POLITECNICO DI TORINO

FACOLTÀ DI INGEGNERIA

Corso di Laurea Magistrale in Ingegneria Civile

Novelty Detection in Beam-like Structures using Extreme Function Theory

Relatore

Prof.ssa Cecilia Surace

Correlatori

Prof. Keith Worden

Ing. Marco Civera

Candidato

Davide Martucci

Ottobre 2018

ACKNOWLEDGEMENT

I would like to thank my thesis advisor, Prof. Cecilia Surace, for her constant support while conducting this research and for her invaluable advises that helped me during all the academic years. Particular thanks to the Engineer Marco Civera for his patient help in facing the inevitable unforeseen problems. Thanks to Prof. Keith Worden for introducing me in this innovative field of study and for the curiosity and passion transmitted to me during this work with extreme competence and professionalism.
A special thanks to my parents, Fernando and Antonella, for their support in all these years, for being an example of life and for their immense sacrifices that allowed me to reach this important achievement. I would like to thank also my brother Adriano, for being always there as only a brother can do. Finally, thanks to all my long-time friends, my university colleagues an all the new friends met during these years that every day have shared with me joy, sacrifice and successes with happiness and love making this experience unique.

RINGRAZIAMENTI

Desidero ringraziare la Prof.ssa Cecilia Surace, relatrice di questa tesi, per il constante supporto durante lo svolgimento di questa ricerca e per gli inestimabili consigli che mi hanno aiutato durante tutto il percorso accademico. Un ringraziamento particolare all'Ing. Marco Civera per il suo paziente aiuto nel fronteggiare gli inevitabili imprevisti di percorso. Un ringraziamento anche al Prof. Keith Worden per avermi fatto conoscere e trasmesso la passione per questo innovativo ambito di studio con competenza e professionalità.
Uno speciale grazie ai miei genitori, Fernando e Antonella, per il loro sostegno in questi anni, per il loro esempio di vita e gli immensi sacrifici che hanno permesso il raggiungimento di questo importante traguardo. Ringrazio mio fratello Adriano per essermi sempre stato vicino come solo un fratello sa fare. Ringrazio infine tutti i miei amici storici, i miei compagni di università e tutti i nuovi amici incontrati in questi anni che ogni giorno hanno condiviso con me gioie, sacrifici e successi con affetto e allegria rendendo questa esperienza unica.

Abstract

Damage detection and localisation in beam-like structures using mode shape features is well-established in the research community. It is known that by inserting a localised anomaly in a cantilever beam, such as a crack, its mode shapes diverge from the usual deflection path. These novelties can hence be detected by a machine-learner trained exclusively on the modal data taken from the pristine beam. Nevertheless, a major issue in current practices regards discerning between damage-related outliers and simple noise in observations, avoiding false alarms.

Extreme functions are here introduced as a viable mean of comparison. By combining Extreme Value Theory (EVT) and Gaussian Process (GP) Regression, one can investigate functions as a whole rather than focusing on their constituent data points. Indeed, n discrete observations of a mode shape sampled at D points can be assumed as 1-dimensional sets of n randomly distributed observations. From any given point it is then possible to define its Probability Density Function (PDF) and the Cumulative Density Function (CDF), whose minima, according to the EVT, belong to one of three feasible extreme distributions - Weibull, Frechét or Gumbel. Thus, these functions - intended as vectors of sampled data - can be compared and classified. Anomalous displacement values that could indicate the presence of a crack are therefore identified and related to damage.

In this work, the effectiveness of the proposed methodology is verified on numerically-simulated noisy data, considering several crack locations, levels of damage severity (i.e., depths of the crack), signal-to-noise ratios and boundary conditions, in order to asses the lowest detectable damage level for non-differentiated transverse displacements data related to a finite elements modelled vibrating structure.

Sommario

L'identificazione e la localizzazione del danno in strutture monodimensionali tramite l'utilizzo delle forme modali è molto diffuso nella comunità dei ricercatori. Infatti è ben noto che, inserendo un'anomalia localizzata in un trave semplicemente incastrata, come ad esempio una frattura, le sue forme modali divergono dal suo usuale campo deformativo. Questi cambiamenti possono essere quindi rilevati tramite un processo di apprendimento automatico allenato esclusivamente sulle forme modali appartenenti allo stato integro della trave stessa. Tuttavia, una delle principali problematiche nella pratica corrente riguarda la corretta distinzione tra valori anomali dovuti alla presenza del danno e il rumore delle osservazioni effettuate, in modo da evitare falsi allarmi.

In questo studio, il concetto di Funzioni Estreme è introdotto come un mezzo di comparazione praticabile. Combinando la Teoria dei Valori Estremi (EVT) e la Regressione con Processi Gaussiani, è possibile analizzare le funzioni nella loro interezza invece di concentrare l'attenzione sui dati puntuali che le costituiscono. Infatti, un campione di misurazioni discrete di lunghezza n riguardante una forma modale campionata in D punti può essere assunto come un set monodimensionale di n variabili aleatorie distribuite in maniera casuale. A partire da ogni punto è quindi possibile definire la Funzione di Densità di Probabilità (PDF) e la Funzione di Ripartizione (CDF), le quali, in accordo con la EVT, appartengono ad una delle 3 distribuzioni per valori estreme ammissibili – Weibull, Frechèt o Gumbel. Queste funzioni, intese come vettori di dati campionati, possono essere quindi comparate e classificate. Gli spostamenti anomali che potrebbero indicare la presenza di una frattura sono quindi riconosciuti e correlati al danno strutturale. In questa tesi, l'efficacia della metodologia proposta è stata verificata tramite dati disturbati simulati numericamente, considerando diverse posizioni del danno, dei livelli di magnitudine del danno stesso (ad esempio la profondità della frattura), di intensità del rumore (ad esempio tramite il Signal-to-Noise-Ratio) e configurazioni di vincolo, al fine di poter determinare il più basso livello di danno riconoscibile per spostamenti trasversali non differenziati derivanti dal modello agli elementi finiti della struttura in esame.

Contents

List of Figures

Chapter 1

Structural Health Monitoring

1.1 Introduction

With the continuous advancing in all the fields of science, technology and economy, the human evolution is increasingly strongly grounded on all the various systems, mechanical and not, that constitute the fundamental bare bones of our existence itself. Mankind is able to focus efforts and resources to endeavour to push forward the limit of our societies, building even more enormous large-scale constructions and developing growing daring and sophisticated projects. Imaging nowday a world without infrastructure as bridges, dykes, power stations, manufacturing plants, airplanes, railways and trains, ... is indeed completely not feasible. When considering the huge cost in terms of global investments and human capital of all these achievements is immediately evident how a continuity with the past is heavily required in order to preserve and further improve these fundamental assets. Hence, **maintenance** covers a main role for several reasons: primary, the standard levels of integrity and serviceability of the considered system have to respect opportune limits to prevent critical crisis, such as catastrophic collapses for structures or severe interruptions in case of essential services and the inevitable consequence of loss of life; besides, the intrinsic and extrinsic value of strategic structures, infrastructures, machinery and networks for historical and economical motives has reached over the years an high grade whose are impossible to refrain from and the preservation of those systems become of central interest jointly with the extension of their design lifetime.

All these considerations has to be approached taking into account a relevant aspect of reality: **uncertainty**, mainly classified as *aleatory* for random variations of variables and predictions or *epistemic* for systemic lack-of-knowledge, pervades in both cases the chosen model for predictions and consequently the accuracy and the reliability of safety measurement and quality assessment. Thus, **probabilistic** and semi-probabilistic approaches based on the assumption that exist statistical distributions of the available experimental data result the only way to bridge the gap and mediate between the natural variability of non-deterministic phenomena and the impossibility to have a complete knowledge of the analysed case, mostly for practical and economic reasons.

For example, to give some context that helps understanding the importance of maintenance related to the residential buildings (figure 1.1) and in particular to the Italian situation, what emerges from the 14^{th} ISTAT General Census of the population and housing **[39]** is that on a total of 12,812,528 recorded building units 19.2% was built before 1919, 12.3% between 1919 and 1945, 50.0% between 1946 and 1981, 11.5% from 1982 to 1991 and 7.0% after 1991, with an overall percentage of 81.5% of buildings older than 40 years and close to their design life. Analogously, in the field of civil construction, one need just to think that the four-year investment plan 2015-2019 of the Italian Public Road Administration Authority (ANAS) provides the 40.6% of resources, amounting to 8.2 billion of euro for extraordinary maintenance and safety works **[4]**. Moreover in recent years, infrastructure efficiency has been put into crisis by various phenomena such as the increase of traffic loads, increase in travel speed, changes in the regulations of reference to safety standards. The functionality of road state of art depends strictly on good inspection activity: in fact the lack of a correct and timely maintenance involves an increase of the deterioration and therefore higher repair costs.

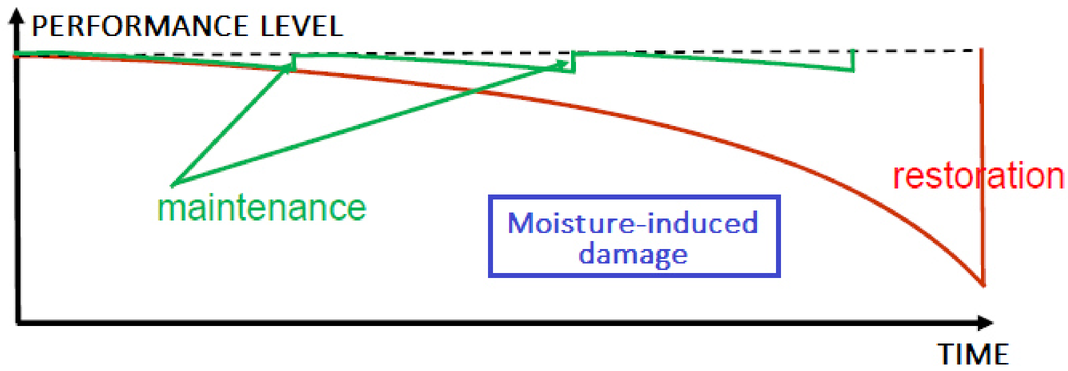

Figure 1.1: Maintenance vs Restoration **[79]**

Unfortunately, it has been reported in recent days the tragic collapse of a part of the stay-cable A10 Polcevera Viaduct 1.2 in Genoa built (only) in 1967, also known as Morandi's Bridge from the name of its designer, during is operational life causing dozen of deaths and injuries and extremely serious consequences for the mobility, the economy and the safety of the town itself with the ulterior imminent danger of flood. Although the causes of the cave-in have not been established yet, the probable failure of a pre-tensed stay and the subsequent failure of the pier and the deck of the bridge shall be undoubtedly recognised in a wide deficiency of ordinary and extraordinary maintenance and with all probability this dramatic epilogue would be avoided with an effective system of structural health monitoring.

Figure 1.2: Stay-cable Polcevera bridge after collapse, Genoa 2018 **[46]**

Even though this fatality is the most widely exposed to media attention for the number of casualties and the strategic importance of the bridge itself, it is not an isolated incident: in the last years a relevant number of bridges of different typologies, static schemes and constructive technologies suffered severe structural damages. Some examples are collected in the figures from 1.3 to 1.6 below; however, as told before, the central role of maintenance and health monitoring is not limited to bridges and civil infrastructures, but it concerns a broad spectrum of engineering applications, ranging from mechanical and aerospace systems to offshore oil platforms and seismic building response.

Figure 1.3: Girder bridge Viaduct 167, Ancona 2017 [**37**]

Collapse caused by pier settlement

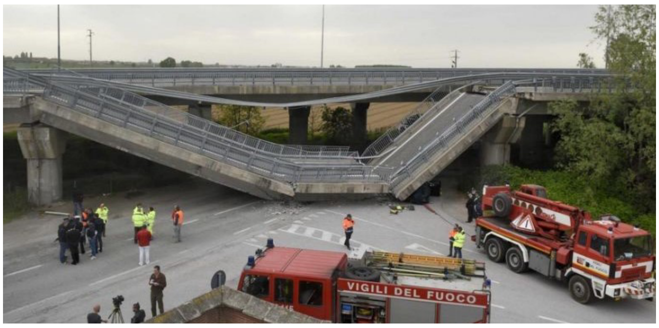

Figure 1.4: Girder bridge Santa Vittoria Viaduct, Cuneo 2017 [**45**]

Failure of the deck under dead load

Figure 1.5: Girder bridge Viaduct 626, Agrigento 2014 [**38**]

Failure of the deck

Figure 1.6: Masonry arch rail bridge, Caltanissetta 2011 [**10**]

Fragile failure of the central span arch

1.1.1 Originality and Organisation of Work

On the aforementioned basis, last decades have seen an increasing interest in the health monitoring of structural systems, involving researchers in multi-disciplinary fields with the aim to develop effective series of procedures and algorithms able to detect, to characterise and to classify the numerous kinds of material damage. Obviously, all the efforts are also focused to respect the implicit economic restrictions, such as for example the type and the number of used sensors. However, in spite of the numerous works inherent theory and applications published in recent years, currently there is not an unified ultimate response to the damage identification and structural monitoring problems and this lack entails a scarcity of real installed systems, especially related to civil structures. Following this well-established pattern, the aim of this Master Thesis work is to study a new methodology that involves genetic optimisation algorithms and machine learning techniques. In particular this study is focused on:

- the analysis of the *transverse mode shapes* of a reference structure in order to establish a **lower detectable damage level**, according to the hypotheses assumed in the data simulation.
- dealing directly with transverse displacements, the **absence of numerical derivation** of data implies the *absence of noise amplification*, with clear consequent advantages in speed and accuracy of analysis.
- developing the algorithm on the basis of the *Extreme Function Theory* leads to a **reduction of false-positive** in novelty detection.
- the adoption of **genetic algorithm** (i.e. *SADE*) enhances statistical robustness of the method without requiring a-priori knowledge of the parameters involved.

This Thesis work is organised as follows: Chapter 1 concerns an introduction to SHM field and it is aimed to give a general overview and a literature review of the current state-of-art; Chapter 2 presents a review of the machine learning techniques adopted here; Chapters 3 and 4 give the theoretical bases of Elasticity, Finite Element and Crack simulation utilised to model the numerical data; Chapter 5 reports the obtained results of analysed case studies; Chapter 6 contains the conclusions of this work and the further perspectives of research.

Part of this work has been presented at the **Modern Practice in Stress and Vibration Analysis Conference** (MPSVA 2018) [**47**], which was held by the Institute of Physic at Clare College in July 2018 in Cambridge, UK.

1.2 Damage Identification Process

Every system is originally designed and built to satisfy a specific need in a given environment with a given level of performance for at least a given service life. Since this strictly defined framework does not correspond exactly to the reality, deeply permeated by uncertainty, in the last 50 years research has been actively focused to implement accurate damage identification strategies because of the related **economic, technological and safety implications** as exposed in the previous introduction. In spite of other widely used monitoring techniques, based on a local analysis that requires an *a-priori* knowledge of the damaged point of the system taken in consideration like Non-Destructive Evaluation (NDE), the Structural Health Monitoring approach is primarily oriented to a global investigation of the structural integrity with the main advantage to analyse vast part of surfaces on the whole. Consequently, also the **definition of damage** itself has to be interpreted from this point of view, moving from a microscopic investigation to a condition-based one, in order to cover the gap between theoretic physical failure phenomena and real engineering applications. According to **[24]**,«*...damage will be defined as changes to the material and/or geometric properties of a structural or mechanical system, including changes to the boundary conditions and system connectivity, that adversely affect current or future performance of that system...*», as far as the system cannot longer perform anymore and the failure occurs. There are several damage and failure classifications based on different criteria, such as effects, severity, detection methods, failure mechanisms and more. A useful collection and comparison of different sources is reported in **[65]**: particularly suitable for the purposes of this work, and thus reported here in figure 1.7, is the severity **classification of failure** taken from the Offshore Reliability Data (OREDA) programme **[52]**:

Critical: A failure which is both sudden and causes the item not to function in one or more essential modes.

Degraded: A failure which is gradual, partial, or both.

Incipient: An imperfection exists that may develop into a degraded or critical failure if corrective action is not taken.

After have defined the object of the analysis, which is the structural damage itself, the problem of damage detection is related the fundamental activity of searching and recognition of patterns in the acquired data. According to **[69]** and to the extended version proposed by **[83]** listed below, it is important to

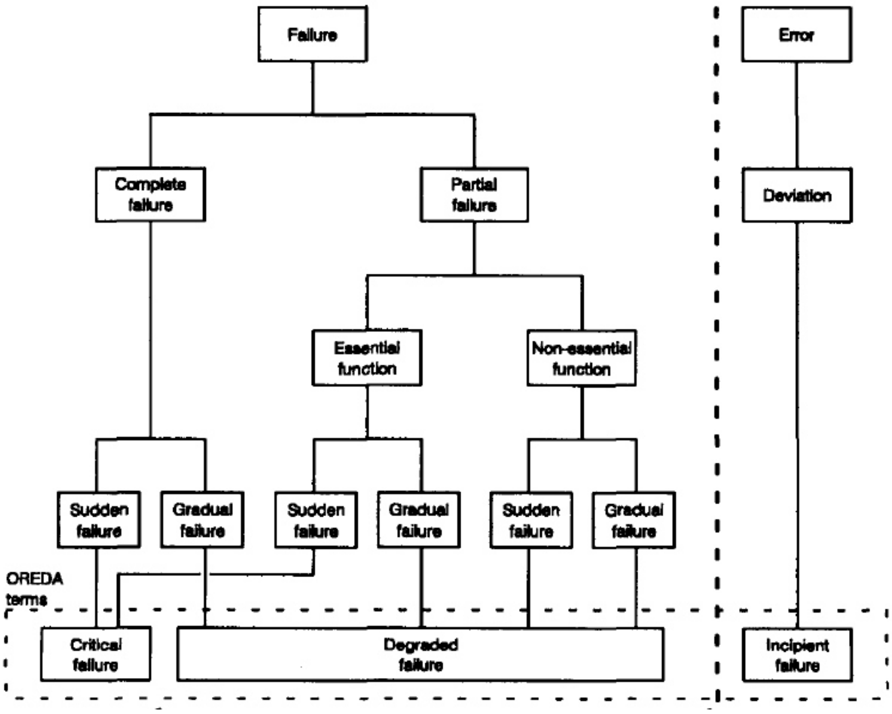

Figure 1.7: OREDA Failure mode classification [52]

define the **hierarchical structure** of the damage identification process, with mandatory sequential levels that allow to organise the different steps of the investigation. Indeed, the information of each underlying step is necessary for the further analyses and all the operations and evaluations have to be properly organised:

1. **Detection**: the method gives a qualitative indication that damage might be present in the structure.

2. **Localisation**: the method gives information about the probable position of the damage.

3. **Classification**: the method gives information about the type of damage.

4. **Assessment**: the method gives an estimate of the extent of the damage.

5. **Prediction**: the method offers information about the safety of the structure, for example it estimates a residual life.

6. (**Smart structures**: self -detection, -diagnosis and -repair [79])

1.2.1 Statistical Pattern Recognition

Although pattern recognition is a traditional activity of science and engineering fields, because of the amount of data taken in consideration and the complexity of the involved calculations, nowday its applications are inseparable from a *machine learning* perspective. Machine learning is a wide field of computer science with a large number of interdisciplinary applications and all its characteristics will be discussed in detail in the next chapter 2. For now it is sufficient to give a first definition and, as proposed by **[9]**, **pattern recognition** «*...is concerned with the automatic discovery of regularities in data through the use of computer algorithms and with the use of these regularities to take actions such as classifying the data into different categories...*». This last statement is not exhaustive since it principally describes a *data-driven* approach to the problem, where a statistical model is built in order to carry out information from data; otherwise, the *inverse problem* approach is likewise relevant in SHM framework and it is mainly based on physical model of the considered structure. The work made in this Thesis refers to the first approach here presented and thus, the focus is to outline the statistical pattern paradigm as organised in **[23]**. A simple and intuitive example of that data-to-decision process, accurate for a single sensor acquisition, is the Waterfall scheme proposed by **[7]** in figure 1.8, while a review of other operational schemes can be found in **[88, 8]**. According to **[23]**, the entire process can be generally divided in four main steps and other subroutines that can recur in different points:

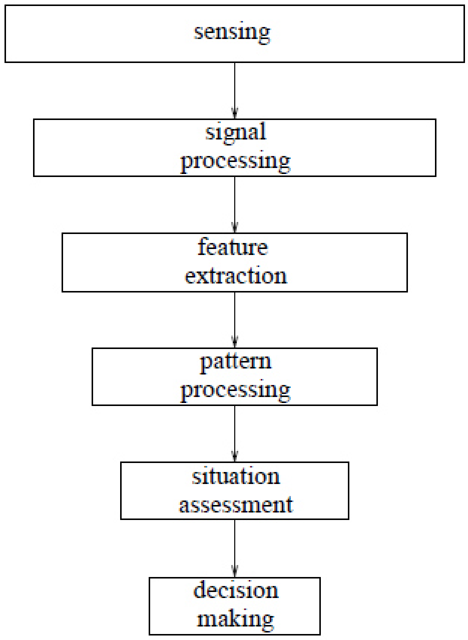

Figure 1.8: Data to Decision (D2D) - Single sensor Waterfall scheme **[88]**

Operational Evaluation :

This stage can be considered as a feasibility phase in which is necessary to evaluate what kind of damage we are interested to analyse (i.e. the higher structural risk), the economic, safety, and environmental conditions in which the monitoring system should operate and its conceptual and technological design.

Data acquisition and preprocessing :
The material acquisition of data concerns a series of issues related to the sensors themselves (i.e sensors location) and the other used technologies. On the basis of the investigated phenomena (i.e. corrosion, fatigue,..), and thus the inputs (i.e. vibrational excitations, laser scanning,...) and the outputs (i.e. dynamic response,...) involved, different operations aimed to improve the quality of the information may be required depending on the implemented process, such as

- *Data Normalisation*, to obtain comparable values (i.e. it is required in case of mode shapes);
- *Data Cleansing*, aimed to reduce epistemic uncertainty of data;
- *Data Compression*, with the objective to reduce the dimension of data and thus the computational effort in storage and calculations;
- *Data Fusion*, to combine several sources for a more complete information

Feature selection and extraction :
As explained in detail in the following paragraphs 1.2.2 and 1.2.3, «.. Sensors cannot measure damage...» and hence, it is necessary to individuate a distinguish feature able to indicate the presence of damage. A this stage, some operations of aforementioned ones can be required or repeated but, more important, this is the application point of all the algorithms and techniques of data mining related to the automatic analysis of machine learning.

Statistical model development :
The final purpose of the process is the damage identification at different levels of the hierarchical structure of analysis as detailed above. To achieve this through statistical pattern recognition, there are basically four different principal types of algorithm, classified on the basis of the available data and the identification goal:

- **Classification**, attributes defined labels to discrete classes of data;
- **Clustering**, autonomously individuates the unknown classes of data;
- **Regression**, evaluates the functional parameters and the evolution of continuous variables;

- **Novelty detection**, detects a change in the variables state, passing from a "normal" state to an "abnormal" or "damaged" one;

Complementary, another important algorithms distinction is made on the basis of the kind of the processed data. Basically, if the algorithm extrapolates all the required initial state information and parameters from the "normal" or "undamaged" observations only, then it is named as **unsupervised learning** algorithm since the data have no labels and they are assumed to come from the pristine state. Otherwise, if the initial multiple data class labels are known, we refer to it as **supervised learning** algorithm because of this initial division of data in different classes [**84**].

1.2.2 Damage Sensitive Features and Identification Methods

The wide literature available covers a large number of methodologies and applications developed in last decades. As well, there are several works focused on summarise and organise the state of art of the structural health monitoring field in a given period: the review presented here derives from a comparison of different exhaustive resources, such as articles [**11, 14, 20, 22, 25, 23, 31, 43, 61, 62, 70, 74, 72, 85**], technical reports [**21, 75**], lectures [**79**] and books [**84, 87**]. Although the large variety of typologies of damage investigation methods, recent researches and applications mostly regards the vibration-based methods since their intrinsic characteristics that properly fit with the nature of data-driven algorithm approach.

In this paragraph is reported a general first classification of the different types of utilised features in order to have an overview of strengths and weaknesses of the various damage identification processes, in particular in civil constructions, while a detailed and referenced review of the adopted metrics can be found in the next section 1.3.

Natural Frequency :
This is probably the most studied feature in damage diagnostic due to the direct correlation between the observations in global structural behaviour related to stiffness, mass and damping variations and the changes in the frequency response. A first limitation common to other modal properties are the restrictions of experimental modal analysis, such as the requirement of structural linearity, time-invariance and reciprocity that unlikely fit with real applications. Another important issue in frequency shift methods is to reach a certain level of accuracy in measurement since the chosen feature itself is not very sensitive to damage and

thus not effective when working with an high level of noise and uncertainty or low level of damage. In spite of this, the ease to measure natural frequencies and to compare their shifts in order to asses the presence of damage, mainly for single-crack in simple structures, made this feature widely used over years providing numerous studies on different applications. Other attempts to reach level upper than 1 of damage identifications hierarchical structure, to deal with multiple cracks scenarios or to extrapolate localised information without involving higher modes showed to be ineffective.

Mode Shape Dispalcement :
Holding the previous assumptions of experimental modal analysis, mode shapes presents many advantages and have been widely used in last decades up to our days: this Thesis, indeed, it is focused on the analysis of the transverse mode shapes as whole functions. Modal parameters have two principal strength points: firstly, they provide spatial information of the structure and thus entail the development of damage localisation method in addition to damage assessment; in second place, they present the relevant property of orthogonality that results very useful for similarity comparison and compression techniques (i.e. MAC, PMAC, COMAC, ...). In particular, as previously mentioned, data compression is often fundamental in order to reduce the dimensionality of analysed data, but on the other hand this may cause the side effect of loss of information. Another adverse aspect is the correlation between damage location and the effectiveness in its detection: depending on boundary conditions, mode shapes present zero-displacement points, called *stationary points* or *modal nodes* that result to be less sensitive to damage and consequently affect the analysis itself. Regarding data noise, instead, it plays a double role: although it definitively affects the measurement to the point that application to real structures is in such way difficult, otherwise modal displacement does not suffer of noise amplification due to numerical manipulation (i.e. derivatives).

Mode Shape Curvature :
Strictly related to the aforementioned parameters, curvature is currently considered on of the best damage sensitive features for its capability to efficiently indicate the damage presence together with spatial information and extension. Numerically and operationally (Operational Deflection Shapes), it can be derived with good approximation from mode shapes by numerical backward, forward and central derivation but it is easy to operate a data cleansing phase in order to reduce the disturbing action

of noise (i.e. subtracting the baseline of undamaged state) since its variations is directly related and localised in correspondence of damage. Moreover, its correlation with strain allows several miscellaneous operations with other features or metrics, such as dynamic flexibility, and strain energy described below (i.e. Dynamic Flexibility Curvature Method or Frequency Curvature Response).

Dinamycal Flexibility :
Defined as the inverse of the stiffness matrix, the flexibility matrix puts in direct correlation the displacements and the related d.o.f., showing as important property an higher sensitiveness to damage effect for lower modes. Otherwise, this feature still requires a large number of measurement points, weakness in common with the other modal features, while does not guarantee sufficient accurateness in the estimation of damage location. As assessed before, there are several metric available in literature that, involving dynamical flexibility also in combination with other features, including analysis of changes in flexibility, Stiffness Error Matrix Method, Residual Flexibility, enhance more robustness in the estimations in particular related to damage localisation.

Strain Energy :
From elastic theory it is known that stresses in a structural element flow following the most rigid feasible path; hence, every variation of this state that might occur in the structure, like a geometrical discontinuity caused by an edge-crack or the related reduction of the element stiffness, leads to a different internal stress distribution and consequently it produces a variation in the strain energy of deformation. Since this change in structural response is basically localised close to damage location, it is possible to perform the damage identification up to levels 3 and 4 of the previous scheme through the definition of opportune damage indexes (i.e. Elementary Energy Quotient). Past applications of methods based on this feature showed off as main advantage a better stability when dealing with data affected by a relevant disturbing noise, while these processes nevertheless present problems to correctly evaluate multiple cracks scenarios or incomplete modal information.

Time domain methods :
Linear time series methods in the context of diagnosis of vibrating structures are widely used because they offer numerous advantages. Continuous monitoring measurements directly refer to time domain and thus no re-elaboration of data that may cause a loss of information are needed. In

addition to this ease of application, these models are able to correctly preform evaluation of damage detection and qualification based on incomplete models and data without requiring physical or numerical simulated reference models. However, partiality of adopted model has as consequent side-effect a limitation on the extent feasible range of damage investigation. Time models suits very well with the data analysis approach, entailing detection of damage from the vibration measurements by the use of filtering and signal processing techniques like Wavelet signal decomposition or Auto-Regressive (AR) and the Auto-Regressive-Moving-Average (ARMA) models and their modified versions.

Frequency domain methods :
Following the development of new algorithms that improve the evaluation of the Fast Fourier Transformation (FFT), frequency-domain-based methods gain an extensive central role in the damage detection studies because of their stability and accurateness. As first advantage, algorithms directly based on the Frequency Response Function (FRF) show off a great capability to deal with incomplete measurements for the intrinsic nature of the used function itself, avoiding the necessary manipulation the extrapolate modal data since they are derived from time series. Moreover, through signal processing it is possible to compensate biases and errors due to data acquisition and extraction. Furthermore, by defining opportune indexes to compare frequency responses it possible to evaluate from the carried information novelty detection, damage extension and location. On the other hand, effectiveness and accuracy of the results still depends on the amount of the measurement points and their position respect to the defect to investigate. Recently, miscellaneous techniques involving at once time and frequency, such as Wavelet Analysis, Spectral Pattern Methods and H-H Transform, have been shown a lot of advantages in most of the requirements of the damage identification process, from data fusion and feature extraction to pattern recognition, while avoiding the requirement of stationary signals.

Matrix update based methods :
Involving different structural parameters, including the ones listed above, these methods combine measured and numerical simulated data in an optimisation process in order to approximate with the best possible accuracy the real structure. Analytical and numerical models constitute the reference model that is iteratively updated taking into account the actual measurements data by the imposition of objective functions to be minimised, constraints equations and other numerical schemes. Naturally,

these methods have some limitations due to computational issues like the accuracy of the initial model and the number of parameters to update. Some of most used approaches are the Matrix-Update Method and the Eigenstructure Assignment Method (based on residual evaluation), the Optimal Matrix Method (direct closed-form solution), the Sensitivity Based Methods (Taylor's series approximated perturbation), Hybrid Matrix and the Computational Intelligence Method.

Non-linear methods :
Real-world applications are often characterised by a non-linear behaviour or by a deviation from a linear response when a discontinuity occurs in the structure. All the aforementioned features and methods hold under the main assumptions of linearity and this results in a restrictive limitation of applicability. For instance breathing cracks, yielding of metallic elements with strain hardening property, structural damping, delamination in composite materials, fatigue phenomena or hysteretic behaviour are all examples of non-linear-responses. Although is difficult to correctly implement models capable to take into account all the several possible non-linearities that behave in different ways, non-linear damage identification methods are spreading for their potential and for the vast number of damage-sensitive features that can be analysed and used as damage indexes. Main challenges in the evolution of these methods concern the accurate evaluation of the predominant non-linear behaviour of some structures in their pristine state and to enhance a more sensitive distinction for those systems that exhibit linear response under low level of excitations or when affected by small damage. Many of the previous features are adapt to be studied removing the hypothesis of linearity and in addition some common non-linear features are the Harmonic Distortion, the Coherence Function, the Holder Exponent, Non-linear Output Frequency Response Functions (NOFRF) or Modified Local Damage Factor (MFLD).

Artificial Neural Networks :
Nowday, the increasing interest in the study of human being and human evolution has met a melting point with other disciplines for the inestimable potentiality and complexity of our characteristics. In particular, from a computational point of view, the ability of our brain to learn, elaborate and store information is something that the most modern and powerful computers can only try to imitate. On this basis, Artificial Neural Network (ANN) algorithms mime the architecture, at different levels of sophistication, of neurons and neural system and have been applied

to a large variety of fields originating new paradigms for artificial intelligence (named Deep Learning) not only capable to analyse data, but also to automatically learn, adapt and evolve in response to the received inputs. Regarding the SHM field, ANNs are non-linear functional operators characterised by the main advantages of learning and memory abilities, adaptivity, robustness, stability and parallel processing. These black-box, model-free and adaptive tools enhance fine detection, localisation and sizing of damage also in complex structures, with the major issues of a huge computational effort and higher entanglement of network models. Literature related to different networks and their applications is very wide: however it is not of central interest here and a citation of the most used algorithms as the Multi-Layer Perceptron (MLP) or the Time Delay Neural Network (TDNN) is sufficient.

Genetic Algorithm Optimisation methods :
Analogously to previous methods, Genetic Algorithms (GA) are stochastic search methods based on the Darwin's theory of evolution of population and survival of the fittest individual. Basically these methods consist of three main steps, reproduction, cross-over and mutation aimed to perform the optimisation of vectorial data encoded as chromosomes. The cost of fitting is specified through an objective function that allows to identify and discard the worst individuals of the random population: optimisation does not require any initial guess or other a-priori knowledge, and the use of the gradient with the numerical implication of derivatives is avoided. Direct advantages of this approach is the finding of global optimum simply repeating several times the process, the ease of implementation of the matching stage and the statistical robustness of estimations, in spite of a possible huge computational effort. In the SHM field these algorithms are widely used such intermediate optimiser in numerous applications, but often their direct application is minded to compare the changes in the vibrational measurements before and after damage to identify the structural damage. Several versions of GA algorithms are available in literature, such as the Differential Evolution (DE), the Particle Swarm Optimisation (PSO), the Ant Colony Optimisation (ACO) or the Firefly Algorithm (FA).

1.2.3 Fundamental Axioms

Only recently research community has established the first cardinal points of the structural health monitoring field, classifying them as fundamental axioms as proposed by [**86**]:

I. All materials have inherent flaws or defects.

II. The assessment of damage requires a comparison between two system states.

III. Identifying the existence and location of damage can be done in an unsupervised learning mode, but identifying the type of damage present and the damage severity can generally only be done in a supervised learning mode.

IV. Sensors cannot measure damage. Feature extraction through signal processing and statistical classification is necessary to convert sensor data into damage information.

V. Without intelligent feature extraction, the more sensitive a measurement is to damage, the more sensitive is to changing operational and environmental conditions.

VI. The length-scale and the time-scale associated with damage initiation and evolution dictate the required properties of the SHM sensing system.

VII. There is a trade-off between sensitivity to damage of an algorithm and its noise rejection capability.

VIII. The size of damage that can be detected from changes in system dynamics is inversely proportional to the frequency range of excitation.

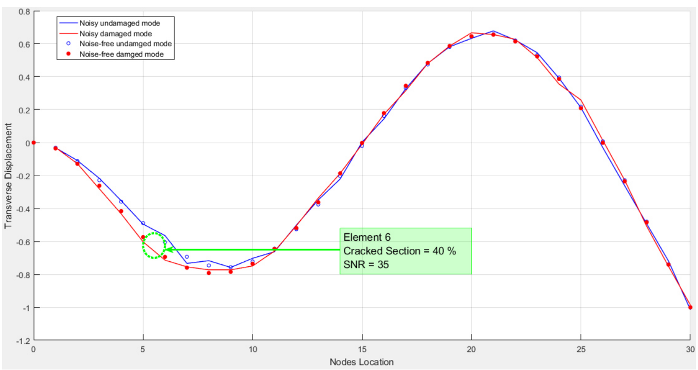

Figure 1.9: Example Ax. II - Comparison of different states of a mode shape

1.3 State of Art: literature review of mode shape-based methods

Mode shape data have been largely used since the early stage of research in damage detection because of the capability of this feature to carry information not only of multiple cracks occurrences, but also regarding their locations and extensions. The ease of data sensing of mode shapes is a strong advantage in using this feature, while experience showed off an higher sensitiveness compared to frequencies analysis. However, the accuracy of vibrational measurements remains limited by the technological issues of available sensors and the related integrity of data against the disturbing presence of epistemic noise. The focal point of the analysis, hence, concerns with the evaluation of one or more opportune metrics able to return a quantitative characterisation of damage. Moreover, modal data give access through mathematical manipulation, such as derivatives, to higher order cinematic fields of the studied structure (i.e. rotations, curvature) that present discontinuities strictly linked with structural properties variations, like geometry, stiffness, flexibility, ... and more.
Available literature on mode shape methods is very wide: some of most relevant works are presented here following a chronological/thematic order. One of the first proposed metric is the Modal Assurance Criterion (MAC) **[3]** (1992) and the similar modified criteria critically reviewed in **[2]** (2003). Based on the orthogonality property of mode shapes ϕ_i, ϕ_j, where ϕ^T and ϕ^* are the transpose and the conjugate respectively, the MAC returns a real scalar index from 0 to 1 of vectors consistency as,

$$MAC = \frac{\left|\phi_i^T \phi_j^*\right|^2}{\phi_i^T \phi_i^* \phi_j^T \phi_j^*} \tag{1.1}$$

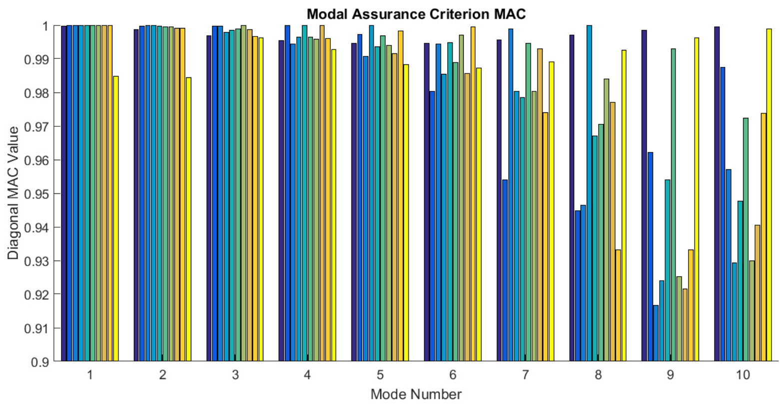

Figure 1.10: Diagonal MAC of a 10-d.o.f cantilever beam

Results can be visually interpreted by immediately comparing the level of consistency of matched mode shapes as showed in figure 1.10 above for a 10-d.o.f.s cantilever beam with a reduction of elementary stiffness of 15% in each element of ϕ_j, respectively.
Analogously, combining eigenvectors and eigenfrequencies ω, **[92]** (1985) proposed the Yuen Function a as a index of distortion of damaged mode shapes over position,

$$Y_i = \frac{\phi_i}{\omega_i} - \frac{\phi_j}{\omega_j} \tag{1.2}$$

Results showed a correlation with position of crack and strain energy of the studied beam: higher discontinuities were detected close to the clamped end, while the differences is slightly reduced where strain energy is low.
On the same pattern, **[53]** (1991) proposed the analysis of curvature κ changes along position x for the relation with bending moment, deriving it from mode shape measurements through the central difference approximation with a step h (while backward and forward rules are used for the extreme elements)

$$\begin{aligned} & \kappa(x) = \phi''(x) \approx \frac{M(x)}{EI} \\ with \qquad & \phi''_m \approx \frac{\phi_{m-1} + 2\phi_m + \phi_{m+1}}{h^2} \end{aligned} \tag{1.3}$$

and the damage index named Mode Shape Curvature (MSC) is generally defined as,

$$MSC = \Delta\kappa_j = \sum_{i=1}^{N} \left| (\phi_{i,j}^D)'' - (\phi_i^U)'' \right| \tag{1.4}$$

The extension of this method was proposed by **[64]** (1997) using a Laplacian operator in order to obtain a generalised evaluation of the second difference suitable also for 2-dimensional problems. Generally, curvature is a good feature to investigate since its higher order contributes to amplify modal discontinuities; otherwise, this amplification is collaterally reflected on noisy data if second order derivative is obtained by deriving transverse displacements. An example of use of squared curvature to index damage is found in **[68]**, while an experimental verification of several methods can be found in **[60]** (2009). Other implementations are the Curvature Damage Factor (CDF) **[81]** and the Normalised Curvature Ratio (NCR) **[42]**.
In **[40]** (1995) the inherent relation between mode shapes and modal strain energy was used to define new indexes α_j describing severity and β_j, standardised in the Damage Localisation Indicator Z_j, describing location of damage, over incomplete mode shapes as in equations 1.5, where apexes ^{T} and * refer

to transpose and conjugate respectively, NM to available mode shapes and NE the number of members, while K is the modal stiffness and C collects the geometric properties. Normalisation, as usual, involves the mean $\bar{\beta}$ and standard deviation σ_β and allows the identification of flaws on pattern recognition bases by accepting or rejecting null and alternate hypotheses. In this method, as the aforementioned ones, results becomes more significative when the baseline of normal conditions is subtracted to damaged data and the analysis is focused on the differences between the two states only (figure 1.11). A comparative study on the effectiveness of the previous methods can be found in **[71]** (2000).

$$\alpha_j = \frac{[\phi_i^T C_{j0} \phi_i]}{\phi_i^{*T} C_{j0} \phi_i^*} \frac{K_i^*}{K_i} - 1$$

$$\beta_j = \frac{\sum_{i=1}^{NM} \left(\phi_i^{*T} C_{j0} \phi_i^* + \sum_{k=1}^{NE} \phi_i^{*T} C_{k0} \phi_i^* \right)}{\sum_{i=1}^{NM} \left(\phi_i^T C_{j0} \phi_i + \sum_{k=1}^{NE} \phi_i^T C_{k0} \phi_i \right)} \frac{K_i}{K_i^*} \tag{1.5}$$

$$Z_j = \frac{\beta_j - \bar{\beta}}{\sigma_\beta}$$

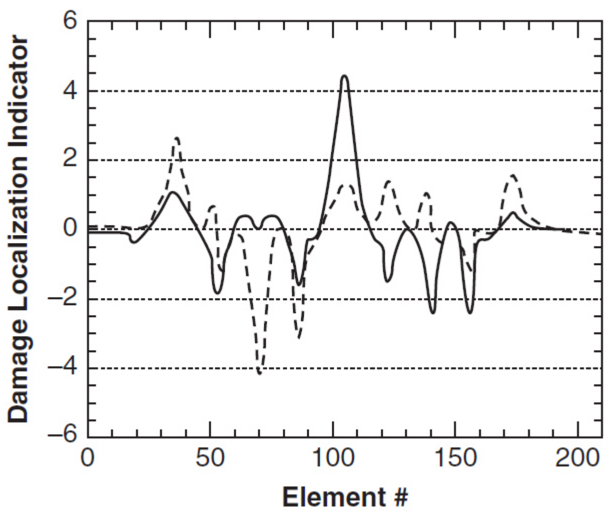

Figure 1.11: Study of I-40 Bridge, damaged element n. 106 **[84]**

A miscellaneous approach involving a variation of MAC, the multiple damage location assurance criterion (MDLAC) introduced by **[48]** for frequencies, was presented in **[73]** (2000) for incomplete mode shapes. Partial mode shapes where combined with the analytical ones to perform localisation of defect by the evaluation of a MDLAC value for mode shapes,

$$MDLAC(\delta D_j) = \frac{|(\Delta\phi)^T \cdot (\delta\phi\delta D_j)|^2}{(\Delta\phi)^T \cdot \Delta\phi \cdot (\delta\phi\delta D_j)^T \cdot (\delta\phi\delta D_j)} \tag{1.6}$$

where $\Delta\phi$ is the measured, incomplete, discrete mode shape difference vector and $\delta\phi$ is the analytical mode shape difference at the same d.o.f.s, while δD_j is the size of damage at location j preliminarily estimated. This method showed off a particular effectiveness in flaws localisation on the basis of partial information also for non-linear structures.
A completely different approach was followed by **[91]** (2001) implementing a real-number encoded genetic algorithm to directly minimise an objective function, instead to update a structural model for iterative evaluation of damage effects. From the different evaluated objective functions, the best results were obtained with a target J comprehensive of frequencies and modes shapes at the same time,

$$\begin{aligned} J = \sum_{i=1}^{NM} W_{\omega,i}^2 \left(\left[\frac{\omega_i(\alpha) - \omega_i^0}{\omega_i^0} \right]^A - \left[\frac{\omega_i^D - \omega_i^U}{\omega_i^U} \right]^E \right)^2 \\ + \sum_{i=1}^{NM} W_{\phi,i}^2 \sum_{i=1}^{NP} \left(\left[\phi_{ij}(\alpha) - \phi_{ij}^0 \right]^A - \left[\phi_{ij}^D - \phi_{ij}^U \right]^E \right)^2 \end{aligned} \tag{1.7}$$

where W are the weights of the cost function, the apexes A and E refer to analytical and experimental data, D and U to the damaged and undamaged state, NM and NP to the available modes and the measurement points, α is a stress reduction factors and 0 refers to the initial value, respectively. The genetic optimisation enhances detection, localisation and sizing of damage in an effective way in 1-d and 2-d structures.
In **[1]**(2002), again an higher order feature of displacement fields was investigated, taking in consideration the changes in rotations. It was carried out that changes of rotation of mode shapes are robust to localise single and multiple cracks with different sizes and more sensitive respect to transverse displacements. An alternative damage index is found in **[41]**, where the mode shape slope at k^{th} coordinate for the i^{th} mode is evaluated with the first derivative approximation on 5 points as,

$$\Delta(\phi_{i,k})' \approx \frac{\phi_{i,k-2} - 4\phi_{i,k-1} + 6\phi_{i,k} - 4\phi_{i,k+1} + \phi_{i,k+2}}{2h} \tag{1.8}$$

and the Mode Shape Slope Damage Factor (MSSDF) is

$$MSSDF_k = \frac{\left|\Delta(\phi_k^D)' - \Delta[\phi_k^U)'\right|}{max\left|\Delta(\phi_{k=1,...,n}^D)' - \Delta[\phi_{k=1,...,n}^U)'\right|} \tag{1.9}$$

Keeping focusing on the discontinuities caused by damage presence, **[82]** (2007) and **[58]** (2008) improved a detection method based on the irregularity profile of the mode shapes due to damage only by subtracting the normal baseline of displacements evaluated by filtering to smooth noisy waveforms. The roughness profile R is defined as,

$$\begin{aligned} w(x_0) &= \int_{-\infty}^{\infty} z(x_0 + x)h(x)dx \\ R(x_0) &= z(x_0) - w(x_0) \end{aligned} \tag{1.10}$$

where z is the height of the mode shape and $h(x)$ is the smoothing function and w is the waviness of the the mode shape. Results showed an effective response for realistic simulations ($SNR \approx 40dB, \frac{a}{h} \approx 0.3$) and low sensors resolution. **[34]** and **[17]** followed a probabilistic approach adopting the joint log-

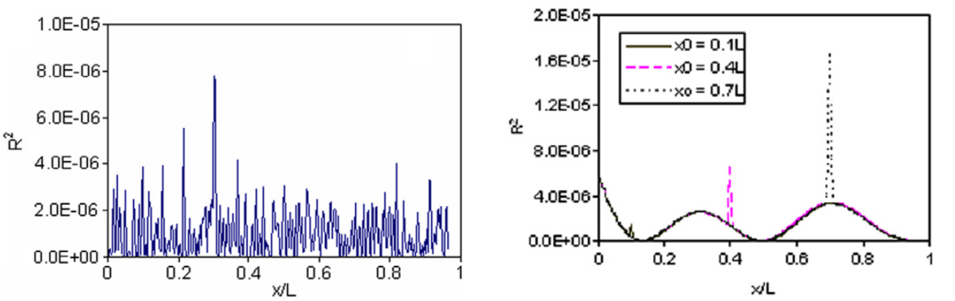

(a) Noisy Roughness profile - 1st mode, $\frac{x}{L} = 0.3$, $\frac{a}{h} = 0.3$, $SNR = 40dB$

(b) Filtered Roughness peaks - 3td mode, 3 cracks

Figure 1.12: Irregularity method applied to a cantilever beam **[82]**

arithmic marginal likelihood evaluated on a piecewise kernel as indicator of damage. The process allow to detect and localise multiple cracks with an acceptable sensors resolution in an effective manner without requiring differentiation that always results in an amplification of noise **[18]**. Further improvement of this approach is **[15]**, where Treed Gaussian Processes (TPG) are used to selectively reduce the possible damaged configurations in order to assess locations and sizes of possible cracks by a treed convergent iteration over subclasses of the characteristic crack parameters.

Chapter 2

Machine Learning and Gaussian Processes

2.1 Definition of Machine Learning problems

If the latter half of the past century has been strongly characterised by the digital revolution with the beginning and the technological development of computers, nowday, with the increased computational power and the advancing in sensor technology, new interdisciplinary paradigms are becoming of central interest in many scientific fields such as big data analysis, data mining, artificial intelligence, natural inspired computation or internet of things, to cite some examples. The *IV Industrial Revolution* is, indeed, firmly rooted on these basis with the final aim to develop automatic and highly innovative products, services and methodologies: a definition that well suits with the purposes of Structural Health Monitoring, where data analysis, computational and sensing devices and decision processes are jointly applied to monitor and to predict the current and the future state of structural elements. In this context, **machine learning** covers a prominent transversal position and, recalling the definition proposed in [**49**], it is «... *the set of methods that can automatically detect patterns in data, and then use the uncovered patterns to predict future data, or to perform other kinds of decision making under uncertainty*...>. As told before, often these methods are contaminated with natural inspired artificial computation, that concerns with developing technology to enable computers to solve problems that commonly could be solved only by humans by taking inspiration from already existent natural models and solutions. To cite an example of this approach, the aforementioned *Multi-Layer Perceptron* (section 1.2.2) mimes the interaction among several neurons in order to provide outputs from a series of mapped input features (figure 2.1).

In other words, what *experience* represents in the human decision process is emulated by the machine in a probabilistic way on the basis of the input data sampled in an opportune training set. This **training phase** is finalised to estimate, by tuning them through an optimisation step, the governing parameters of an adaptive model, which constitutes the reference baseline of knowledge of the algorithm. To ensure the statistical reliability of the estimations, generally an intermediate **validation phase**, performed on a opportune validation set separated form the training one, is required. Final predictions using the already tuned algorithm, like classification or novelty detection, is the **generalisation phase**, where a not-intersecting test data set is used to match probabilistic thresholds and in some case reward criteria to extrapolate generally valid predictions that fit with the recognised pattern [9]. Typically, learning algorithms are classified by considering the type of available input data or distinguishing the type of resulting output. While the second criterion has been already presented in section 1.2.1, in the first case the three different classes are subdivided as follows,

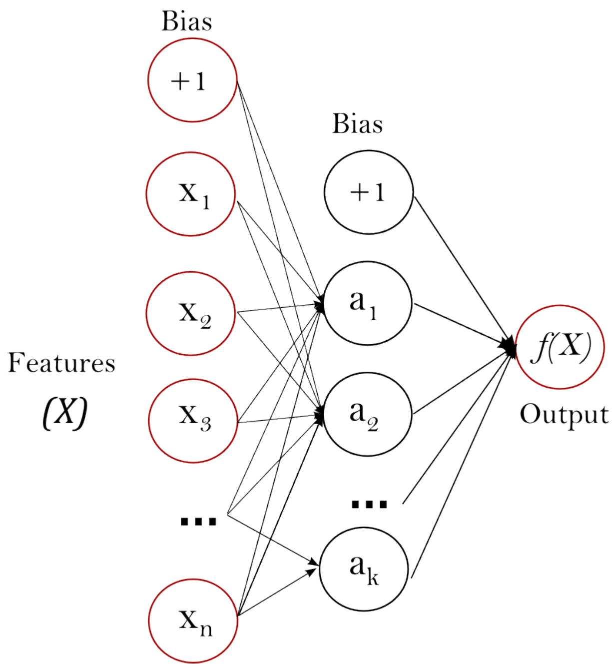

Figure 2.1: Multi-Layer Perceptron network, an example of artificial natural inspired model

Supervised Learning :
The algorithm is trained on data from every feasible state and the label of each case is known (i. e. undamaged/damaged state). Basically this procedure consists of teaching to the machine how to do something and then to let it use the model with a general rule that correlates input and output. The major disadvantage is the requirement of prior knowledge of all states, which implies an higher cost in the data acquisition phase in economic and time-consuming terms.

Unsupervised Learning :
Starting from unlabelled data acquired from a single case (i. e. undam-

aged state), the algorithm learns how to do something, and use this to discover structure and patterns in data.

Reinforcement Learning :
The adaptive algorithm autonomously interacts with external inputs in order to pursue a given goal while a supervisor rewards or punishes it on the basis of the final achievements (success/fail). In this way the algorithm tries to maximise the reward and develops memory from past experience, improving the quality of further predictions.

2.2 Gaussian Process

Bayesian interpretation of probability concerns with evaluating the confidence of a given estimation, since its approach is based on the data information rather than frequency of occurrence of certain event and the probabilistic model parameters themselves are estimated with a level of uncertainty. As explained in **[63]**, for the n noisy observations $\mathbf{y} = f(\mathbf{x}) + \varepsilon$ of a 1-dimensional (D) problem, disturbed by the independent and identically distributed noise ε with standard deviation σ, the Standard Linear Inference Model can be computed as a Bayesian parametric regression, where the resulting distribution given the *a-priori* knowledge of the phenomena is function of the weights $\mathbf{w}$, following the Bayes's rule,

$$p(\mathbf{w}|\mathbf{y},\mathbf{x},\sigma) = \frac{p(\mathbf{y}|\mathbf{x},\mathbf{w},\sigma)\,p(\mathbf{w})}{p(\mathbf{y}|\mathbf{x},\sigma)} \tag{2.1}$$

where $p(\mathbf{w})$ is the *prior* probability Density Function (PDF) that expresses our initial beliefs on the distribution, $p(\mathbf{y}|\mathbf{x},\mathbf{w},\sigma)$ is the *likelihood* PDF given the observations, $p(\mathbf{y}|\mathbf{x},\sigma)$ is the normalising constant named *marginal likelihood* and $p(\mathbf{w}|\mathbf{y},\mathbf{x},\sigma)$ is the *conditional posterior* joint distribution. A key factor in all

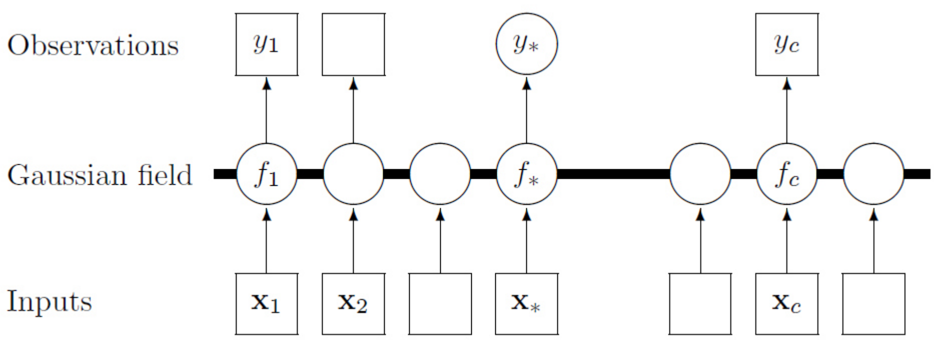

Figure 2.2: Gaussian Process Regression scheme **[63]**

probabilistic and semi-probabilistic approaches used in sciences and technology fields regards the assumptions on the statistical distributions of the available experimental data. On the basis of the well-known Central Limit Theorem (CLT), Gaussian or Gaussian-like probability distributions are mostly used. The noisy observations $\mathbf{y}$, that in this case are the beam transverse displacements at the node locations $\mathbf{x}$, have a Gaussian joint distribution of the target values $\mathbf{f}^*$ and the function values at the test locations $\mathbf{x}^*$ defined as follows,

$$p\left(\mathbf{f}^* | \mathbf{x}, \mathbf{y}, \mathbf{x}^*\right) \sim \mathcal{N}\left(m^*, K^*\right) \tag{2.2}$$

where m^* is the predictive mean and K^* is the predictive covariance matrix, expressed as,

$$m^* = k\left(\mathbf{x}^*, \mathbf{x}\right)\left[k\left(\mathbf{x}, \mathbf{x}\right) + \sigma_n^2\right]^{-1}\mathbf{y} \tag{2.3}$$

$$K^* = cov(\mathbf{f}^*) = k\left(\mathbf{x}^*, \mathbf{x}^*\right) - k\left(\mathbf{x}^*, \mathbf{x}\right)\left(k\left(\mathbf{x}, \mathbf{x}\right) + \sigma_n^2\right)^{-1} k\left(\mathbf{x}, \mathbf{x}^*\right) \tag{2.4}$$

The resulting multivariate Gaussian probability distributions take the form,

$$p = \frac{1}{\sqrt{2\pi^D |K^*|}} \exp\left[-\frac{1}{2}(\mathbf{f}^* - m^*)^T K^{*-1}(\mathbf{f}^* - m^*)\right] \tag{2.5}$$

The prior information of the process is specified in the covariance matrix K^*, in this case assumed as a *Squared-Exponential.* In the one dimensional case it can be expressed in the form,

$$k_y(x_p, x_q) = \sigma_f^2 \exp\left[-\frac{1}{2l^2}(x_p - x_q)^2\right] + \sigma_n^2 \delta_{p,q} \tag{2.6}$$

where $\delta_{p,q}$ is the Kronecker delta and l, σ_f, σ_n are the *hyperparameters,* whose optimisation is based on the *marginalisation property* of the *marginal Likelihood* (ML). The variables x_p and x_q are the nodal locations of the training data data set corresponding to different position indices p, q. The ML is taken in the negative logarithmic form (NLML), since it is easier to perform a minimisation, resulting in,

$$NLML = \log p\left(\mathbf{y} | \mathbf{x}, l, \sigma_f, \sigma_n\right) = \frac{1}{2}\mathbf{y}^T L_{xx}^T \backslash \left(L_{xx} \backslash \mathbf{y}\right) + \sum \log\left(diag\left(L_{xx}\right)\right) + \frac{n}{2}\log 2\pi \tag{2.7}$$

where L_{xx} is the lower Cholesky decomposition of the covariance matrix $k(\mathbf{x}, \mathbf{x})$ and the operator "\" indicates the left matrix division, required for a faster computation of the matrix inversion. From 2.7 follows the three partial derivatives constituting the gradient used to optimise it (CGO 2.4.1) evaluated with the derivation chain rule:

$$\begin{aligned}
\frac{\partial NLML}{\partial l} &= -\frac{1}{2} trace\left[A * \sigma_f^2 \exp\left(\frac{(x_p - x_q)^2}{2l^2}\right)\frac{(x_p - x_q)^2}{l^2}\right] \\
\frac{\partial NLML}{\partial \sigma_f} &= -\frac{1}{2} trace\left[A * 2\sigma_f^2 \exp\left(\frac{(x_p - x_q)^2}{2l^2}\right)\right] \\
\frac{\partial NLML}{\partial \sigma_n} &= -\frac{1}{2} trace[A * 2\sigma_n^2] \\
& \qquad\qquad\qquad\qquad\qquad with \\
A &= \left(\left(L_{xx}^T \backslash \left(L_{xx} \backslash \mathbf{y}\right)\right)\left(L_{xx}^T \backslash \left(L_{xx} \backslash \mathbf{y}\right)\right)^T - K_{XX} I\right)
\end{aligned} \tag{2.8}$$

At the end of the iterative minimisation process, when the difference in likelihood value is smaller than a given tolerance, the obtained hyperparameters are the best ones fitting the covariance function on the **training data** considered. In figure 2.3 is showed and example of regression, where 3 random posterior are inferred on 5 observations with a confidence interval represented in grey.

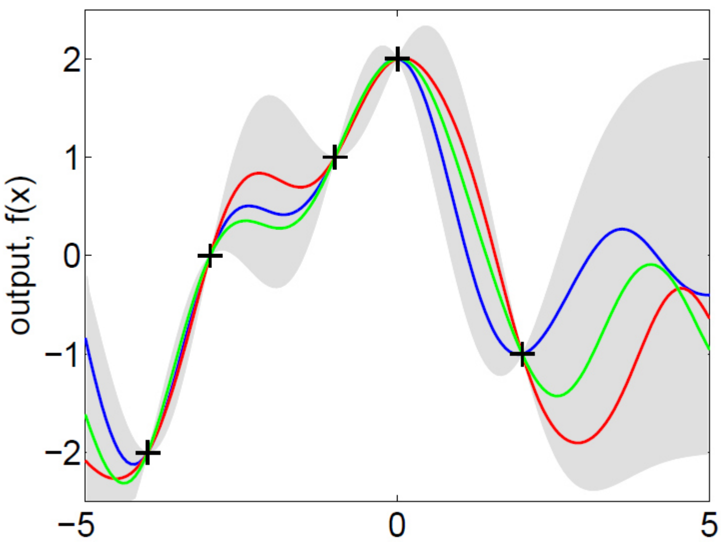

Figure 2.3: Example of Regression **[63]**

2.3 Extreme Function Theory

Extreme Value Statistics (EVS), based on *Extreme Value Theory* (EVT) **[26]**, has been established specifically to handle the values of the independent random variables failing in the tails of the distribution of interest **[13, 32, 44]**. This is particularly interesting in the field of Structural Health Monitoring (SHM). Indeed, most widely used damage detection techniques revolve around outlier detection (see, e.g., **[89]** and **[90]**), which in turn needs, in some sense, a sort of "thresholding" between data taken from damaged and undamaged conditions. This is due to the assumption that some features in the output recorded from the structure in an abnormal situation will be above the so-determined threshold. *Extreme Values Theory* is an ideal statistical framework for evaluating the significance of **extreme values** departing from the normality model and the concept has already been exploited in this sense **[67]**.
It must be remarked that normality, or normal condition, refers here to the pristine state of the structure; Gaussian is used instead to indicate the normal probability distribution function (PDF), to avoid any confusion. Nevertheless, when dealing with extreme deviations from the mean, hypothesising Gaussianity may misguide.
EVT is by definition a point-wise approach, generally applied to univariate data or extended to other low-dimensional spaces. It can be adapted for functional applications adopting the *Extreme Function Theory* (EFT) **[16]** to identify **extreme functions** from a given n-dimensional multivariate Gaussian distribution; in the case proposed here, the functions are the mode shapes of the structure, interpolated from n discrete observations. Hence, defining a single value of PDF (equation 2.5) for each tested function as $\mathbf{z} = f_n(\mathbf{f}^*)$ and taking the Gaussian probability $\mathbf{z}$ in its logarithmic form ($lz = log(\mathbf{z})$) allows a better distinction between the more extreme normal functions (undamaged mode shapes) from the abnormal ones (damaged mode shapes) resulting in a reduction of wrong identifications.

As known form the EVT the Generalised Extreme Value (GEV) distribution for minima (L),

$$L(lz, \mu, \sigma, \gamma) = 1 - exp\left\{ -\left[1 + \gamma\left(\frac{\mu - lz}{\sigma}\right)\right]^{-\frac{1}{\gamma}} \right\} \tag{2.9}$$

where μ, σ, and γ denote, respectively location, scale, and shape of the GEV distribution. The GEV distribution combines ones in a unique model the three feasible limit distributions for the minima values, *Gumbel* (G), *Frechét* (F) and

Weibull (W) (equation 2.10) **[26]**,**[90]**,

$$
\begin{aligned}
GUMBEL: L_G(lz,\lambda,\delta,\beta) = &\quad 1 - exp\left[-exp\left(\frac{lz-\lambda}{\delta}\right)\right] \\
&\qquad with \quad -\infty < lz < +\infty, \quad \delta > 0 \\
FRECHÉT: L_F(lz,\lambda,\delta,\beta) = &\quad \begin{cases} 1 - exp\left[-\left(\frac{\delta}{lz-\lambda}\right)^{\beta}\right] & if \quad lp \leq \lambda \\ 1 & if \quad lz > \lambda \end{cases} \\
WEIBULL: L_W(lz,\lambda,\delta,\beta) = &\quad \begin{cases} 0 & if \quad lz \leq \lambda \\ 1 - exp\left[-\left(\frac{lz-\lambda}{\delta}\right)^{\beta}\right] & if \quad lz > \lambda \end{cases}
\end{aligned}
\tag{2.10}
$$

where the parameters λ, δ and β represent, respectively, the location, the scale and shape of the model distribution. A direct correlation with the parameters of the 3 feasible limit minima distributions is reported in **[55]**,

$$
\begin{aligned}
GUMBEL: &\quad if \quad \gamma \to 0, \quad L_G(lz,\lambda,\delta,\beta) \\
&\qquad \mu = \lambda, \ \ \sigma = \delta \\
WEIBULL: &\quad if \quad \gamma < 0, \quad L_W(lz,\lambda,\delta,\beta) \\
&\qquad \mu = \lambda + \delta, \ \ \sigma = \frac{\delta}{\beta}, \ \ \gamma = -\frac{1}{\beta} \\
FRECHET: &\quad if \quad \gamma > 0, \quad L_F(lz,\lambda,\delta,\beta) \\
&\qquad \mu = \lambda - \delta, \ \ \sigma = \frac{\delta}{\beta}, \ \ \gamma = \frac{1}{\beta}
\end{aligned}
\tag{2.11}
$$

To individuate the anomalous mode shapes that could indicate the presence of a damage in the beam structure, it is necessary to discern them from the mode shapes that fall in a normal range. After reconstructing the CDF it is possible to define a threshold lz_{lim} in correspondence of a given quantile α, in this case set to the lower 1%. For the test data set, a new logarithmic posterior probability lz_{test} is now calculated from equation (2.5) for each tested mode shapes. When a logarithmic probability falls in a quantile $\alpha^{'}$ beyond the defined limit α, the value is recorded as an outlier and the entire mode shape identified as taken from a damaged structure.

2.4 Optimisation Methods

The search of the optimum model solution for a given problem with unknown parameters requires an iterative process where a defined target or *objective function* needs to be maximised (or minimised) to reach the related best function values fitting the input information (equation 2.12). The fundamental paradigm of an optimisation algorithm must ensures, according to **[50]**, three main properties:

- **Robustness**, performing well on a wide variety of problems in their class.
- **Efficiency**, not requiring too much computer time or storage.
- **Accuracy**, able to identify a solution with precision, without being overly sensitive to errors in the data or to the arithmetic rounding errors that occur when the algorithm is implemented on a computer.

Computational issues, instead, limit the theoretical feasible process, imposing a trade-off among convergence rate, storage requirements, robustness and speed. Usually, a further requirement is to find the *global optimum* of the domain among the possible *local optima*, because of the latter implies a lack of knowledge on the problem that misguides the final estimation with strong biases and errors. If the domain is unbounded the optimisation is defined as *unconstrained*; otherwise, if restrictions are imposed on the variables space as scalar or functions, the objective function is evaluated on a specified range of values and the optimisation is called *constrained*. Moreover, to be statically reliable, an optimisation algorithm should prevent *under-* and *over-fitting* (figures 2.4), namely the inadequate or the excessive and wrong adaptability of the model to a given analysed sample of values in fulfilment of the *Occam's razor* principle.

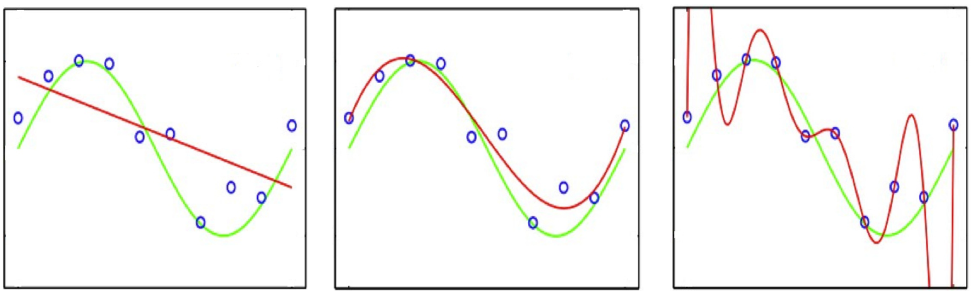

(a) Under-fitting (b) Good fitting (c) Over-fitting

Figure 2.4: Flexibility in fitting of a model

An ulterior distinction depends on the type of used approach in the chose of the model: if it is fully specified and a rule to define the initial condition is assigned it is called *deterministic* (2.4.1), while «...*stochastic* optimisation algorithms (2.4.2) use the quantifications of the uncertainty to produce solutions that optimise the expected performance of the model...»**[50]**.

In mathematical notation the minimisation problem (and analogously the maximization) over an arbitrary real set X of a continuous objective function $f : X \to \mathbb{R}$ is **[36]**:

$$min_{x\in X} \;\; f(x) \tag{2.12}$$

where if $X = \mathbb{R}^n$ the problem is defined unconstrained, otherwise constrained. Operatively, the formulation of the optimisation process can be resumed in the following steps:

- Individuation and definition of variables
- Chose of the solution representation
- Definition of the solution space definition
- Definition of the objective function
- Definition of solution quality measure criteria
- Constraints explication

In the context of this Thesis work, in the next two paragraphs are outlined the working principles of the optimisation algorithms involved in the development of the process.

2.4.1 Gradient Methods

Line-search methods are powerful deterministic algorithms widely used to perform unconstrained optimisation. The basic working principle is the *descent method*, which is the search for the faster direction p_k that ensures a decrease of the objective function f. The problem formulation is restated as,

$$x_{k+1} = x_k + \alpha_k p_k \tag{2.13}$$

where the positive scalar α is called the *step length*. The simplest application is the *Steepest Descent* (SD) which performs minimisation in the direction of the negative gradient, but it is often inefficient because the orthogonality of searching directions does not ensure the fastest convergence. To overcome this limit an **inexact line search** is required in order to iteratively estimate the best step length and the resulting more rapid descend search direction. The *Conjugate Gradient Optimisation* (CGO), introduced by **[35]** in the linear formulation and modified for non-linear problems by **[27]**, is one of the most used algorithm based on the adaptive line search strategy because it approximates quadratically the estimation without requiring Hessian matrix evaluations or large storage and computational effort in matrix inversion (figure 2.5). Line search starts by choosing as initial guess the steepest descent direction p_k and an appropriate step length α_k is now calculated as

$$\alpha_{k+1} = \quad min \; f(x_k + \alpha_k p_k) \tag{2.14}$$

The new search direction is evaluated by combining the steepest descent g_i direction at the new iterate of equation 2.13

$$g_i = \nabla f(x_{k+1}) \tag{2.15}$$

with the previous search direction expressed as,

$$p_{k+1} = -g_i + \beta p_k \tag{2.16}$$

where β is a real scalar value depending on the gradient g_i defined according different formulations, such as the Fletcher-Reeves or Polak-Ribière-Polyak conditions. The variation of the step length α, instead, is subjected to the Wolfe-Armijo or Wolfe-Powell conditions. Finally, the iterative loop ends returning the global minima estimated with a given approximation **[50]**.

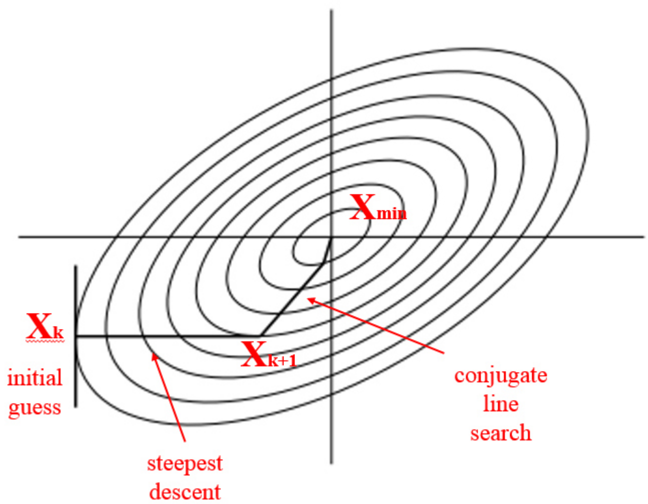

Figure 2.5: Conjugate Gradient Optimisation scheme

2.4.2 Genetic Algorithms

Genetic Algorithms (GA) are random heuristic optimisation method based on the evolution process of DNA structure, where the optima estimations are reached through a phase of *intensification* in which the solution is locally perturbed to fast look for the best fitting and a phase of *diversification* in which a greater part of solution is changed to avoid local minima. Generally, according to **[30]**, GA present the following properties:

- works with a coding of the parameters set
- searches from a populations of points
- uses objective function instead of gradient
- uses probabilistic rules
- has memory of previous search results

In the paradigm introduced by **[76]** for *Differential Evolution* (DE) algorithm, an initial random population of n individuals is encoded in a chromosome structure, where each individual represents a gene of the genetic heritage to propagate during the **reproduction** phase. The reproduction probability to transmit the favourable or disadvantageous attributes depends on the fitting cost to minimise that each case have when matched with the objective function. A *child* chromosome is created starting from two random selected parents vectors of the population: to avoid any bias the child vector is processed through a **mutation** phase (intensification) in which it is scaled and perturbed in order to obtain an new element. A successive **cross-over** step (diversification) combines the child vector with an independent one to obtain the *trial* vector of parameters used to fit the objective function. On the basis of the Mean Squared Error (MSE) of fitting cost the gene would be transmitted or not to the next population by a binomial matching. A schematic overview of the algorithms is showed in figure 2.6. Simply repeating the process different times, genetic algorithms of DE type enhance robustness in the estimation while avoiding local minima, without requiring any a-priori knowledge on the defined range of parameters. The self-adaptive (SADE) modified version of the genetic differential algorithm proposed by **[59]** has been applied to perform fitting, where the adaptive feature of the optimisation does not require the specification of the initial parameters, such as the scaling factor or the crossover ratio that are iteratively estimated.

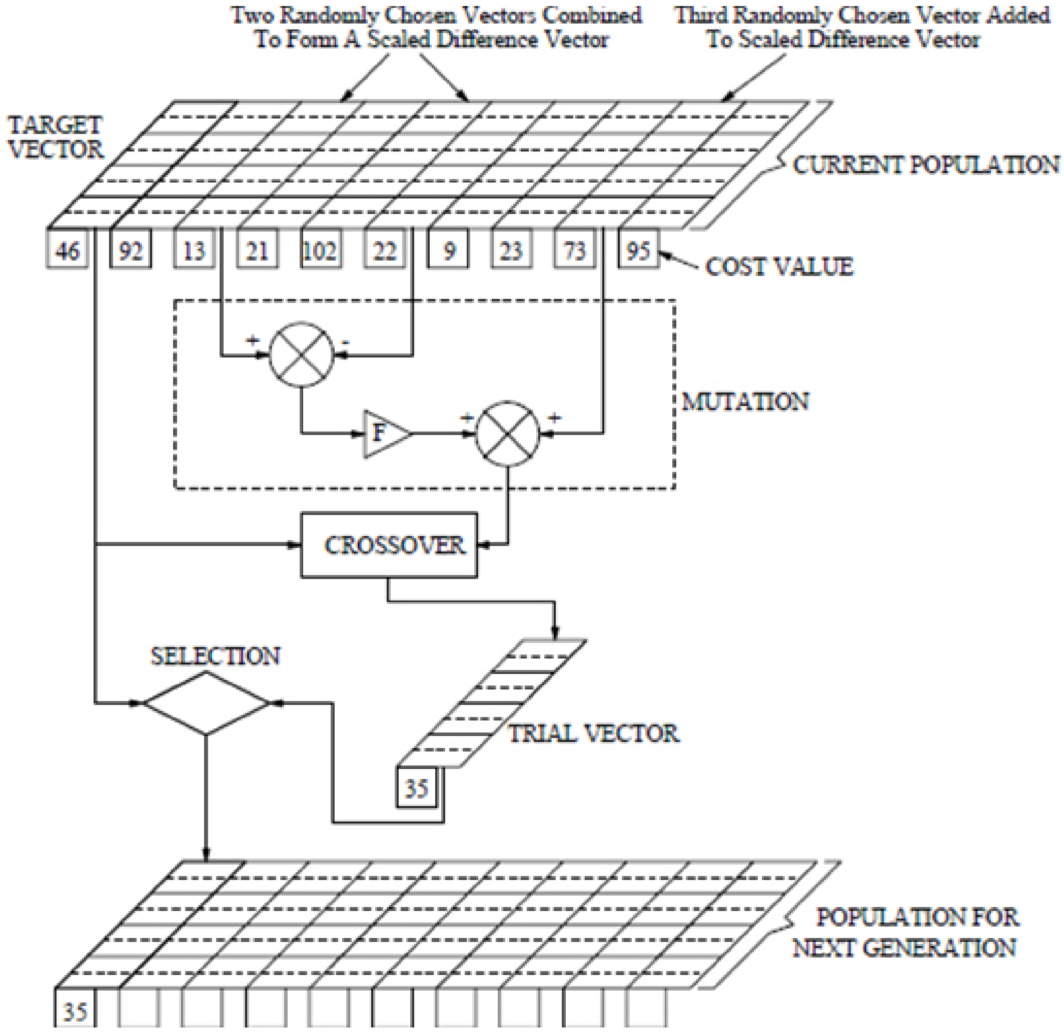

Figure 2.6: Flow chart of Differential Evolution Genetic Algorithm **[90]**

Chapter 3

Beam Elastic Model

3.1 Introduction

The model of a beam-like structure, with one main longitudinal dimension along the beam axis, is often adopted as reference model for more complex analysis because it is simple to describe directly its behaviour. In the simulations considered in the next chapters the interest is focused on evaluating the displacements of a vibrating cantilever beam in the undamaged and damaged states, with the main assumption of linearity in both of them. These assumptions of linearity present obvious advantages in mathematical dissertation although the model remains still capable to approximate in an effective way the structural behaviour in most of the practical cases: common materials such as steel, concrete or reinforced concrete can be modelled as linear or can be linearised to equivalent sections since their global properties can be assumed as elastic, homogeneous and isotropic.

The sections below present a review of some theoretical aspects regarding the deformation process of a deformable elastic beam modelled according to the mono-dimensional Euler-Bernoulli theory in the static and dynamic configurations. The further implementation in MatLab® of the undamaged and the damaged models is formulated using the Finite Element Methods (FEM), a numerical and computational method widely used to approximate continuous problems, so also a review of this calculus approach is given, focusing on the aspects applied to the related analysis.

3.2 Static Deflection of Continuous Beam

A general description of the deflection behaviour of a beam was given by Timoshenko **[78]** taking into account the effects of shear, particularly relevant when dealing with thick beams, where rotational inertia contributes significantly with the rigidity of the beam. Although formulated some centuries before, the classical **Euler-Bernoulli** beam theory represents a particular and simplified case of the Timoshenko's one and its validity holds under certain main restrictions. The two fundamentals hypothesis are :

- Conservation of plane sections - The cross sections of the beam in the undeformed state are plane and remain plane during the deformation process and thus, the centroidal axis is a longitudinal symmetry axis.
- Orthonormality - The plane cross sections originally orthogonal to the centroidal axis remain orthogonal to the deformed centroidal axis during the deformation process, implying the isotropy property.

From the previous kinematic hypotheses follows that the shear strains are null and consequently the shear stresses as well (beam infinitely rigid in shear). This condition suites only with the behaviour of slender beams where the order of thickness is smaller than the length one and the contributes of shear strain and rotational inertia can be ignored if compared with the effects of bending **[5]**. Furthermore, other simplifying hypotheses are made in the analysis:

- All the displacements are considered small and they can be evaluated with a first order approximation.
- The equilibrium of the structure is considered in an undeformed state.
- The constitutive behaviour of the structure is linear elastic.
- The Poisson's effect is neglected.
- The longitudinal axis of the beam is straight.
- The cross section A is prismatic (rectangular) and remains constant along the span.
- The mass distribution remains constant along the span (constant volumetric density ρ).

The linearisation of the describing equations of the elastic equilibrium due to the assumption of small displacements and the linear elastic behaviour have the main consequence of the applicability of the *principle of superposition of* *effects*. The global solution can obtained summing the solutions of the single response for a given action and the use of all linear operators is allowed. This last property will results relevant in next chapters when the simulated data will be processed as Gaussian distributed. In spite of this, the assumed linearity issues some limitations such as in the case of non-linear constitutive behaviour or when geometric non-linearities are present.

Considering an infinitesimal element of a beam subjected to simple bending (figure 3.2), thus to bending moment M_z and shear force V_y, and ignoring the displacements in lateral direction z caused by the Poisson's effect, the displacements field

$$\{u\} = \{ \begin{matrix} u & v & \varphi_x \end{matrix} \}^T \tag{3.1}$$

is determined by 2 independent displacement components $u(x,y)$ $v(x,y)$ and the related rotation $\varphi_x = \varphi(x)$. The hypothesis of plane section normal to the longitudinal axis implies big curvature radius r and consequently small curvature κ, while considering only transverse forces the uncoupled axial displacement $u(x)$ results null. The elementary rotation (figure 3.1) can be expressed as:

$$\varphi(x) \approx tan\left(\varphi_x\right) = \frac{dv}{dx} \tag{3.2}$$

with the approximation of the tangent based on the small displacements assumption. Consequently, the curvature is:

$$\kappa = \frac{1}{r} = \frac{d\varphi_x}{dx} \tag{3.3}$$

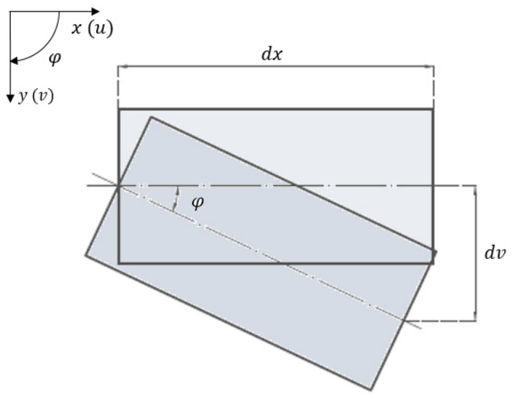

Figure 3.1: Elementary rotation of an infinitesimal element

Since axial translation and shear deformation are neglected, the increment of transverse displacement due to bending moment is:

$$dv = \varphi_x dx \tag{3.4}$$

and thus, the relation between the transverse displacement and the curvature is represented by the second order derivative:

$$\kappa = \frac{d^2 v}{dx^2} \tag{3.5}$$

The stress-strain *De Saint-Venant* relations allow to express the curvature in function of the bending moment M_z for an arbitrary material point distant y from the centroidal axis and for a given section A. Defining:

- from the kinematic relations, the longitudinal elastic axial strain ε_x

$$\varepsilon_x = \frac{\partial u}{\partial x} = -y\frac{d\varphi_x}{dx} = -y\frac{d^2 v}{dx^2} \tag{3.6}$$

- from the Hooke's constitutive relations, the corresponding elastic axial stress σ_x

$$\sigma_x = E\varepsilon_x = -Ey\frac{d^2 v}{dx^2} \tag{3.7}$$

- the moment of inertia I_z, or rather the second moment of area A along the z-axis

$$I_z = \int_A y^2 dA \tag{3.8}$$

and combining the previous equations 3.6, 3.7, 3.8 with the *De Saint-Venant* formulation of the characteristic external forces, the resulting in-plane bending moment M_z **[78]** is expressed as

$$M_z = \int_A \sigma_x y dA = -EI_z\frac{d^2 v}{dx^2} = EI_z\kappa(x) \tag{3.9}$$

where the product EI_z is the *flexural rigidity*. This differential expression 3.9 is the **equation of linear elasticity** and represents the governing equation for the inflected beam in function of the bending moment M_z. Alternatively, it is possible to formulate the differential equation 3.9 taking in consideration directly the applied orthogonal external load instead of the end forces. Expressing the shear V_y as the variation along the x-axis of the bending moment M_z

$$\frac{dM_z}{dx} + V_y = 0 \tag{3.10}$$

The equilibrium of the infinitesimal beam element subjected to a transverse distributed load $p(x)$ represented in figure 3.2 resulting from equation 3.10 is:

$$\frac{d^2 M_z}{dx^2} = -p(x) \tag{3.11}$$

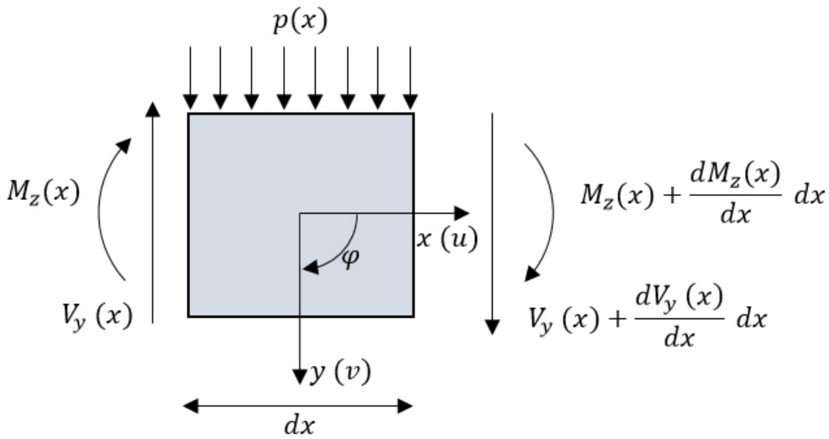

Figure 3.2: Equilibrium of the infinitesimal beam element

Thus, the governing equation of linear elasticity can be rewritten as a differential equation of the fourth order (the second member is valid for a constant elastic modulus and constant cross section):

$$\frac{d^2}{dx^2}\left(EI_z\frac{d^2 v}{dx^2}\right) = EI_z\frac{d^4 v}{dx^4} = p(x) \tag{3.12}$$

With a null external load $p(x) = 0$, the general **exact solution** for the transverse displacement is a third order polynomial in the form:

$$v(x) = \frac{ax^3}{6} + \frac{bx^2}{2} + cx + d \tag{3.13}$$

and can be solved in closed form by finding the 4 integration constants with the definition of 4 Dirichlet's boundary conditions, with the sign convention of figure 3.3:

$$\begin{gathered} v(0) = v_1 \\ v(l) = v_2 \\ \left.\frac{dv}{dx}\right|_{x=0} = \varphi_1 \\ \left.\frac{dv}{dx}\right|_{x=l} = \varphi_2 \end{gathered} \tag{3.14}$$

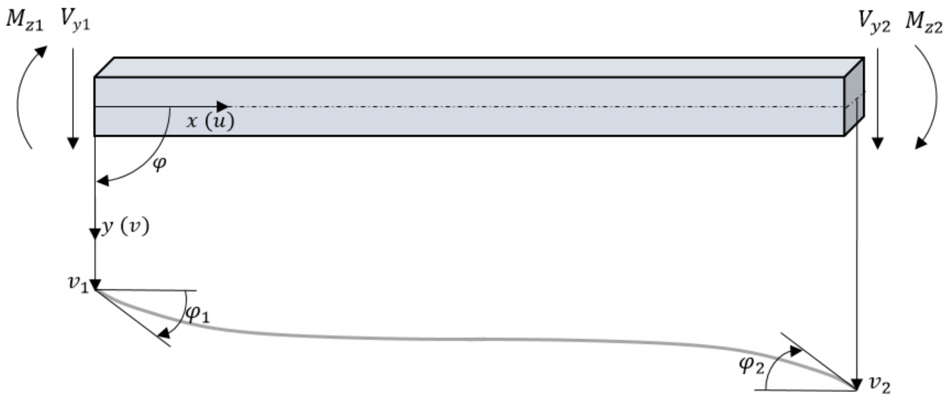

Figure 3.3: Sign convention for the Euler beam element

The final expression of the differential equation 3.13 after the determination of the constants gives the expression of the transverse displacement for a beam subjected to a translation in node 1 v_1, null transverse displacement v_2 in node 2 and zero rotations φ_1, φ_2 in node 1 and in node 2:

$$v(x) = \left[1 - 3\left(\frac{3x^2}{l^2}\right) + 2\left(\frac{x^3}{l^3}\right)\right] v_1 \tag{3.15}$$

Solving the equation 3.12 in an analogous way for the other cases (all the transverse displacements and rotations), the displacements field is fully determined and consequently, from the principle of strength of materials, it is possible to evaluate the element end member forces vector $\{P^e\}$:

$$\{P^e\} = \{\ V_{y1} \quad M_{z1} \quad V_{y2} \quad M_{z2}\ \}^T \tag{3.16}$$

This yields to the definition of the **elastic stiffness matrix in local coordinate system $\mathbf{K^e}$**, in which each column represents the response due to the uncoupled action of transverse displacement v_1, rotation φ_1, applied in node 1, and displacement v_2, rotation φ_2 applied in node 2, respectively :

$$\begin{Bmatrix} V_{y1} \\ M_{z1} \\ V_{y2} \\ M_{z2} \end{Bmatrix} = \begin{bmatrix} \frac{12EI_z}{l^3} & \frac{6EI_z}{l^2} & -\frac{12EI_z}{l^3} & \frac{6EI_z}{l^2} \\ & \frac{4EI_z}{l} & -\frac{6EI_z}{l^2} & \frac{2EI_z}{l} \\ & \textbf{Sym} & \frac{12EI_z}{l^3} & -\frac{6EI_z}{l^2} \\ & & & \frac{4EI_z}{l} \end{bmatrix} \begin{Bmatrix} v_1 \\ \varphi_1 \\ v_2 \\ \varphi_2 \end{Bmatrix} \tag{3.17}$$

Or rewritten in compact matrix notation:

$$\{P^e\} = [K^e]\{u\} \tag{3.18}$$

3.3 Undamped Free Vibrations of Continuous Beam

The dynamic analysis of the continuous beam is based on the mono dimensional wave theory formulated by D'Alembert, in which is expressed the dependency of wave propagation on space and time. Also in this case, a more general solution comprehensive of the effects of rotational inertia and longitudinal forces is obtained from the Rayleigh **[66]** and Timoshenko **[77]** theories and a comparison among the different models can be found in **[33]**. Instead, holding all the hypotheses assumed in the previous section 3.2, the free flexural (small) vibrations for the particular case of the Euler-Bernoulli can be described taking into account the effects of **transverse inertial forces**, in the form:

$$p^I(x,t) = -\rho A \frac{d^2 v}{dt^2} \tag{3.19}$$

A main simplification respect to the real behaviour of structure is not considering the viscous damping among the internal forces. The element, in fact, is considered purely elastic and consequently its response is conservative. This assumptions holds the linearity property of elastic solids, that as told before, is basic for the further elaboration of vibrations as Gaussian process. The transverse displacement of a vibrating beam due only to inertial forces are expressed rewriting the equation of linear elasticity 3.12 as:

$$\frac{d^4 v}{dx^4} = -\frac{\rho A}{EI_z} \frac{d^2 v}{dt^2} \tag{3.20}$$

The previous equation is a partial differential equation with separable variables and the solution can be obtained by applying the Fourier method:

$$v(x,t) = \phi(x) f(t) \tag{3.21}$$

hence the equation of motion 3.20 results:

$$\frac{d^4\phi(x)}{dx^4} f(t) + \frac{EI_z}{\rho A}\phi(x)\frac{d^4 f(t)}{dt^2} = 0 \tag{3.22}$$

which can be separated in two uncoupled ordinary differential equations (ODE):

$$\begin{aligned} \frac{d^2 f(t)}{dt^2} + \omega^2 f(t) = 0 \\ \frac{d^4\phi(x)}{dx^4} - \frac{\rho A\omega^2}{EI_z}\phi(x) = 0 \end{aligned} \tag{3.23}$$

The first of 3.23 depends only on time variable and is a second order linear homogeneous ODE, which has the characteristic equation in the form:

$$\ddot{y} + \omega^2 = 0 \tag{3.24}$$

and hence admits the different characteristics roots:

$$y = \pm i\omega \tag{3.25}$$

that give the general solution:

$$f(t) = C_1 e^{i\omega t} + C_2 e^{-i\omega t} \tag{3.26}$$

or rewriting it using the Euler-Cotes relation the previous equation becomes:

$$f(t) = A\sin(\omega t) + B\cos(\omega t) \tag{3.27}$$

that is the equation of motion of the **elementary harmonic oscillator** with undamped free-vibrations, where the constant ω has the physical meaning of the angular frequency of the system, related to the period T of 1 cycle of the system:

$$\omega = \frac{2\pi}{T} \tag{3.28}$$

The particular solution of 3.27 depends on the coefficients A and B that can be determined by imposing the Cauchy boundary conditions, such as the initial position f_0 and initial velocity $\dot{f}_0$ at $t = 0$, while the frequency ω depends on the Dirichlet's boundary conditions defined by the imposed restraints. Since ω is also the eigenvalue of the problem and the structure is in this case studied as a continuous system, there will be an infinite number of eigenfunctions $f_i(t)$ and related eigenfrequencies ω_i, one for each of the infinite degree of freedom, also called **natural frequencies**. In correspondence of these values, indeed, as the evaluated roots of the differential equation are not identical, the solution presents mathematical **resonance** traduced physically with an amplification of the motion of the system subjected to a periodical external excitation force acting at a nearly frequency. The first natural frequency is defined *fundamental* because all the other natural frequencies are proportional to this one (eq. 3.29):

$$\omega_i = (k_i l)^2 \sqrt{\frac{\rho A}{E I_z l^4}} \tag{3.29}$$

where l s the length of the element, and it is related to the less rigid vibrational configuration of the system, which consequently presents the largest displacements. The constant k_i, that corresponds also to the multiplying factor

$(\rho A\omega^2)\cdot(EI_z)^{-1}$ in the second equation of 3.23, is called **wavenumber k** and depends on the geometry and on the boundary conditions of the structure. This can be explicated in function of ω through the *dispersion relation*:

$$k^4 = \frac{\omega^2 \rho A}{EI_z} \tag{3.30}$$

Thus, the eigenfunction $\phi(x)$ depends only on space variable and can be solved as a fourth order homogeneous equation, with characteristic equation:

$$y^{IV} - k^4 = 0 \tag{3.31}$$

and the four different characteristics roots:

$$y = \pm k;\ \pm ik \tag{3.32}$$

leading to the general solution:

$$\phi(x) = C_3 e^{kx} + C_4 e^{ikx} + C_5 e^{-kx} + C_6 e^{-ikx} \tag{3.33}$$

or in the alternative Euler-Cotes formulation **[80]**:

$$\begin{aligned}\phi(x) = \beta_1\,[\cos(kx) + \cosh(kx)] + \beta_2\,[\cos(kx) - \cosh(kx)] + \\ +\beta_3\,[\sin(kx) + \sinh(kx)] + \beta_4\,[\sin(kx) - \sinh(kx)]\end{aligned} \tag{3.34}$$

that for the arbitrariness of constants β_i yields to:

$$\phi(x) = C\sin(kx) + D\cos(kx) + E\sinh(kx) + F\cosh(kx) \tag{3.35}$$

where the constants depend on the Dirichlet's boundary conditions defined by the imposed restraints. Similarly to the time case, the system considered continuous is described by an infinite number of eigenfunctions $\phi_i(x)$, one for each of the infinite degree of freedom, and the generic structural deformation $v(x,t)$ is the results of a linear combination of all these vibrational functions (with a more relevant influence coefficient for the first lower shapes). Otherwise, the previous statement implies that each **natural mode shape** is linearly independent and can not be obtained from a linear combination of other modes. Indeed, the eigenfunctions $\phi_i(x)$ present the mathematical property of orthogonality respect to the mass and to the stiffness of the structural element assumed of length l:

$$\int_0^l \phi_i \phi_j \, dx = 0, \qquad if \quad i \neq j \tag{3.36}$$

This relevant characteristic is widely used in several aspects of modes shape functions analysis, as the decoupling of equations of motion in space and time or modal analysis. Moreover, it is used to normalize the mode shapes to the maximum displacement (taken equal to 1) or to normalize with regard to the mass distribution (taken unitary) related to each degree of freedom considered (principal components). Finally, a general expression of the harmonic motion for the natural modes of vibrations taking into account equation 3.21 can be given in the form:

$$v(x,t) = \sum_{i=1}^{\infty} \phi_i(x) \cdot [A_i cos(\omega_i t) + B_i \sin(\omega_i t)] \tag{3.37}$$

The constants A_i and B_i are defined through the imposition of the initial conditions, showing the dependence of the free vibration on the initial displacement and the initial velocity. For each i^{th} mode it is possible to identify an increasing (finite) number of points of maximum deflection, called **nodes**, and points with null displacement, called **antinodes**.

3.4 Transverse Vibration of a Continuous Cantilever Beam

For simple boundary conditions setup it is possible to analytically evaluate the component functions of the equation of motion 3.37, obtaining the related space and time varying eigenvectors. Instead, for more complex systems, it is definitely more convenient in terms of computational effort to use a numerical approach. In this case, the focus is on the cantilever beam configuration and the analytic solution is presented below, while a Finite Element approach will be presented in section 4.1. For the fixed-free beam of length l in figure 3.4 the clamp restraint implies null displacement and null rotations in $x = 0$, while the free end at $x = l$ has unconstrained vibrations and thus null shear and null bending moment (eq. 3.38). The 4 Dirichlet's boundary conditions apply to the eigenfunctions $\phi(x)$ (eq. 3.35)

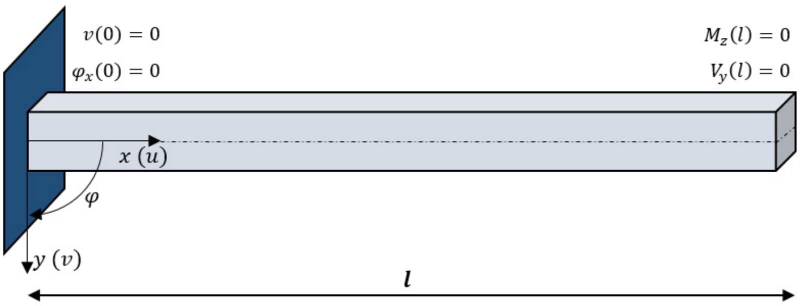

Figure 3.4: Boundary conditions of a cantilever beam

$$\begin{aligned} v(0,t) = \quad & \phi(0) && = 0 \\ \left.\frac{dv}{dx}\right|_{x=0} = \ \varphi_x(0,t) = \ & \left.\frac{d\phi}{dx}\right|_{x=0} && = 0 \\ \left.\frac{d^2v}{dx^2}\right|_{x=l} = M_z(l,t) = \ & \left.\frac{d^2\phi}{dx^2}\right|_{x=l} && = 0 \\ \left.\frac{d^3v}{dx^3}\right|_{x=l} = \ V_y(l,t) = \ & \left.\frac{d^3\phi}{dx^3}\right|_{x=l} && = 0 \end{aligned} \tag{3.38}$$

And thus, results a system of 4 unknowns constants:

$$\begin{bmatrix} 0 & 1 & 0 & 1 \\ 1 & 0 & 1 & 0 \\ -\sin(k_i l) & -\cos(k_i l) & \sinh(k_i l) & \cosh(k_i l) \\ -\cos(k_i l) & \sin(k_i l) & \cosh(k_i l) & \sinh(k_i l) \end{bmatrix} \begin{bmatrix} C \\ D \\ E \\ F \end{bmatrix} = \begin{bmatrix} 0 \\ 0 \\ 0 \\ 0 \end{bmatrix} \tag{3.39}$$

The trivial solution with the determinant not null is not admitted here since it corresponds to the free body rigid motion. Thus the non-trivial solution, with the null determinant, gives the transcendent spectrum equation of all possible frequencies:

$$\cos(k_i l) - \cosh(k_i l) + 1 = 0 \tag{3.40}$$

which yields to the characteristic equation **[80]**:

$$\phi_i(x) = \cosh(k_i x) - \cos(k_i x) - \frac{\cos(k_i l) + \cosh(k_i l)}{\sin(k_i l) + \sinh(k_i l} [\sinh(k_i x) - \sin(k_i x)] \tag{3.41}$$

The characteristic vibration is in the form of equation 3.37, where the constant A_i and B_i depend on the initial conditions at $t = 0$ and are determined using the orthogonality property, resulting:

$$\begin{aligned} A_i &= \frac{2}{l} \int_0^l v(x,0) \phi_i(x) dx \\ B_i &= \frac{2}{l\omega_i} \int_0^l \frac{dv(x,0)}{dt} \phi_i(x) dx \end{aligned} \tag{3.42}$$

Solving numerically equation 3.40, the roots $k_i l$ allow to evaluate the correspondent eigenfrequencies ω_i (eq. 3.29) and the beam vibration in space and time through equations 3.41, 3.42 and 3.37. In the figure 3.5 below, the first 5 solutions for the cantilever beam and related mode shapes are presented, with the positions of the *i nodes* and *i antinodes* for each i^{th} mode.

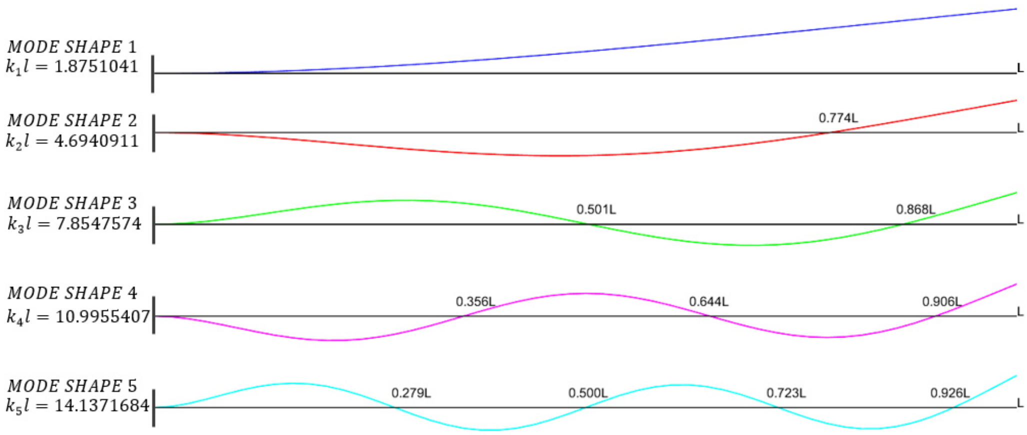

Figure 3.5: First 5 roots and mode shapes for a cantilever beam **[80]**.

3.5 Undamped Free Vibration of Discrete Beam

As introduced before in previous section 3.4, the analytic solution of the dynamic vibrational problem is hardly obtainable for geometrical heterogeneous structure setup since the resolution of the equation of motion 3.37 increases considerably and may require a consistent computational effort. To overcome this problem, in practice the real continuous elements characterized by an infinite number of degrees of freedom (one of each material point) can be considered as **discrete** and the description of the continuous geometry is reduced to a N finite number punctual masses. The Finite Element Analysis discussed more in detail in section 4.1 is one common example of numerical discretization method: splitting the problem in an adequate N finite number of smaller subsets the governing differential equations describing the physical behaviour can be approximated to algebraic equations with an accuracy in the **approximation** related to the number of elements involved (**mesh**). This aspects is of fundamental relevance for automatic calculus, since the computer are basically able to operate with addiction and subtraction, resulting in easier and faster implementation. Moreover, the dynamic problem considered so far has been assumed linear and this enhance the use of the *principle of superposition of effects*: the multiple degrees of freedom system (MDOF) can be studied as the sum of N decoupled responses of each oscillating mass (single degree of freedom (SDOF)).

There are various ways to formulate the discrete mechanical dynamic problem like through the application of the *Virtual Work Principle*, the *Lagrangian equations* or the *Principle of D'Alembert.* On the same line of section 3.3 this last alternative is chosen, which actually consist in an extension of the Virtual Work Principle. According to the D'Alembert Theorem formulation:

The motion of a vibrating mechanical system can be considered in each moment t as a static equilibrium of all the time dependent internal $p^{int}(t)$ and external $p^{ext}(t)$ acting forces and the inertial forces $p^I(t)$.

$$\sum \left[p^{int}(t) + p^{ext}(t) + p^I(t) \right] = 0 \quad , \forall t \geq 0 \tag{3.43}$$

Consider the i^{th} general structural element of mass m_i represented in figure 3.6, where k_i is the stiffness of the spring, c_i is the viscous coefficient of the dashpot, $p_i(t)$ is the time dependent force of volume, $u_i(t) = u_i$ is the time dependent displacement, $\dot{u}_i$ and $\ddot{u}_i$ are respectively the velocity and the acceleration and e_j is the generic versor.

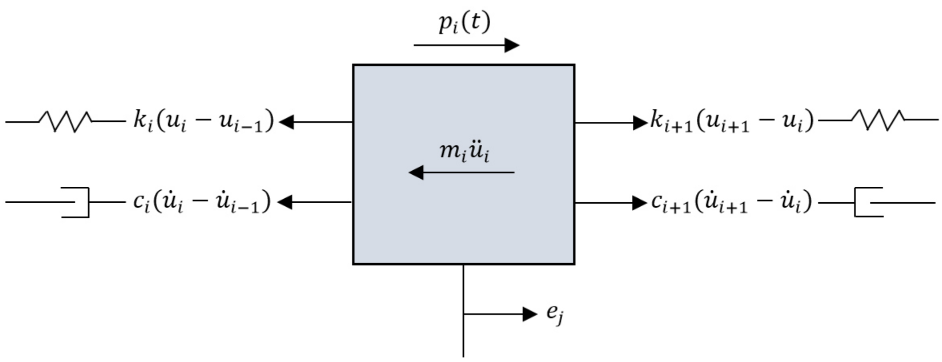

Figure 3.6: Dynamic equilibrium of the i^{th} interconnected element with elastic springs and viscous dampers **[56]**.

The internal forces $p_i^{int}(t)$ are divided in two classes: the *conservative* force due to elastic spring $p_i^{EL} = k_i u_i(t)$ dependent on the displacement and the *non-conservative* force due to viscous damper $p_i^{NC} = c_i \dot{u}_i(t)$ dependent on the velocity. The external forces $p_i^{ext}(t)$, instead, can act punctually, on surface or on the entire volume of the element, but in this case only the last force $p_i(t)$ is considered. The fictitious inertial force is defined as the product between the mass and the acceleration $p_i^I = m_i \ddot{u}_i$. The equilibrium of equation 3.43 becomes:

$$\sum_{i=1}^{N} \left[p_i^{EL}(t) + p_i^{NC}(t) + p_i^I(t) \right] = \sum_{i=1}^{N} \left[p_i(t) \right] \tag{3.44}$$

that can be rewritten as **[56]**:

$$\begin{aligned} \sum_{i=1}^{N} \big[m_i \ddot{u}_i(t) e_j - c_i \dot{u}(t)_{i-1} e_j + (c_i + c_{i+1}) \dot{u}_i(t) e_j - c_{i+1} \dot{u_{i+1}}(t) e_j + \\ - k_i u_{i-1}(t) e_j + (k_i + k_{i+1}) u_i(t) e_j - k_{i+1} u_{i+1}(t) e_j - p_i(t) \big] = 0 \end{aligned} \tag{3.45}$$

and in compact matrix notation, avoiding to report the time dependence is:

$$[M]\{\ddot{u}\} + [C]\{\dot{u}\} + [K]\{u\} = \left\{p\right\} \tag{3.46}$$

where all the matrices are of **dimension N × N**. When the structure is assumed linear with constant $[M]$ and $[K]$, the damping is neglected $[C] = 0$ and the in absence of external forces$\left\{p\right\}$, the equation 3.46 describes the undamped free-vibrations:

$$[M]\{\ddot{u}\} + [K]\{u\} = \{0\} \tag{3.47}$$

The mass matrix [M] is real, diagonal (symmetric) and positive defined for obvious physical reasons. The stiffness matrix, instead, is real, tridiagonal (symmetric) and non-negative defined, because is not necessary that the system is bounded and a null value corresponds to a rigid motion of the degree of freedom. These attributed properties have the physical meaning of proportional relations between the stiffness matrix and the elastic energy and between the mass matrix and the kinetic energy of the considered body. Thus, the coefficients of each matrix represent respectively the mass and the stiffness influence on the motion for each element with regard to the related degree of freedom. Similarly to the continuous case of equation 3.21, the motion can be expressed as the product of two vectors:

$$u(t) = \sum_{i=1}^{N} \phi_i f_i(t) \tag{3.48}$$

where the vector $\{\phi\}$ is a constant vector of displacements and $\{f\}(t)$ is the harmonic scalar time varying vector expressed as:

$$f_i = A_i \sin(\omega_i t - \alpha) \tag{3.49}$$

in which A_i are the amplitudes and α the phase of the oscillations dependent on the initial conditions. The **harmonic solution** means that all the degrees of freedom move in phase, reaching the zero and the max amplitude at the same instant (synchronous motion). Introducing equation 3.49 in equation 3.47 and pre-multiplying for $\{\phi\}^T$:

$$\{\phi\}^T[M]\{\phi\}\{\ddot{f}\} + \{\phi\}^T[K]\{\phi\}\{f\} = \{0\} \tag{3.50}$$

Splitting the scalar products analogously to continuous equation 3.23 the 2 left members result equal to a non negative constant vector $\{\omega\}$:

$$\frac{\{\ddot{f}\}}{\{f\}} = -\frac{\{\phi\}^T[K]\{\phi\}}{\{\phi\}^T[M]\{\phi\}} = -\{\omega^2\} \tag{3.51}$$

Leading to the differential homogeneous equation in the form:

$$\ddot{f} + \omega^2 f = 0 \tag{3.52}$$

From the previous equation results the governing system of linear algebraic equations:

$$\left(-\omega^2[M] + [K]\right)\{\phi\} = \{0\} \tag{3.53}$$

That represents a linear algebraic eigenproblem in the canonical form:

$$[K]\{\phi\} = \omega^2[M]\{\phi\} \tag{3.54}$$

The trivial solution $\{\phi\} = 0$ correspond to a system in its state of rest, while the non trivial solution is obtained only if the determinant is null and implies the linear independence of the equations 3.53:

$$\det\left(-\omega^2[M] + [K]\right) = 0 \tag{3.55}$$

Which is the polynomial characteristic equation of order N and so admits N **eigenfrequencies** ω_i (square roots of the N roots of the polynomial) that for the properties of the matrices involved enunciated before are real and non-negative eigenvalues. Relevant is that the eigenfrequencies are also the square root of the ratio between the stiffness and the mass of the i^{th} element:

$$\omega_i = \sqrt{\frac{K_i}{M_i}} \tag{3.56}$$

At each of these solutions corresponds one of the N **eigenvectors** ϕ_i that express the geometrical **natural mode shapes** of vibration of the system and, being defined trough the ratio of equation 3.51, are uniquely associated to the correspondent eigenvalue except for an arbitrary constant non-zero scale factor. Moreover, the eigenvectors are orthogonal respect to the mass and stiffness matrices. For two different mode shapes $\{\phi\}_p$ and $\{\phi\}_q$ holds:

$$\begin{aligned} \{\phi\}_p^T[M]\{\phi\}_q = 0 \qquad & if \\ \{\phi\}_p^T[K]\{\phi\}_q = 0 \qquad & p \neq q \end{aligned} \tag{3.57}$$

In order to have comparable values of the mode shapes (since they are defined with the exception of the arbitrary constant) it is usual to normalize them. Two of the more common **normalisation** procedures are the *unitary scaling*, dividing each value for the largest absolute component of the mode itself, or using the orthogonal condition 3.57 to the *unitary mass* obtaining:

$$\begin{aligned} \{\phi\}^T[M]\{\phi\} = [I] \\ \{\phi\}^T[K]\{\phi\} = [\Lambda] \end{aligned} \tag{3.58}$$

where $[I]$ is the identity matrix and $[\Lambda] = diag(\omega_i^2)$.

Chapter 4

Finite Element Analysis

4.1 Finite Element Method

Instead of using the exact solution of the continuous static (3.12) and dynamic (3.22) equations, the *Finite Element Method* (FEM) is a discrete method based on an approximated formulation that evaluates the displacements of a countable number of points called **nodes** and connects them interpolating with appropriate functions. Thus, all the components of the structural model, such as the geometrical description, the mathematical governing laws, the materials' properties and the acting loads have to be formulated in their discrete forms and the precision of the results depend on the density of elements employed to describe the model (**mesh**). Obviously, the finite elements used have same spatial dimensions of the analysed system: a beam is split in linear segments, a surface is generally modelled with two-dimensional elements such as triangles and rectangles, continuous volumes are described through cubic elements. All the assumed approximations are held by *Virtual Work Principle* (VWP):

Considering a statically admissible system of external forces (volumetric forces $\{P_A\}$ and surface forces $\{s_A\}$) and internal stresses $\{\sigma_A\}$) and a kinematically admissible system of strains $\{\varepsilon_B\}$ and displacements $\{\delta u_B\}$, a necessary and sufficient condition for the equilibrium is that, for any given (virtual) displacement field δu, the virtual work δW_{ext} of external loads of system A applied to the displacements of system B is equal to the internal work δW_{int} of internal stresses of system A applied to the strains of system B (eq. 4.1).

$$\begin{gathered}\delta W_{int} = \delta W_{ext} \\ \int_\Omega \{\sigma_A\}^T \{\varepsilon_B\} d\Omega = \int_\Omega \{P_A\}^T \{\delta u_B\} d\Omega + \int_\Gamma \{s_A\}^T \{\delta u_B\} d\Gamma\end{gathered} \tag{4.1}$$

The previous expression is called *"weak formulation"* because is obtained by partial integration through the application of the extended *Green's Theorem*. Moreover, the VWP is directly related with the *Principle of D'Alembert* and has a general validity independently of the constitutive law of the material: actually, the FEM can be applied to a large variety of physical problems, making of this method a powerful analysis tool to solve, i.e., variational problems or equations that do not present a closed analytic solution. The interpolation functions for nodal displacements, also referred to as **shape functions**, are often polynomials where their degree is determined by the number of d.o.f and their accuracy depend on the number of interpolation points. For example, splitting the element with two internal nodes (figure 4.1) and using the cubic polynomial results:

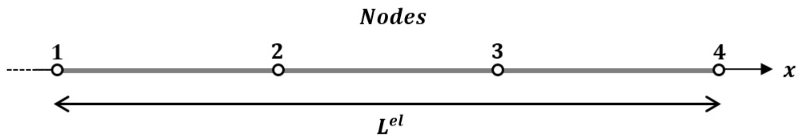

Figure 4.1: Element nodes for cubic interpolation

The standard procedure, for a linear element subjected only to a longitudinal displacements, consists to approximate the displacement field $\hat{u}$ (where the hat denotes the approximation) with a system of d (correspondent to the number of d.o.f.) 3^{th} degree polynomials: **[19]**:

$$\hat{u}(x) = \alpha_1 + \alpha_2 x + \alpha_3 x^2 + \alpha_4 x^3 = \begin{bmatrix} 1 & x & x^2 & x^3 \end{bmatrix} \begin{bmatrix} \alpha_1 \\ \alpha_2 \\ \alpha_3 \\ \alpha_4 \end{bmatrix} = \{P\}\{\alpha\} \tag{4.2}$$

Substituting the point wise values of the x_i nodal positions and the nodal displacements $\hat{u}_i$, the system of equations 4.2 becomes:

$$\begin{bmatrix} \hat{u}(x_1) \\ \hat{u}(x_2) \\ \hat{u}(x_3) \\ \hat{u}(x_4) \end{bmatrix} = \begin{bmatrix} 1 & x_1 & x_1^2 & x_1^3 & x_1^3 \\ 1 & x_2 & x_2^2 & x_2^3 & x_2^3 \\ 1 & x_3 & x_3^2 & x_3^3 & x_3^3 \\ 1 & x_4 & x_4^2 & x_4^3 & x_4^3 \end{bmatrix} \begin{bmatrix} \alpha_1 \\ \alpha_2 \\ \alpha_3 \\ \alpha_4 \end{bmatrix} \tag{4.3}$$

Expressing the previous equation in compact notation, the resulting expression of the unknown linear coefficient $\{\alpha\}$ is:

$$\{\hat{u}\} = [C]\{\alpha\} \rightarrow \{\alpha\} = [C]^{-1}\{\hat{u}\} \tag{4.4}$$

Thus, combining the previous relation with equation 4.2, the longitudinal displacement approximation is:

$$\hat{u}(x) = \{P\}[C]^{-1}\{\hat{u}\} = \begin{bmatrix} N_1^e & N_2^e & N_3^e & N_4^e \end{bmatrix} \begin{bmatrix} \hat{u}(x_1) \\ \hat{u}(x_2) \\ \hat{u}(x_3) \\ \hat{u}(x_4) \end{bmatrix} \tag{4.5}$$

The interpolating shape functions $\{[P\}[C]^{-1}$ collect the terms of the corresponding linear combination related to the nodal displacements:

$$\mathbf{N^e} = \begin{bmatrix} N_1^e & N_2^e & N_3^e & N_4^e \end{bmatrix} = \begin{bmatrix} 1 & x & x^2 & x^3 \end{bmatrix} \begin{bmatrix} 1 & x_1 & x_1^2 & x_1^3 & x_1^3 \\ 1 & x_2 & x_2^2 & x_2^3 & x_2^3 \\ 1 & x_3 & x_3^2 & x_3^3 & x_3^3 \\ 1 & x_4 & x_4^2 & x_4^3 & x_4^3 \end{bmatrix}^{-1} \tag{4.6}$$

The main problems in the evaluation of shape functions is that the inverse of matrix $[C]$ may do not exist, be ill-conditioned or hard to express in a general form. In this exemplification case of a linear one dimensional element the shape functions are required to be continuous and so to have only $\mathscr{C}^0$ continuity, while in the case of the Euler-Bernoulli beam they have to have $\mathscr{C}^1$ continuity in order to integrate the second order derivatives due to he presence of rotations. To overcome these issues it is useful to adopt directly interpolating functions as **Splines**, **Fourier functions**, **Exponential functions**, **Hermitian polynomial** or **Lagrange polynomial**. Commonly these functions are conveniently expressed in terms of local dimensionless coordinates ξ obtained normalizing the global coordinates x (isoparametric element) **[19]**(figure 4.2):

$$\xi = 2\frac{x - \bar{x}_{i,i+1}}{L^{el}} \tag{4.7}$$

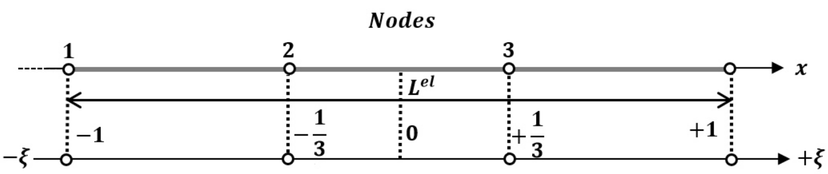

Figure 4.2: Normalized local coordinate system

In the considered case of a cubic interpolation, the third order Lagrangian polynomial for the isoparametric element has to be of the form:

$$\mathscr{L}_i^p(\xi) = \prod_{j=1, j\neq i}^{p+1} \frac{(\xi - \xi_j)}{(\xi_i - \xi_j)} \tag{4.8}$$

Hence, the 4 resulting shape functions are evaluated in 4.9 and showed graphically in figure 4.3:

$$
\begin{gathered}
N_1^e = \mathscr{L}_1^3 = \frac{[\xi-(-\frac{1}{3})]\,[\xi-\frac{1}{3}]\,[\xi-1]}{[(-1)-(-\frac{1}{3})]\,[(-1)-\frac{1}{3}]\,[(-1)-1]} = -\frac{9}{16}\left(\xi+\frac{1}{3}\right)\left(\xi-\frac{1}{3}\right)\left(\xi-1\right) \\
N_2^e = \mathscr{L}_2^3 = \frac{[\xi-(-1)]\,[\xi-\frac{1}{3}]\,[\xi-1]}{[(-\frac{1}{3})-(-1)]\,[(-\frac{1}{3})-\frac{1}{3}]\,[(-\frac{1}{3})-1]} = +\frac{27}{16}\left(\xi+1\right)\left(\xi-\frac{1}{3}\right)\left(\xi-1\right) \\
N_3^e = \mathscr{L}_3^3 = \frac{[\xi-(-1)]\,[\xi-(-\frac{1}{3})]\,[\xi-1]}{[\frac{1}{3}-(-1)]\,[\frac{1}{3}-(-\frac{1}{3})]\,[\frac{1}{3}-1]} = -\frac{27}{16}\left(\xi+1\right)\left(\xi+\frac{1}{3}\right)\left(\xi-1\right) \\
N_4^e = \mathscr{L}_4^3 = \frac{[\xi-(-1)]\,[\xi-(-\frac{1}{3})]\,[\xi-\frac{1}{3}]}{[1-(-1)]\,[1-(-\frac{1}{3})]\,[1-\frac{1}{3}]} = +\frac{9}{16}\left(\xi+1\right)\left(\xi+\frac{1}{3}\right)\left(\xi-\frac{1}{3}\right)
\end{gathered}
\tag{4.9}
$$

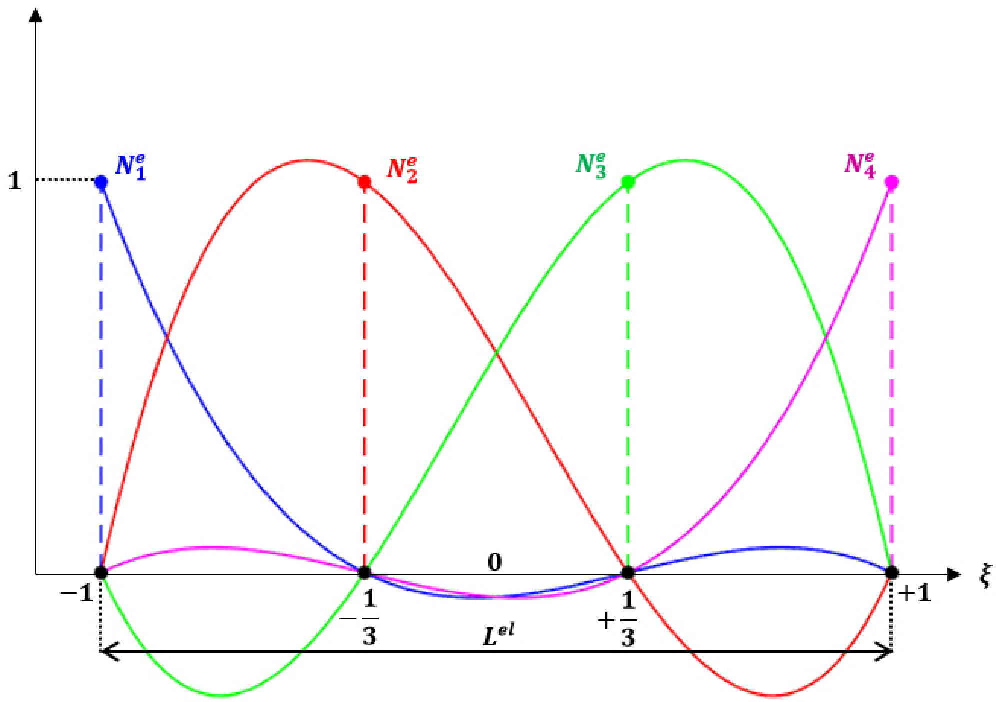

Figure 4.3: Isoparametric Lagrange cubic polynomial interpolation.

Introducing now the time dependence of displacements for the dynamic analysis purpose, similarly to equation 4.5, the displacements field can be expressed as:

$$\{\hat{u}\}_{(x,t)} = [N]_{(x)}\{\hat{u}_0\}_{(t)} \tag{4.10}$$

where $\{\hat{u}_0\}(t)$ are the time dependent nodal displacements. Recalling from the linear elasticity theory **[12]** the stress-strain relations, in discrete form results:

$$\begin{aligned} \{\hat{\varepsilon}\}_{(x,t)} = [\partial]\{\hat{u}\}_{(x,t)} = [\partial][N]_{(x)}\{u_0\}_{(t)} = [B]_{(x)}\{u_0\}_{(t)} \\ \{\hat{\sigma}\}_{(x,t)} = [E][\partial][N]_{(x)}\{u_0\}_{(t)} = [E][B]_{(x)}\{u_0\}_{(t)} \end{aligned} \tag{4.11}$$

where the $[B]_{(x)}$ is the deformation matrix. Introducing the previous equation 4.11 in the equation of V.W.P. 4.1, since the virtual displacements are arbitrary **[28] [29]**, is possible to obtain the discrete formulations of the other mathematical terms of the static and dynamic governing equations 3.18, 3.43 and 3.47 as:
- the elastic element stiffness matrix $[K^e]$

$$[K^e] = \int_0^{L^{el}} [B]^T_{(x)} EI_z [B]_{(x)} dx = \int_{-1}^{+1} [B]^T_{(x)} EI_z [B]_{(x)} \frac{L^{el}}{2} d\xi \tag{4.12}$$

- the consistent element mass matrix $[M]^e$

$$[M^e] = \int_0^{L^{el}} \rho A [N]^T_{(x)} [N]_{(x)} dx = \int_{-1}^{+1} \rho A [N]^T_{(x)} [N]_{(x)} \frac{L^{el}}{2} d\xi \tag{4.13}$$

- the generalized load vector of volumetric external forces $\{p\}^{ext}$

$$\{p\}^{ext}_{(t)} = \int_0^{L^{el}} [N]^T_{(x)} \{F_v\}_{(x,t)} dx = \int_{-1}^{+1} [N]^T_{(x)} \{F_v\}_{(x,t)} \frac{L^{el}}{2} d\xi \tag{4.14}$$

- the inertial mass forces vector $\{p\}^I$

$$\{p\}^I_{(t)} = -\left(\int_0^{L^{el}} \rho A [N]^T_{(x)} [N]_{(x)} dx\right)\{\ddot{u}_0\}_{(t)} = -[M]\{\ddot{u}_0\}_{(t)} \tag{4.15}$$

The previous equations represent the structural model of one single element. The whole structure is considered as the aggregation of N_e disjointed elements and the full global mass $[M]$ and stiffness $[K]$ matrices are built by directly assembling the N_e sub-matrices (*Direct Stiffness Method*), overlapping them at the coincident nodes and taking into account the opportune boundary conditions and internal restraints. These will lead to the implementation of matrices of dimension $D \times D$, where D is the product between the number of elements and the number of considered d.o.f.

$$\begin{aligned} [K] = \sum_{e=1}^{N_e} [K^e] \qquad D \times D \\ [M] = \sum_{e=1}^{N_e} [M^e] \qquad D \times D \end{aligned} \tag{4.16}$$

4.2 Euler-Bernoulli Elastic Cantilever Beam

Consider the Euler-Bernoulli cantilever beam of figure 3.4, subjected to bending moment M_z and shear force V_y under the hypotheses of chapter 3. Since the structure is linear and straight with a constant section, it can be modelled with enough accuracy as beam finite element with only two end nodes n and thus two degrees of freedom d for each node. The resulting transverse displacement field and the external load vector are, respectively:

$$\{v\}_{(x)} = \left\{ \begin{array}{cccc} v_1 & \varphi_1 & v_2 & \varphi_2 \end{array} \right\}^T \tag{4.17}$$

$$\{P\} = \left\{ \begin{array}{cccc} V_{y1} & M_{z1} & V_{y2} & M_{z2} \end{array} \right\}^T \tag{4.18}$$

Since the beam homogeneous differential equation is 3.12, the displacement field 4.17 can approximated with a polynomial at least of order $n \times d - 1 = 2 \times 2 - 1 = 3$:

$$\hat{v}_i(x) = \alpha_1 + \alpha_2 x_i + \alpha_3 x_i^2 + \alpha_4 x_i^3 \tag{4.19}$$

Following the standard procedure, equation 4.4 becomes:

$$\{\hat{v}\}_{(x)} = \left\{ \begin{array}{cccc} N_{v_1}(x) & N_{\varphi_1}(x) & N_{v_2}(x) & N_{\varphi_2}(x) \end{array} \right\} \left\{ \begin{array}{c} \hat{v}_1 \\ \hat{\varphi}_1 \\ \hat{v}_2 \\ \hat{\varphi}_2 \end{array} \right\} \tag{4.20}$$

where the matrix $[C]$ resulting in equation 4.22 is evaluated directly from the interpolating polynomial, by imposing 4 boundary conditions (eq. 4.21). The solution for the cantilever beam case is obtained imposing the restraints conditions at the fixed end, thus $\hat{v}_1 = 0$ and $\hat{\varphi}_1 = 0$ in node 1.

$$\begin{array}{ll} \hat{v}(0) = \hat{v}_1 = \alpha_1 & \hat{v}(l) = \hat{v}_2 = \alpha_1 + \alpha_2 l + \alpha_4 l^3 + \alpha_3 l^2 \\ \left.\dfrac{d\hat{v}}{dx}\right|_{x=0} = \hat{\varphi}_1 = \alpha_2 & \left.\dfrac{d\hat{v}}{dx}\right|_{x=l} = \hat{\varphi}_2 = \alpha_2 + 2\alpha_3 l + 3\alpha_4 l^2 \end{array} \tag{4.21}$$

$$[C] = \begin{bmatrix} 1 & 0 & 0 & 0 \\ 0 & 1 & 0 & 0 \\ 1 & l & l^2 & l^3 \\ 0 & 1 & 2l & 3l^2 \end{bmatrix} \tag{4.22}$$

The four shape functions of equation 4.20 after the definition of the constants can be calculated in global coordinate:

$$N_{v_1}(x) = 1 - 3\frac{x^2}{l^2} + 2\frac{x^3}{l^3} \qquad N_{\varphi_1}(x) = x - 2\frac{x^2}{l} + \frac{x^3}{l^2}$$
$$N_{v_2}(x) = 3\frac{x^2}{l^2} - 2\frac{x^3}{l^3} \qquad N_{\varphi_2}(x) = -\frac{x^2}{l} + \frac{x^3}{l^2} \tag{4.23}$$

Alternatively, the parametric formulation can be used and recalling the normalized coordinate conversion 4.7 the previous equations 4.23 can be expressed as the *Lagrangian Polynomial* or related to the *Hermitian Polynomial* **[6]**:

$$N_{v_1}(\xi) = \frac{1}{4}(1-\xi)^2(2+\xi) \qquad N_{\varphi_1}(\xi) = \frac{l}{8}(1-\xi)^2(1+\xi)$$
$$N_{v_2}(\xi) = \frac{1}{4}(1+\xi)^2(2-\xi) \qquad N_{\varphi_2}(\xi) = \frac{l}{8}(1+\xi)^2(\xi-1) \tag{4.24}$$

Analogously to the transverse displacement, it is also possible to approximate the expression for curvature κ (eq. 3.5) simply deriving with respect to x the shape functions expressions, implying the requirement of the $\mathscr{C}^1$ continuity condition due to the presence of the second order derivatives of transverse displacement field. This leads, according with equation 3.9, to the definition of the deformation matrix $[B]$, which collects the shape functions second derivatives:

$$[B] = -\left\{ \frac{d^2 N_{v_1}}{dx^2} \quad \frac{d^2 N_{\varphi_1}}{dx^2} \quad \frac{d^2 N_{v_2}}{dx^2} \quad \frac{d^2 N_{\varphi_2}}{dx^2} \right\} \tag{4.25}$$

Adopting the interpolating shape function expression in global coordinates, recalling the equations 4.12 and 4.13, the discrete form of the stiffness matrix $[K]$ and the consistent mass matrix $[M]$ 4.26. Since for a prismatic member with constant cross-section the displacement field interpolated from the nodal values concurs with the exact solution obtained from the equation of elasticity 3.12, the resulting matrix is the same for the exact solution 3.17 and for the approximated one.

$$[K] = \begin{bmatrix} \frac{12EI_z}{l^3} & \frac{6EI_z}{l^2} & -\frac{12EI_z}{l^3} & \frac{6EI_z}{l^2} \\ & \frac{4EI_z}{l} & -\frac{6EI_z}{l^2} & \frac{2EI_z}{l} \\ & \textbf{Sym} & \frac{12EI_z}{l^3} & -\frac{6EI_z}{l^2} \\ & & & \frac{4EI_z}{l} \end{bmatrix} \qquad [M] = \frac{\rho A}{420}\begin{bmatrix} 156l & 6l^2 & 54l & -13l^2 \\ 22l^2 & 4l^3 & 13l^2 & -3l^3 \\ 54l & 13l^2 & 156l & -22l^2 \\ -13l^2 & -3l & -22l^2 & 4l^3 \end{bmatrix} \tag{4.26}$$

4.3 F. E. Model of a Cracked Cantilever Beam

The analytic solution of cracked structure is not simple since the presence of the localized discontinuity causes non-linear variations in the stress, strain and displacement fields. However, it is much easier to model the system with a F.E. approach because according to *De Saint-Venant*, the effects of the crack presence can be limited in the neighbourhood of the damaged region and thus only the damaged element formulation need to be modified. The solution reported in this section is the one proposed by **[57]** where the the stiffness matrix for the damaged element $[K^d]$ is derived through the definition of the **stress intensity factors**. Considering the cantilever beam with a cracked section in figure 4.4:

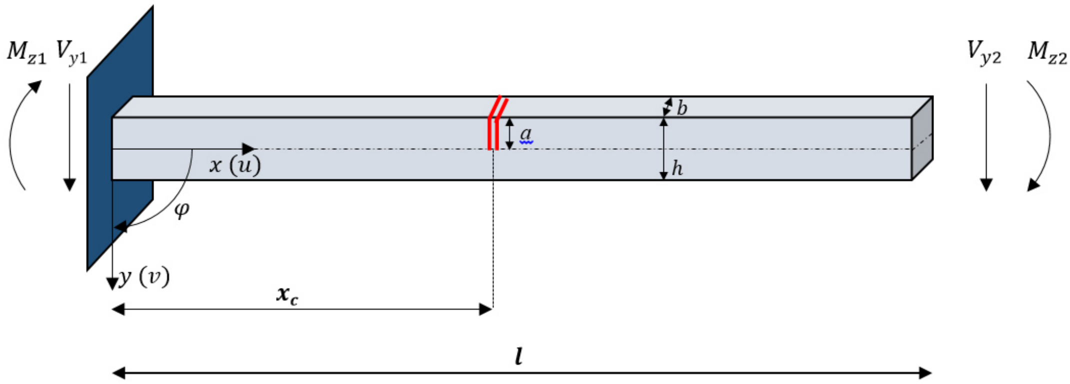

Figure 4.4: Convention for a beam with crack

Neglecting the shear deformation, the strain energy for the damaged element is:

$$W = W^E + W^D \tag{4.27}$$

where the elastic component W^E, common for all the undamaged elements, is:

$$W^E = \frac{1}{2EI_z}\int_0^l (M+Vx)^2 dx = \frac{1}{2EI_z}(M^2 l + MVl^2 + V^2 l^3) \tag{4.28}$$

and the additional strain energy due to crack W^D is:

$$W^D = b\int_0^a \left(\frac{(K_I^2 + K_{II}^2)}{E'} + \frac{(1-\nu)K_{III}^2}{E} da\right) \tag{4.29}$$

The K coefficients are, respectively, the *stress intensity factors*, for the opening, in-plane sliding and out-of-plane sliding mechanisms (figures 4.5).

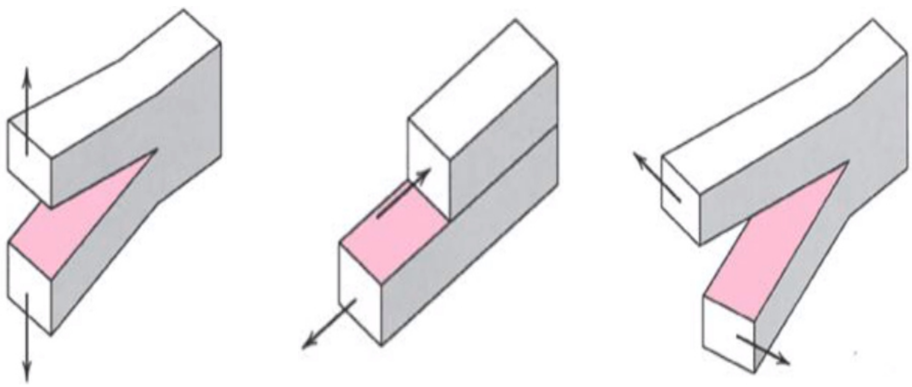

(a) KI Opening (b) KII In-plane slide (c) KIII out-of-plane slide

Figure 4.5: Types of cracking

The elastic modulus E', instead, for plane strain conditions is defined in function of the Poisson's coefficient ν as:

$$E' = \frac{E}{1+\nu} \tag{4.30}$$

Taking in to account only the transverse bending displacements, equation 4.29 becomes:

$$W_M^D = \int_0^a \frac{(K_{IM} + K_{IV})^2 + K_{IIV}^2}{E'} da \tag{4.31}$$

with the three stress intensity factors for the opening due to bending moment K_{IM} and shear K_{IV} and for in-plane sliding due to shear K_{IIV} :

$$\begin{gathered} K_{IM} = \left(\frac{6M}{bh^3}\right)\sqrt{\pi a}F_I(\frac{a}{h}) \\ K_{IV} = \left(\frac{3Vl}{bh^2}\right)\sqrt{\pi a}F_I(\frac{a}{h}) \\ K_{IIV} = \left(\frac{V}{bh}\right)\sqrt{\pi a}F_{II}(\frac{a}{h}) \end{gathered} \tag{4.32}$$

where the empirical factors F_I and F_{II} are:

$$F_I = \sqrt{\left(\frac{2}{\pi\frac{a}{h}}\tan\left(\frac{\pi\frac{a}{h}}{2}\right)\right)}\frac{0.923+0.199\left(1-\sin\left(\frac{\pi\frac{a}{h}}{2}\right)\right)^4}{\cos\left(\frac{\pi\frac{a}{h}}{2}\right)}$$

$$F_{II} = \left(3\frac{a}{h}-2\left(\frac{a}{h}\right)^2\right)\frac{1.122-0.561\frac{a}{h}+0.085\left(\frac{a}{h}\right)^2+0.18\left(\frac{a}{h}\right)^3}{\sqrt{1-\frac{a}{h}}} \tag{4.33}$$

Remembering that the flexibility matrix $[C]$ is the inverse of the stiffness matrix $[K]$ (eq. 4.34), the coefficients for the elastic (undamaged elements) are defined as in equation 4.35

$$[C] = [K]^{-1} \tag{4.34}$$

$$c_{11}^E = \frac{\partial^2 W^E}{\partial V^2}$$

$$c_{22}^E = \frac{\partial^2 W^E}{\partial M^2} \tag{4.35}$$

$$c_{12}^E = \frac{\partial^2 W^E}{\partial V \partial M} = c_{21}^E$$

The additional flexibility terms due to crack c_{ij}^D can be computed analogously to equation 4.34 by substituting the energy W^D and the total flexibility for the damaged element is:

$$c_{ij} = c_{ij}^E + c_{ij}^D \tag{4.36}$$

The equilibrium of the cracked element is showed in figure 4.6 and results (eq. 4.37);

$$\left\{\begin{array}{c} V_i \\ M_i \\ V_{i+1} \\ M_{i+1} \end{array}\right\}^T = [T]\left\{\begin{array}{c} V_{i+1} \\ M_{i+1} \end{array}\right\}^T \tag{4.37}$$

where

$$[T] = \begin{bmatrix} -1 & 0 \\ -l & -1 \\ +1 & 0 \\ 0 & +1 \end{bmatrix} \tag{4.38}$$

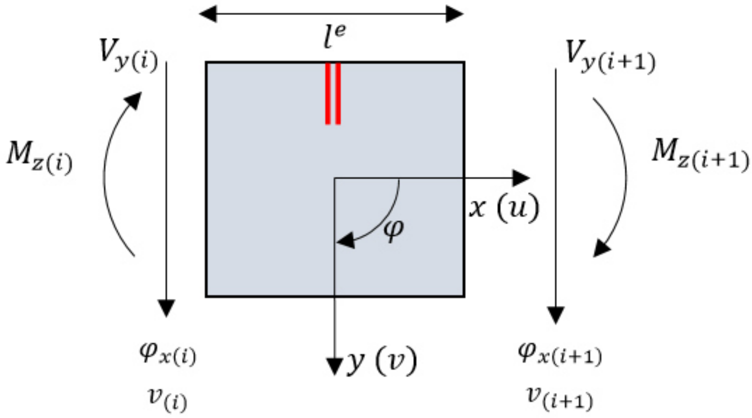

Figure 4.6: Equilibrium of the cracked element

From the V.W.P., the expression for the stiffness matrix of the damaged element $[K^D]$ is:

$$\left[K^D\right] = [T]\,[C]^{-1}\,[T]^T \tag{4.39}$$

and the global stiffness matrix [K] for the N_e elements

$$[K] = \sum_{e=1}^{N_e} \begin{cases} [K_e^E] & if\ \ undamaged\ \ element\ \ (eq.4.12) \\ \\ [K_e^D] & if\ \ damaged\ \ element\ \ (eq.4.39) \end{cases} \tag{4.40}$$

Chapter 5

Novelty Detection in Cracked Structures

5.1 Methodology

The methodology adopted in this study follows the path initiated by **[16, 54]** in order to asses if a given simulated noisy mode shape is damaged or not. Moreover, the rate of success in correct classification is reported since is of primary interest to determine the effectiveness of the used metric, in this particular case the transverse displacement of the cantilever beam. First of all, two large sets of data are simulated with the Finite Element Method, the first one collecting the noisy undamaged transverse modes (UND), while the second one collects the noisy damaged transverse modes (DAM). This step is functional to obtain a robust statistical pool of data from which different subsets will be randomly sampled later, avoiding intersections among them. Since the theoretical mode shapes simulated using the dynamic elastic theory reviewed in previous chapters 3 and 4 are noise-free, the Gaussian i.i.d. noise has been added (at different levels) trough the specification of the *Signal to Noise Ratio* (SNR) (equation 5.3).

Then three subsets of data are randomly sampled for each analysed mode from the parent sets UND and DAM:

- **Training set (TR)**: composed only by the undamaged data.
- **Validation set (VA)**: composed only by the undamaged data
- **Test set (TS)**: composed by the undamaged and the damaged data.

The training set TR is used to train the Gaussian Process, fitting the parameters of the multivariate distribution through the optimisation of the predictive joint conditional *Marginal Likelihood* by minimising its negative logarithmic form with the *Conjugate Gradient Method* **[63]**. Combining the current parameters estimation with the validation set VA leads to the generation of the standardised logarithmic Probability Density Function (PDF).

To individuate the anomalous high displacement values that could indicate the presence of a crack in a structure, it is necessary to discern them among all the nodal displacements that fall in a normal range. To do this, from the logarithmic values of PDF is indeed possible to calculate the correspondent Cumulative Distribution Function (CDF) that, as know from the *Extreme Functions Theory* (EFT), belongs to one of the three feasible extreme distributions **[26]**. In this case, the interest is focused on the minima distributions, since one could expect few occurrences of the anomalous values respect to the normal ones. The defining parameters of the three CDFs are estimated with a Genetic Differential Evolution algorithm, in particular the Self-Adaptive Differential Evolution (SADE) algorithm, because it enhances a better and more stable convergence, avoiding the local minima without requiring an initial guess **[90]**. It is important to note that mode shapes are treated as whole function instead that pointwise, enhancing a reduction in false positives. Finally, a threshold defined to be the 99% confidence interval allows to distinguish if the tested mode shapes data belong to the normal undamaged condition or if they lay in the outer 1% quantile, detecting in this case the presence of the damage. The parameters studied in the different simulations, such as the depth of the crack, the location of the crack and the level of added noise, were varied in order to establish the effectiveness of the used metric and to ensure statistically significative results in the evaluation of the algorithm rate of success, the procedure was repeated several times for each case. A graphical overview of the entire process is showed in figure 5.1, which reports the key steps of the algorithm: the blue coloured initial part is referred to data generation or acquisition, the yellow one is the the training process of the model, the red one are the steps followed to validate the model and, finally, the green part resumes the test and detection steps for damage assessment; red text annotations, instead, reports the main input parameters required that are been varied in the different simulations.

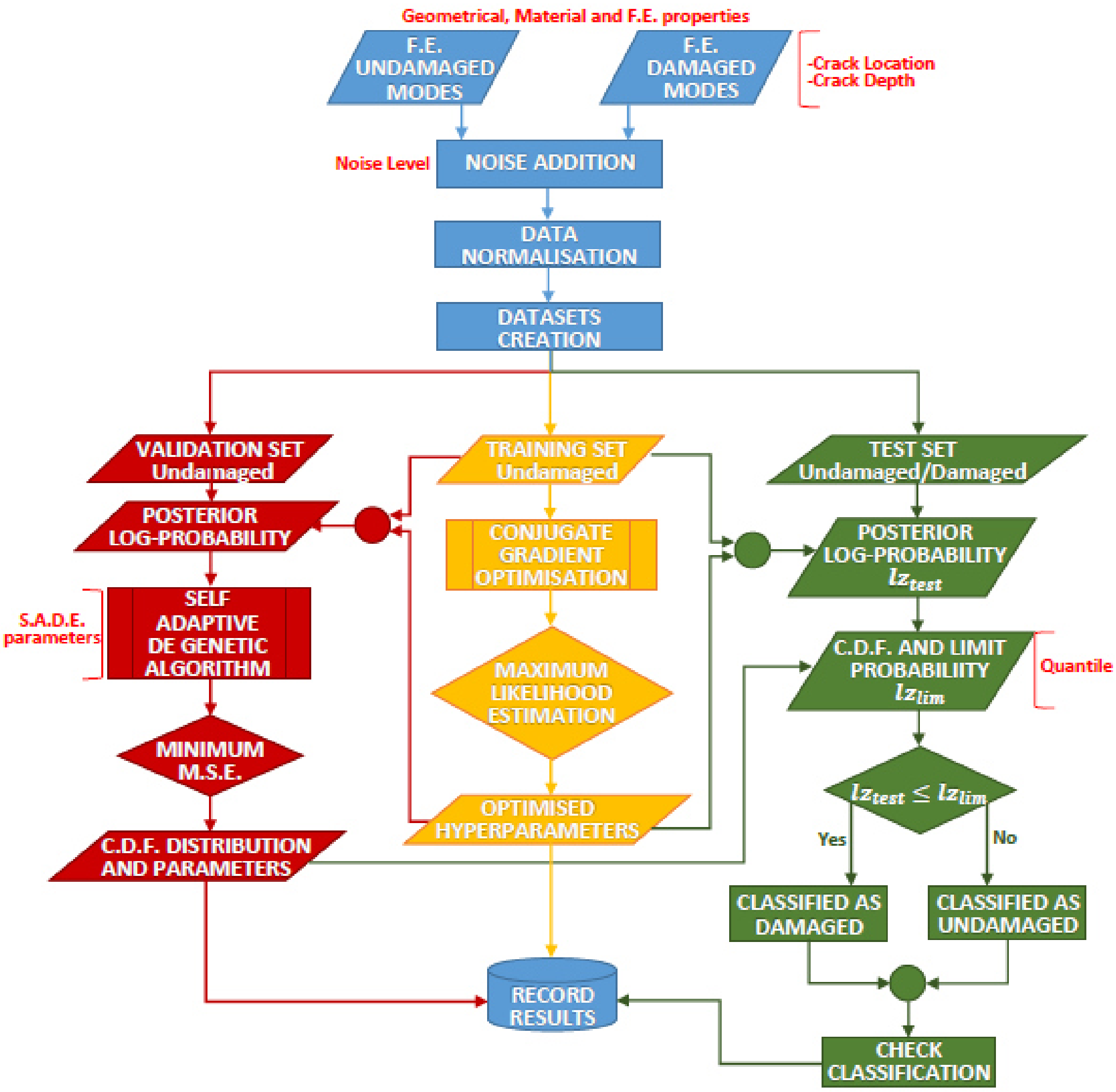

Figure 5.1: Flow Chart: Damage detection algorithm for a edge-cracked cantilever beam using Gaussian process regression with eigenmode displacements.

5.2 Description of the Mode Shapes Data

Starting from the Euler-Bernoulli theory enunciated previously in chapter 3, the undamaged slender cantilever beam used as reference structure has been modelled using the Finite Element Method (chapter 4). The chosen interpolating shape functions are the cubic Hermitian polynomials that, after re-converting the normalised coordinate, leads to the element Stiffness matrix $[K^e]$ 5.1 and to the consistent Mass matrix $[M^e]$ 5.2 approximation. The properties adopted simulate an idealised concrete beam with all the assumptions of the simplified case, such as the absence of shear strains, irrelevance of Poisson's effect, purely elastic material behaviour and the linearisation of crack mechanic. All the parameters are resumed in *table 5.1.*

$$[K^e] = E_u I_z \begin{bmatrix} \frac{12}{l^3} & \frac{6}{l^2} & -\frac{12}{l^3} & \frac{6}{l^2} \\ & \frac{4}{l} & -\frac{6}{l^2} & \frac{2}{l} \\ & \textbf{Sym} & \frac{12}{l^3} & -\frac{6}{l^2} \\ & & & \frac{4}{l} \end{bmatrix} \tag{5.1}$$

$$[M^e] = \frac{\rho A}{420} \begin{bmatrix} 156l & 6l^2 & 54l & -13l^2 \\ 22l^2 & 4l^3 & 13l^2 & -3l^3 \\ 54l & 13l^2 & 156l & -22l^2 \\ -13l^2 & -3l & -22l^2 & 4l^3 \end{bmatrix} \tag{5.2}$$

Section base	b	0.05	[m]
Section height	h	0.05	[m]
Section area	A	2.5 e-3	$\left[m^4\right]$
Moment of inertia	I_z	5.21 e-7	$\left[m^4\right]$
Beam length	L	1	[m]
Elements number	N_e	50	[m]
Element length	l	0.02	[m]
Elastic modulus (UND)	E_u	7.00 e10	$\left[\frac{N}{m^2}\right]$
Density	ρ	2700	$\left[\frac{kg}{m^3}\right]$
Poisson's coefficient	ν	0.3	[-]

Table 5.1: E.B. cantilever beam F.E.M. parameters

After defining the mass and stiffness matrices is straightforward to calculate the natural frequencies and the related natural mode shapes of the system. The eigenmodes calculated consist of two degrees of freedom (transverse displacement and rotation): after selecting the d.o.f of interest these values have been normalised scaling them to the maximum displacement and copied several times to generate the base of the data set UND.

The data simulated so far are noise-free since they derive directly from the theoretical F. E. model. To give them the aleatory behaviour that they would have in reality is necessary the addition of the Gaussian white noise, specifying its level by the definition of the Signal to Noise Ratio (SNR), expressed in Decibel $[Db]$:

$$SNR = 20\log_{10}\left(\frac{A_{signal}}{A_{noise}}\right) \tag{5.3}$$

where A_{signal} is the noise-free signal amplitude and A_{noise} is the amplitude of the added noise.

As known from the Fracture Mechanics (ch. 4), the crack behaviour implies a non-linearity in the dynamic response of considered structure. It is primarily due to the localised geometrical discontinuity in the continuous, but also it activates an opening and closing mechanism, which dissipates energy during the motion. Neglecting this last factor, the governing equation of motion can be linearised operating a transformation in the stiffness matrix $[K^e]$ in order to obtain an **equivalent linear stiffness matrix** $[\mathbf{K^e_{EQ}}]$ capable to take into account the effects of crack presence through the stress intensification factors, as the solution proposed by **[57]**. Consequently, the main parameters influencing the stiffness of the structure will result the *normalised crack depth* $a[m]$ and the *normalised crack location* $x_c[m]$: the first one is limited from the Griffith's energetic fracture failure criteria to be smaller then 50% of the height of the section, while the second one is not allowed at the edge of the structure has it has been modelled according to the *De Saint-Venant* theory. The mass matrix, instead, is assumed to remain constant in the cracked structure. Again, after the F.E. calculation and the normalisation, the Gaussian noise is added following the procedures of the undamaged state (equation 5.3) to build the damaged data set (DAM). Under these hypotheses, figure 5.2 below shows the comparison between undamaged and damaged states of the first theoretical mode shape of vibration and the related natural frequencies, where for representational clearness the crack aperture is taken a = 40% of height section h and x_c = 10% of beam length L:

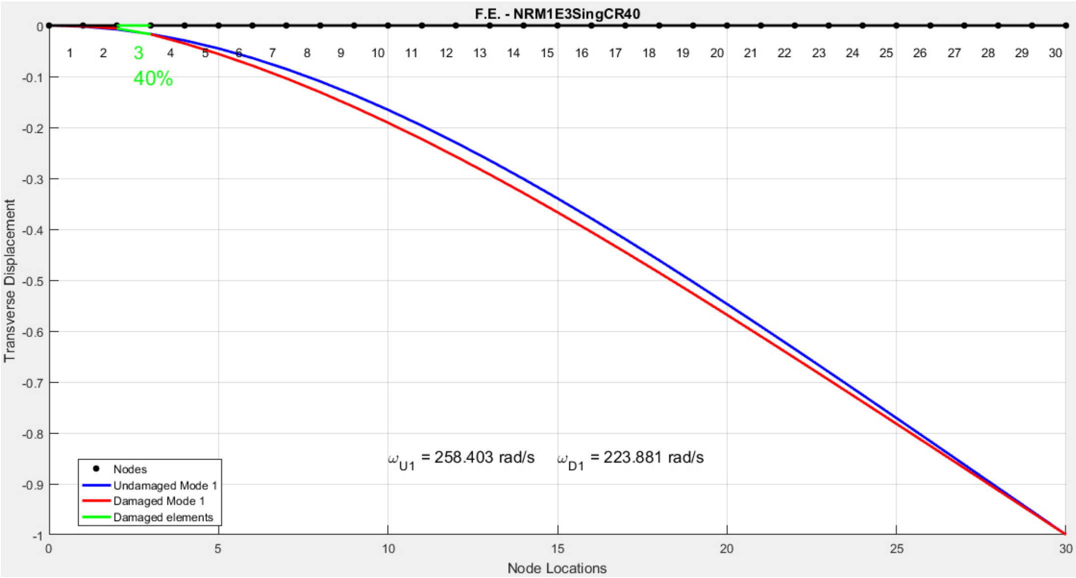

Figure 5.2: F.E. Mode 1: damage location 10% of length, crack depth 40% of section.

After the noise addition, instead, the available modal information coming from the relative displacements of the two compared beams results dependent on the magnitude of the noise itself. Figures 5.3, 5.4 and 5.5 show the comparison of a single copy of the N_e undamaged and damaged displacements of the first three modes, where in case I) SNR=20 dB the noise covers most of the information, while in case II) where SNR=50 dB is a more clear case. Finally, the 2 parent data sets UND and DAM and the randomly sampled TR, VA and TS sets are created with the following number of aleatory copies 5.2. Remembering that each mode is composed by N_e values, the final dimensions are:

SET	Name	Copies	Dimension
Undamaged	UND	2000	60000
Damaged	DAM	2000	60000
Training	TR	30	900
Validation (U30)	VA_1	200	4500
Validation (U50)	VA_2	90	4500
Test	TS_1	100	3000
Test	TS_2	100	5000

Table 5.2: Dimensions of data sets

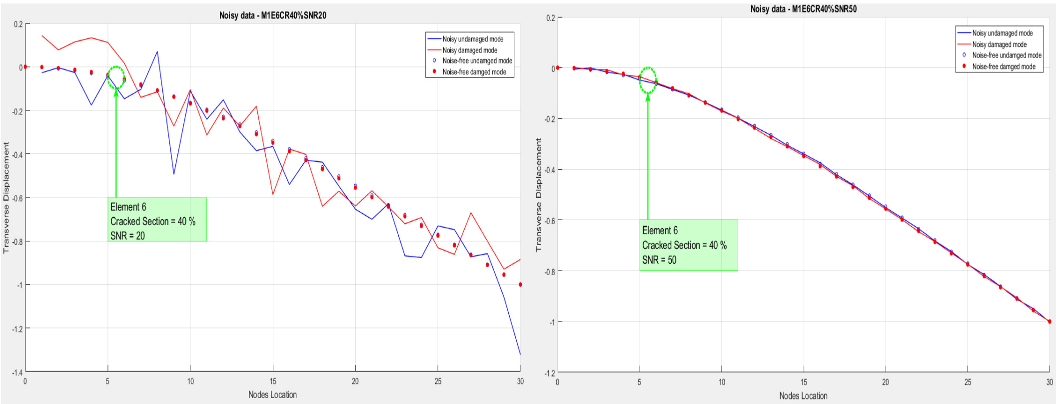

Figure 5.3: Noisy data Mode 1 - I)SNR=20 II)SNR=50 || a=40% || $x_c = 30\%$

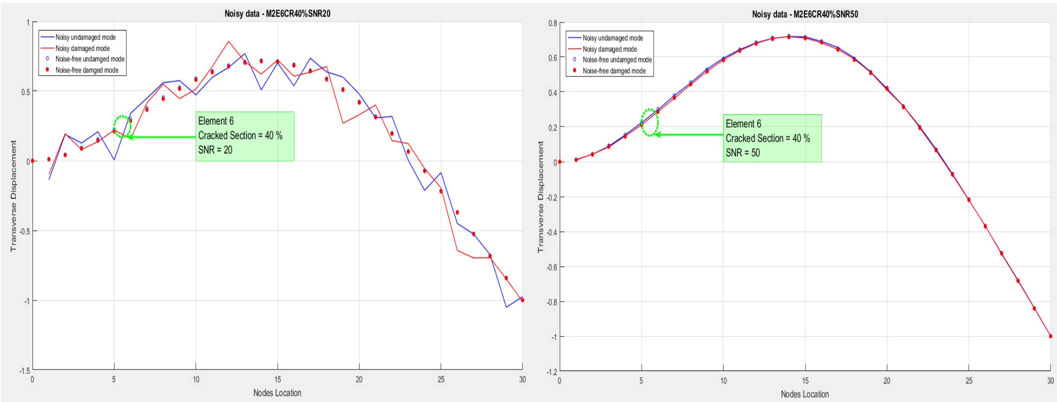

Figure 5.4: Noisy data Mode 2 - I)SNR=20 II)SNR=50 || a=40% || $x_c = 20\%$

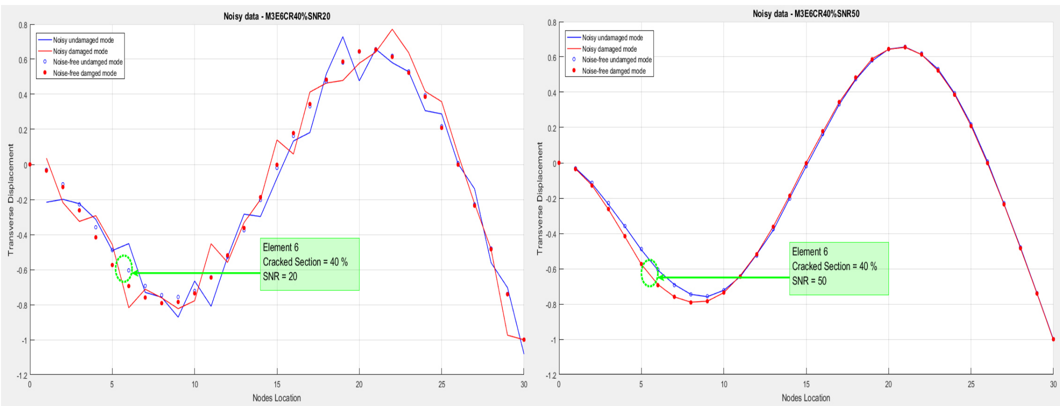

Figure 5.5: Noisy data Mode 3 - I)SNR=20 II)SNR=50 || a=40% || $x_c = 20\%$

5.3 Training of the Gaussian Process

The mode shape displacements simulated so far, holding their main property of linearity, can be assumed as a 1-dimensional (D) set of n Gaussian distributed aleatory observations y dependent on the node locations x. Recalling the probability theory of section 2.2, the Gaussian Process interpolates the transverse displacement data through the application of a Bayesian linear regression in order to reconstruct the generating continuous function. The training phase of the process consists in the estimation of the hyperparameters of equation 2.6 on the bases of the data coming form the training data set TR. After that optimisation is performed, the posterior mean and covariance (equations 2.3, 2.4) allow to obtain the inferred function values over the tested input points. Figures below show different cases of noisy measurements fitting (SNR=20 dB) of the second mode shapes of a simply supported beam: while case 5.6 is referred to a sensors network of 11 equispaced elements, case 5.7a consists of only 4 random measurements points and case 5.7b is instead evaluated on the continuous input space.

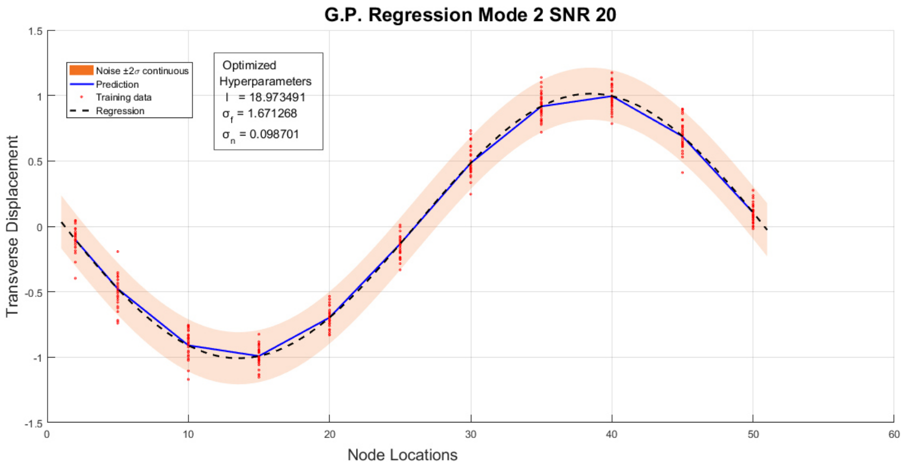

Figure 5.6: G.P. Regression of a mode shape

In case of figure 5.6 above, the 95% confidence interval represented in pale orange remains almost constant, since the chose of equispaced measurement points implies a constant knowledge over the considered system. The discrete prediction represented with a piecewise blue line fit properly with the continuous regression (black dashed line) of the mode shape (figure 5.7b). Otherwise figure 5.7a shows off how the sensing settlement is not sufficient to correctly estimate the transverse displacements and it results in a coarser approximation: in particular the characteristic horizontal length scale l, which represents the distance of uncorrelation of the data in the input space, is reduced of 3 times respect to the other cases and thus it means that the processed data have a more uncorrelated trend.

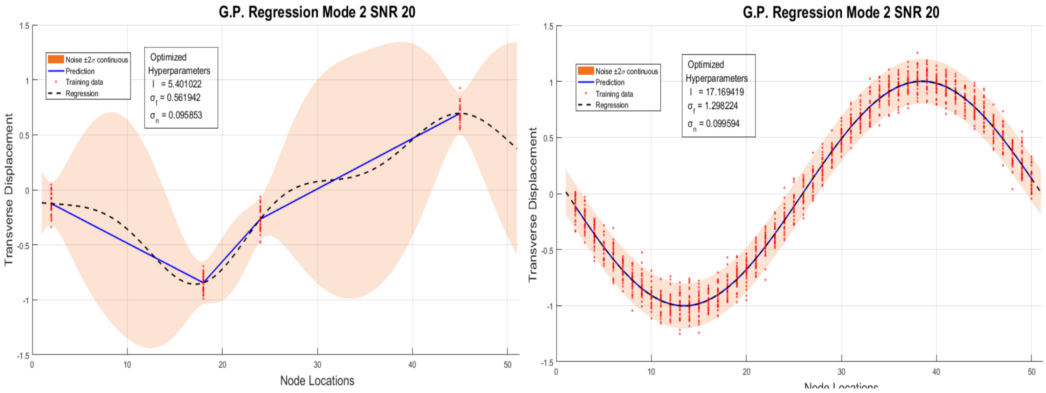

(a) (b)

Figure 5.7: Comparison with different cases of regression

5.4 Validation and C.D.F. Fitting

A first posterior probability (equation 2.5) is calculated conditioning the Validation data set VA on the Training data set TR, in order to make statistically relevant the further results coming form this data combination and independent from the Test data TS. The Gaussian probability is taken in its logarithmic form and processed through a genetic *Differential Evolution* algorithm to estimate the related Cumulative Distribution Function (CDF) of the minima extreme distributions. It is important to remark that the mode shapes data are treated as a whole function rather than pointwise measurements, since the aim is to obtain a single value of probability expressing the level of similarity between the compared mode shapes. Moreover, it should be remarked that CDF has to be fit in its lower tail ($\approx$ 10%) because of the low occurrence frequency of extreme events like damage that deviates from the normal condition of the pristine state.

As known form the *Extreme Function Theory* reviewed in section 2.3, for the minima values there are three parametric feasible limit distributions (Gumbel, Weibull, Frechét) plus the Generalised Extreme Values distribution, where the parameters of scale, shape and location are unknown. Adopting the DE non-linear optimisation method, the empirical CDF is set to be the target function of the algorithm **[90]** while the best parameters are selected on the base of the minimum fitting cost computed as Normalised Mean Squared Error (NMSE) after around 1000 evaluations. Having no clue on the possible range of parameters, D.E. algorithm enhances robustness in the estimation without any initial guess and avoids the local minima due to its heuristic approach of trying different random possible solutions and the multiple repetitions of the entire process. Since the limit distribution of the considered transverse mode shapes is unknown, all the three possibility are investigated and compared with to correspondent results obtained with the GEV. The used initial parameters for the DE algorithm are resumed in the table below 5.3: when the variant of Self-Adaptive Differential Evolution is applied, the specification of the scale factor and the crossover ratio become useless and these parameters are iteratively estimated by the algorithm itself. The empirical CDF (F), as well known, is obtained through the assignment of a family of distributions to a given data set by defining the plotting position and is generally expressed in the form:

$$F = \frac{i-\alpha}{n+1+2\alpha} \tag{5.4}$$

where α is a coefficient varying between 0 and 1. Numerous different plotting position were proposed over the years and a review is found in **[51]**. In the context of the analysed cases the *Hazen* plotting position is adopted, since it is a distribution dependent position suitable for all the EV distributions.

Range used data	10%
Plotting position	Hazen
Population size	30
Number of runs	10
Number of generations	100
Scale factor	0.9
Crossover factor	0.5

Table 5.3: Differential Evolution input parameters

Along the different simulations, the data do not show a clear convergence to a single distribution, but the CDF varies mainly between the Gumbel and the Frechét distributions, while the Weibull one occurs in a lower number of estimations, independently from the crack location, the damage level, the added noise or the mode considered.

An example of the resulting count of estimated distributions for the first mode of a cantilever beam with $SNR = 65dB$ is reported in figure 5.8, while in table 5.4 are showed the average estimated parameters over 1000 repetitions.

Figures from 5.9 to 5.11 show the reconstructed CDF (a), the logarithmic NMSE fitting cost (b) and the probability plot (c) of a single case for each distribution, using only the lower 10% of the available validation data set VA_1. The range was chosen to ensure enough data to analyse while remaining in the lower tail. From the probability plot 5.10c it is clear how the the attraction domain is incorrect since there is not any recognisable linear trend in spite of the other 2 cases.

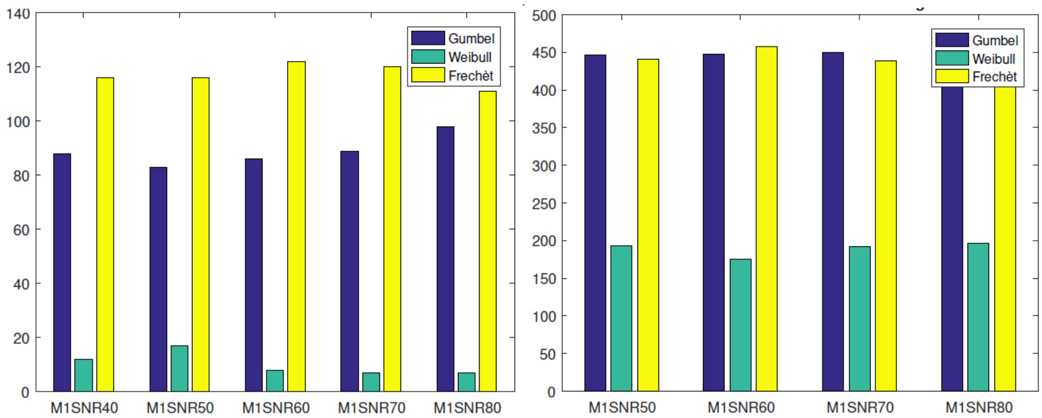

(a) Estimation on 10% of validation data (b) Estimation on 5% of validation data

Figure 5.8: Comparison of estimated CDFs

Average	Gumbel	Frechét	Average	GEV
β	0	5.2779	γ	0.1068
δ	1.6366	5.0831	σ	1.3213
λ	69.4483	73.2554	μ	68.9589
NMSE	1.4351	1.4490	NMSE	1.1118

Table 5.4: CDF average parameters over 1000 repetitions

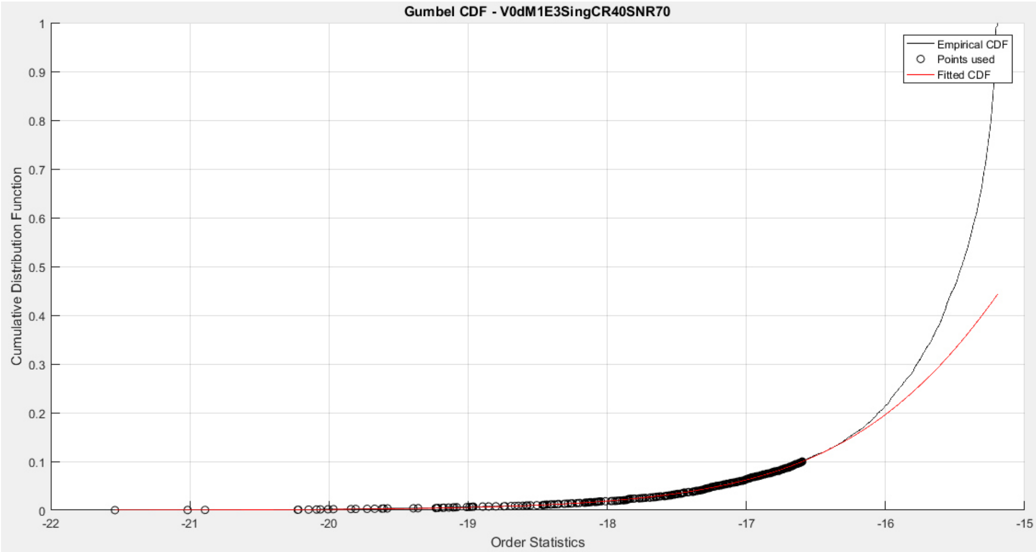

(a) Reconstructed Gumbel C.D.F. using 10% of VA_1 data set

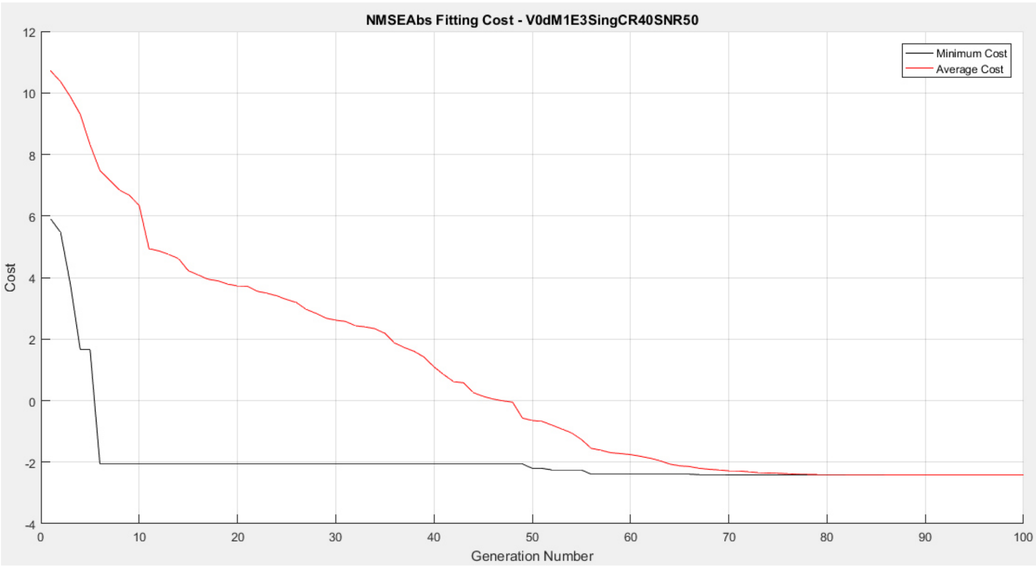

(b) Evolution of logarithmic fitting cost - Gumbel C.D.F.

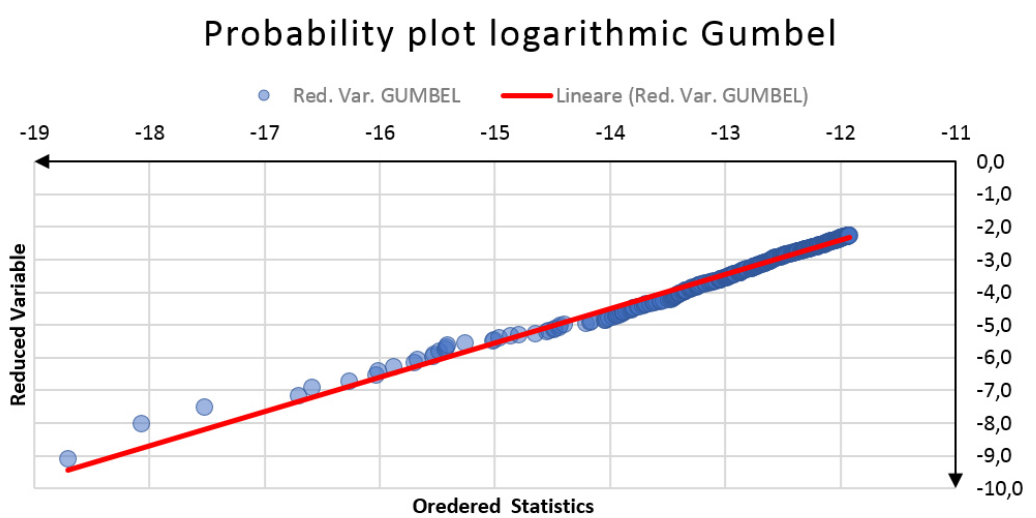

(c) Probability Plot - Gumbel C.D.F.

Figure 5.9: Example of Gumbel C.D.F. estimation

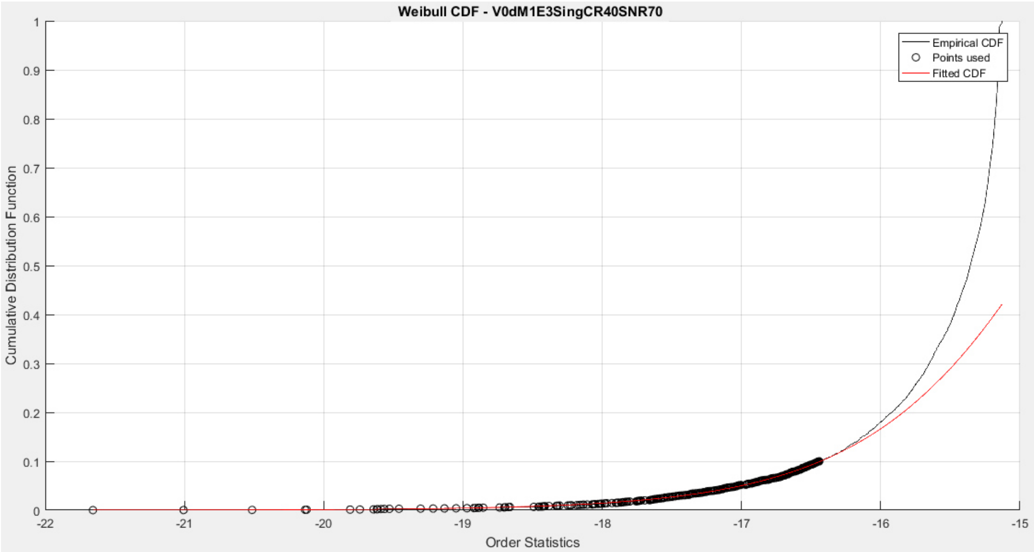

(a) Reconstructed Weibull C.D.F. using 10% of VA_1 data set

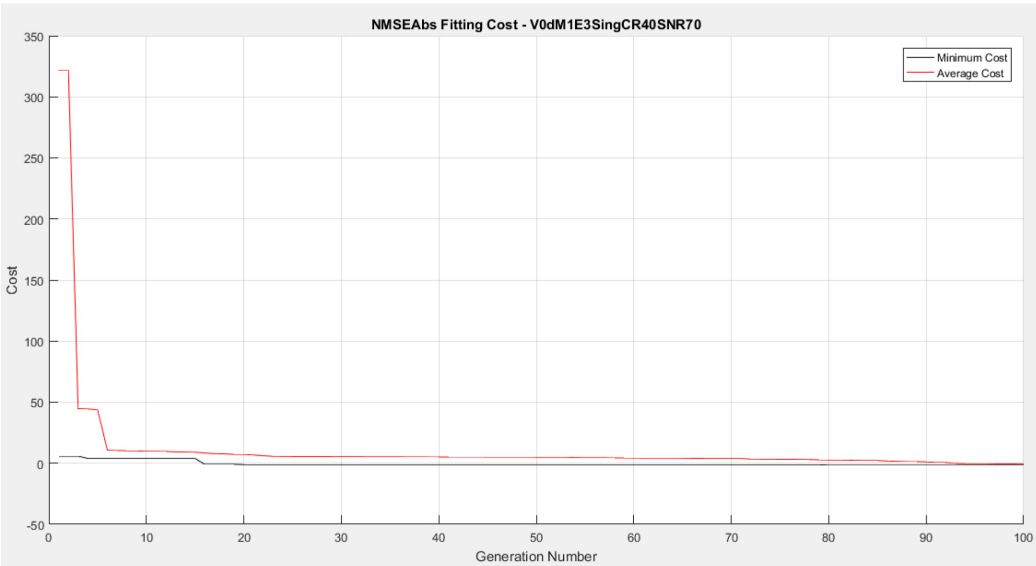

(b) Evolution of logarithmic fitting cost - Weibull CD.F.

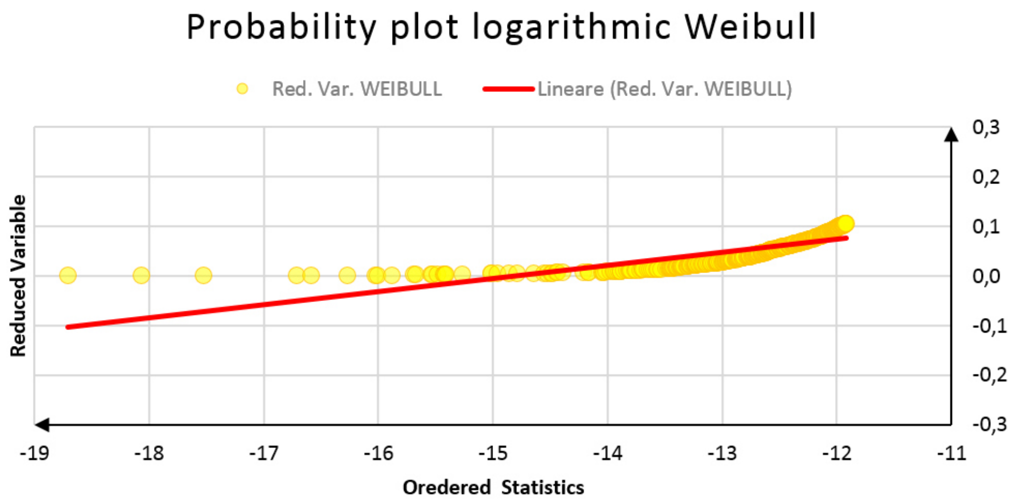

(c) Probability Plot - Weibull C.D.F.

Figure 5.10: Example of Weibull C.D.F. estimation

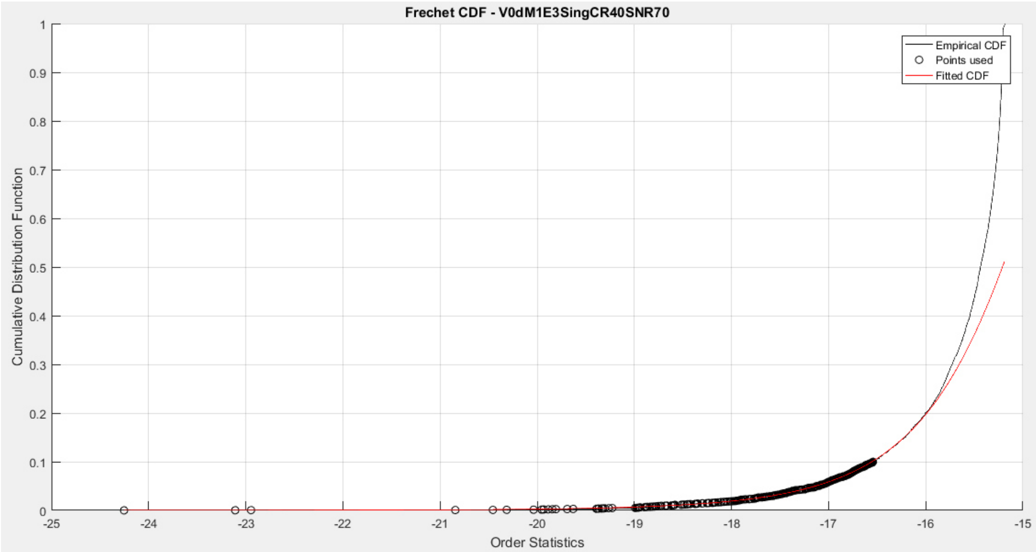

(a) Reconstructed Frechét C.D.F. using 10% of VA_1 data set

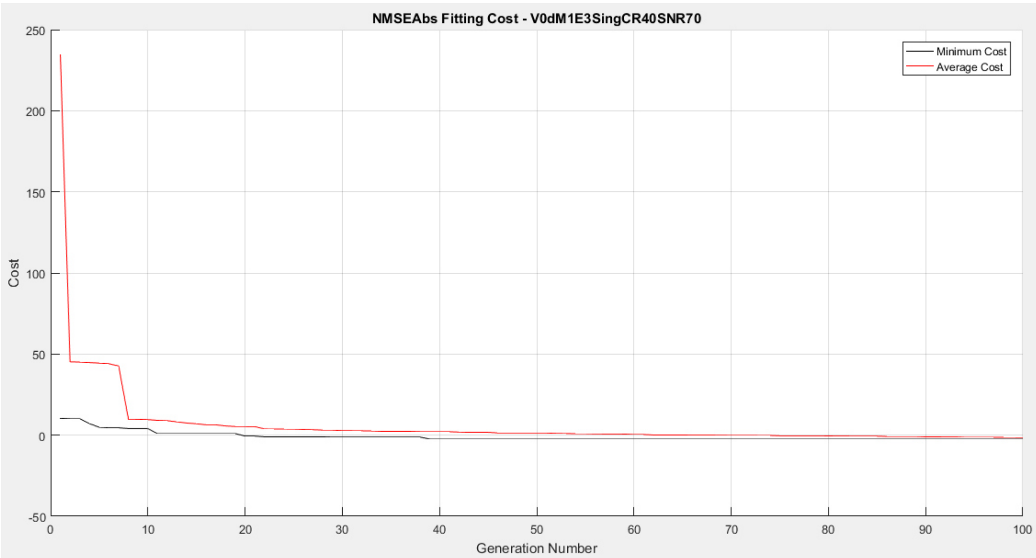

(b) Evolution of logarithmic fitting cost - Frechét C.D.F.

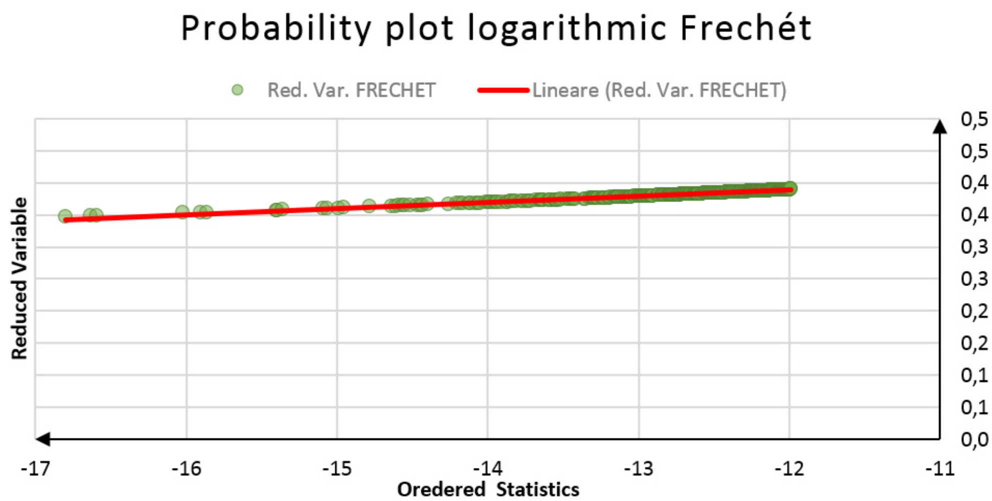

(c) Probability Plot - Frechét C.D.F.

Figure 5.11: Example of Frechét C.D.F. estimation

5.5 Threshold Definition and Damage Detection

After reconstructing the Cumulative Distribution Function it is possible to define a threshold in correspondence of a given quantile α, simply inverting the equations of feasible limit distributions 2.10. In this case, the quantile is set to be the lower 1% and the this leads to the three limit logarithmic probabilities $lz_{lim} = log(\mathbf{z_{lim}})$ for each minima extreme distribution:

$$\begin{gathered} GUMBEL: lz_{lim} = \Big[log\big(-\log(1-\alpha)\big)\Big] * \delta + \lambda \\ FRECH\acute{E}T: lz_{lim} = -\Big\{\Big[\big(-log(1-\alpha)\big)^{\frac{1}{\beta}}\Big]^{-1} * \delta - \lambda\Big\} \\ WEIBULL: lz_{lim} = \Big[\big(-log(1-\alpha)\big)^{\frac{1}{\beta}}\Big]\delta + \lambda \end{gathered} \tag{5.5}$$

and for the Generalised Extreme Value distribution is,

$$lz_{lim} = -\left\{\frac{\sigma * \Big[\big(-log(1-\alpha)\big)^{-\gamma} - 1\Big]}{\gamma} - \mu\right\} \tag{5.6}$$

For the Test data set TS is now calculated a new logarithmic posterior probability lz_{test} from the equation 2.5 and confronted with the limit for each analysed transverse displacement. When a value is found beyond the limit, so:

$$lz_{test} \leq lz_{lim} \tag{5.7}$$

that value is recorded as an outlier and the mode is identified as damaged. Since the TS data set contains undamaged and damaged mode shapes, when an undamaged mode shape is detected as damaged it is recorded as "false positive" and, the other way, when a damaged mode shape is not recognised a misclassification as "false negative" is reported.

5.6 Results

The details of the obtained results and the theoretical proof for different case studies of a reference cantilever beam are showed in the following figures from 5.12 to 5.17. The results are displayed as comprehensive graphics where the x-axis and y-axis represent the crack location and the crack depth, respectively, while the coloured cells are the percentage of successful identifications of damaged modes. The effectiveness of the employed algorithm in detecting a change in the behaviour of the structure when a simulated damage is present is studied by several simulations with a non-optimised Matlab ® code to investigate the influence of the different parameters. In particular the varied parameters are:

- Crack location, between 1% and 99% of the beam length
- Crack magnitude, between 5% and 40 % of the beam height section
- Noise Level (*SNR*), between 40 and 80 dB
- Number of sensors

Initially, the different simulations were elaborated taking into account all the FE nodes as sensor locations in order to assess the correctness of the method. Successively, the number of input was reduced to verify the performance of the algorithm when dealing with fewer measurement points. The implemented damage detection algorithm is primary applied to a reference cantilever beam and successively it has been extended to other boundary conditions.

Moreover, a comparison with the pointwise approach of the *Extreme Value Statistics* is done in order to asses the advantages and the disadvantages of the *Extreme Function Theory* approach and to evaluate the accuracy of the proposed method.

5.6.1 Damage Detection in a Cantilever Beam

As one would expect, peaks of error occur near the free end, since the crack influence decreases moving away from the clamped end, and in correspondence of the null-displacement points (i.e. modal nodes) (see figure 3.5). Analogously, the same trend is found analysing the crack depth, since a more damaged section obviously implies bigger displacements and thus a higher deviation with respect to the normal behaviour of the beam: this basically leads to more displacement data points that are recognised in the process as falling beyond the acceptable limit deriving from the definition of the 99% quantile confidence interval. Less intuitive is the peak of error located around the 20% of beam length for the first mode of the particular boundary conditions of the cantilever beam: when a crack occurs in this location, the Euclidean distance between damaged and undamaged mode shapes is very small thus a correct detection result is difficult.

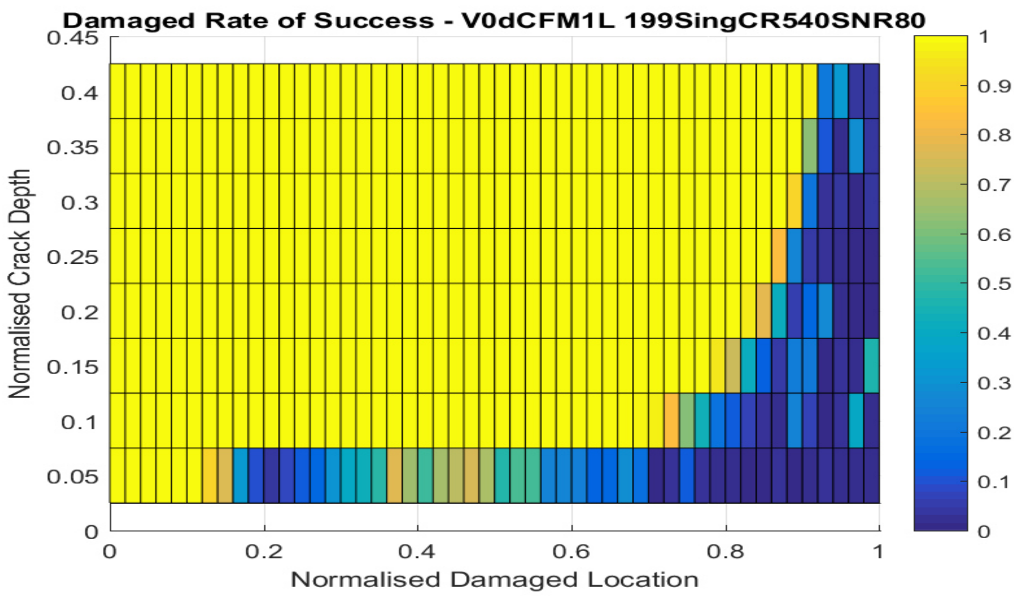

Figure 5.12: Rate of Successful detections Cantilever Beam (CB) - Mode Shape (MS) 1 with SNR=80 dB

Figure 5.13 shows the changes in relative difference of normalised absolute transverse displacements between the undamaged and the damaged state of a cantilever beam when a single edge crack is placed in different location along the beam. The resulting Euclidean distance is showed in figure 5.14, while the correspondence between peaks of the error in detection and peaks in the curve representing the complementary normalised Euclidean distance is evi-

dent from the figures 5.12 and 5.15.
The Euclidean distance between the pristine transverse mode shape $P = (p_1, p_2, ...p_n)$ and the damage one $Q = (q_1, q_2, ...q_n)$ has been evaluated for the n-dimensional space as,

$$\sqrt{(p_1 - q_1)^2 + (p_2 - q_2)^2 + ... + (p_n - q_n)^2} = \sqrt{\sum_{k=1}^{n} (p_k - q_k)^2} \tag{5.8}$$

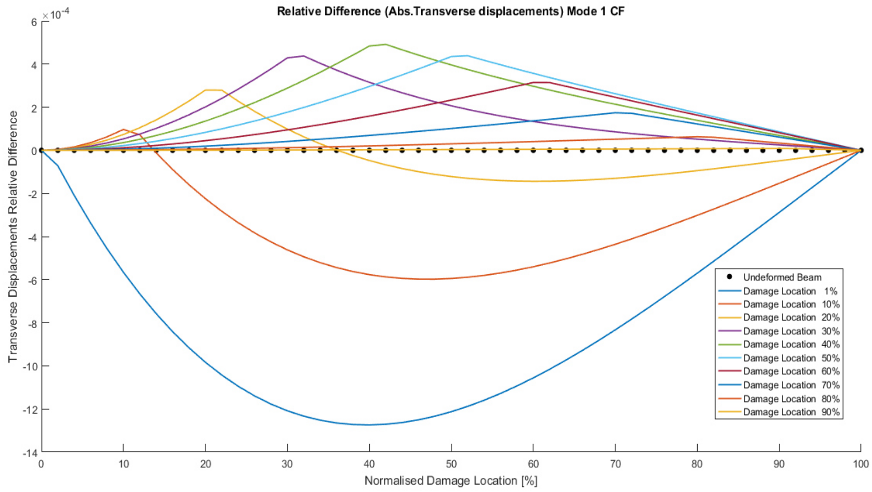

Figure 5.13: CB - MS 1, Relative difference in absolute transverse displacements

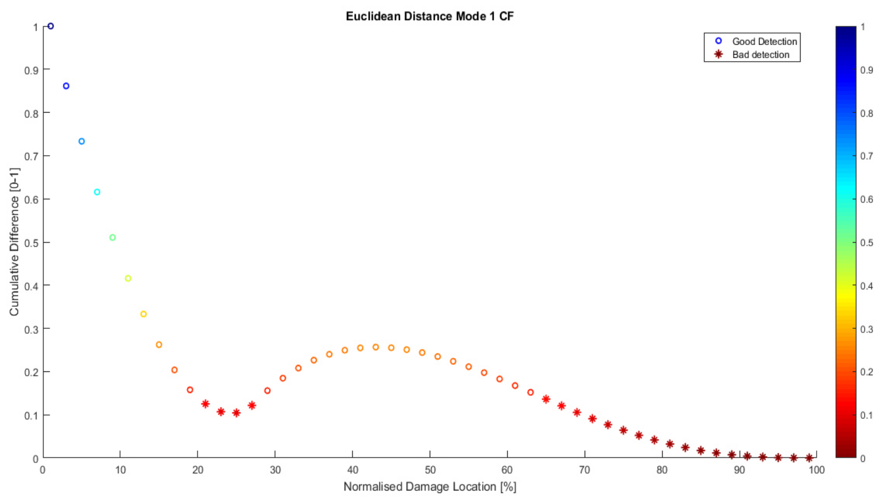

Figure 5.14: CB - MS 1, normalised Euclidean distance

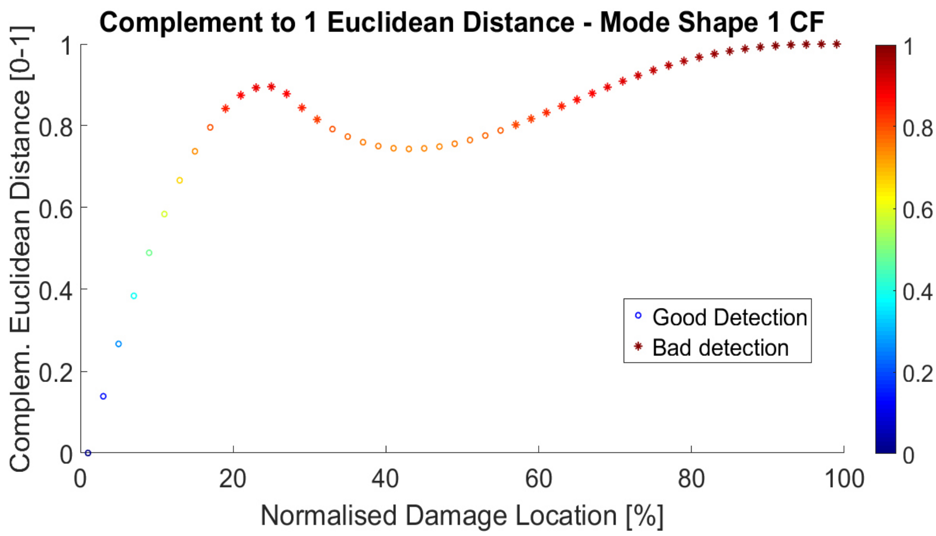

Figure 5.15: CB - MS 1, complementary normalised Euclidean distance

Moreover, the rate of correct detections increases while decreasing the disturbing presence of the noise: if figure 5.12 with a noise correspondent to $SNR = 80\ dB$ shows a rate of successful identifications of ≈ 100% in most of the analysed cases detecting also the small cracks, in figure 5.16, instead, the successes decrease significantly and much less no damaged mode shapes are correctly identified.

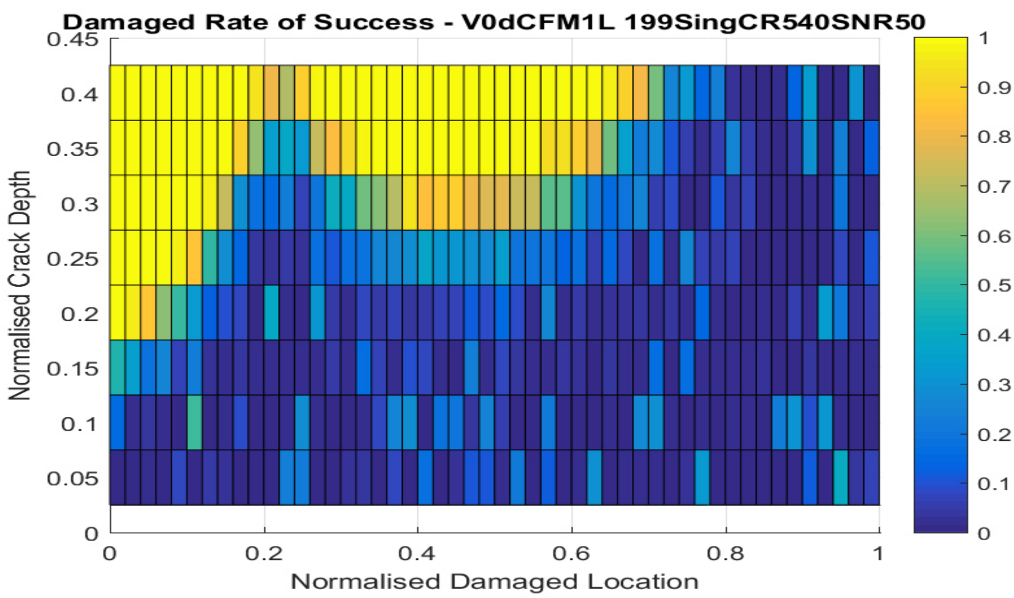

Figure 5.16: Rate of Successful detections CB - MS 1, SNR=50 dB

The effect of FE discretisation seems to be negligible and there are not relevant differences between a coarser but acceptable mesh and a more refined one. More relevant is, instead, the number of nodes considered as sensor locations and thus involved in the formation of datasets: figure 5.17a it is evaluated with a coarser discretisation of 30 elements (instead of 50) and taking into account all of them as sensor locations while figure 5.17b, instead, considers 11 sensors among the 31 nodes.

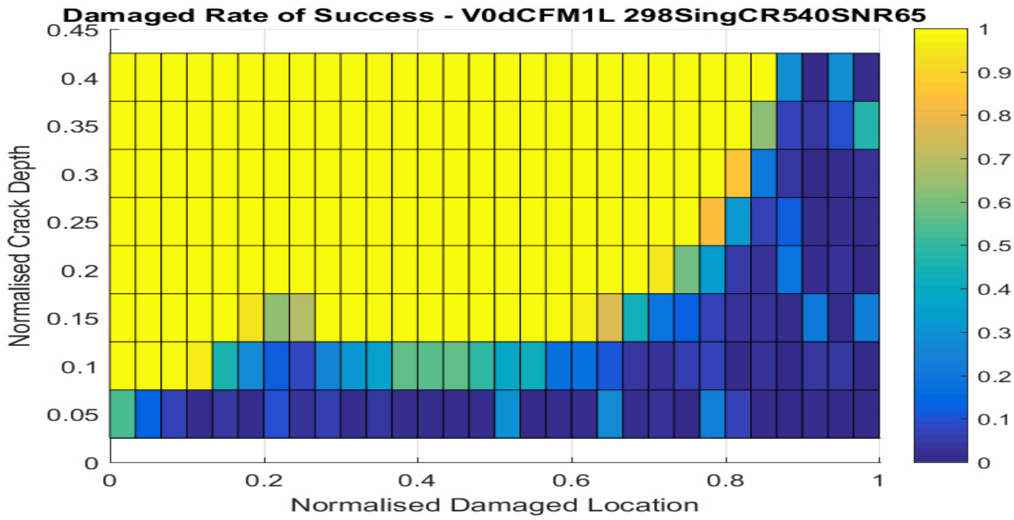

(a) Rate of Successful detections CB - MS 1, considering 30 sensors.

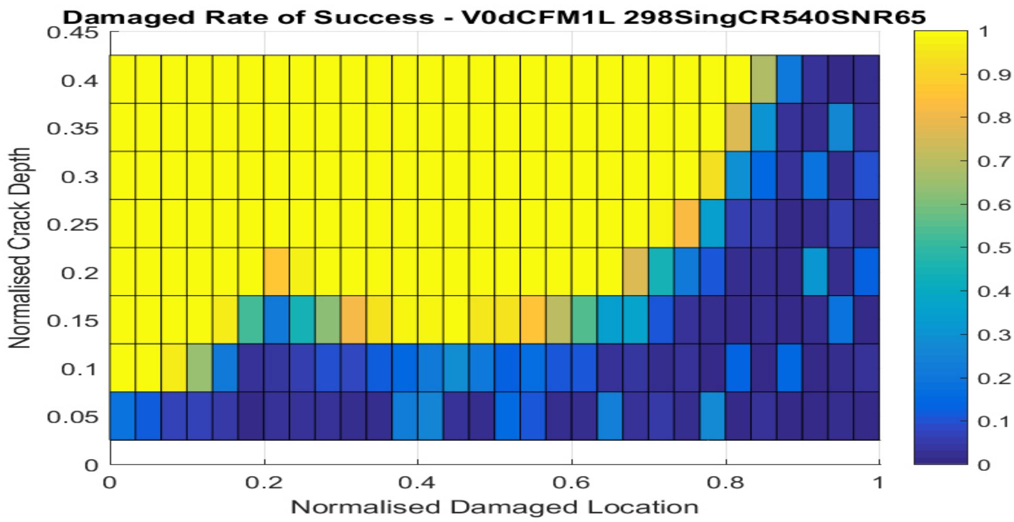

(b) Rate of Successful detections CB - MS 1, considering 11 sensors.

Figure 5.17: Results CB - MS 1 SNR=65 dB

Finally, a last observation regards the false identifications: the rate of false identifications remains almost constant in all the simulations and can be related to the intrinsic statistical uncertainty of the model. However, switching approach from EFT to EVT it is possible to note how the number of "false positives", that are undamaged modes identified as damaged decreases; otherwise, the number of "false negative", that are not detected damaged mode shapes increases as results from the comparison between figures 5.16 in 5.18a. This is due to the total number of available outliers (figure 5.18b) that the algorithm can process to make a prediction on the state of the tested mode shapes and, hence, a trade-off is necessary to balance both situations.

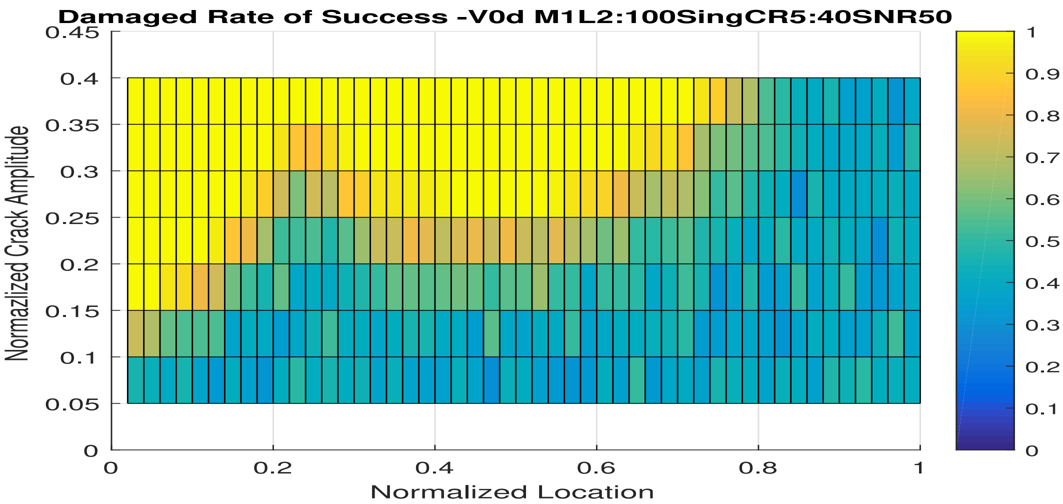

(a) Rate of Successful detections CB - MS 1, pointwise approach

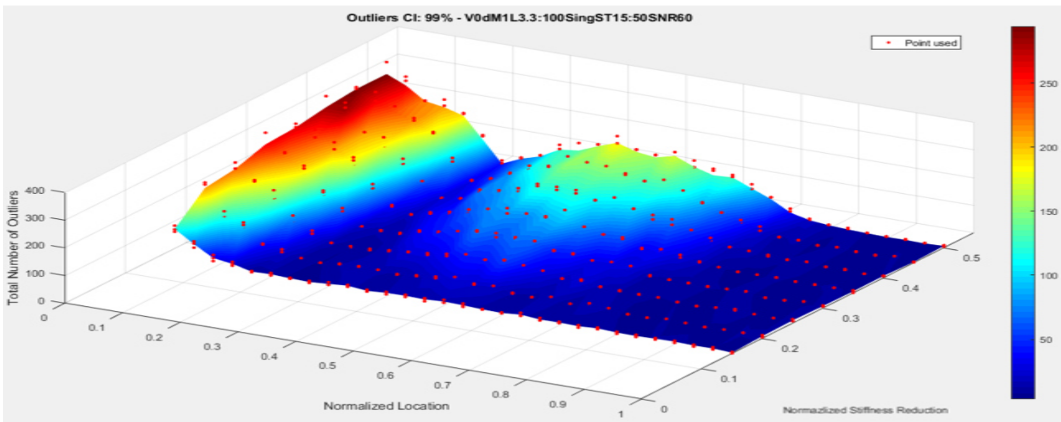

(b) Outliers CB - MS 1

Figure 5.18: Results pointwise approach CB - MS 1 SNR=50 dB

5.6.2 Higher Modes and other Boundary Conditions

Cantilever Beam (CB) - SNR 80 dB

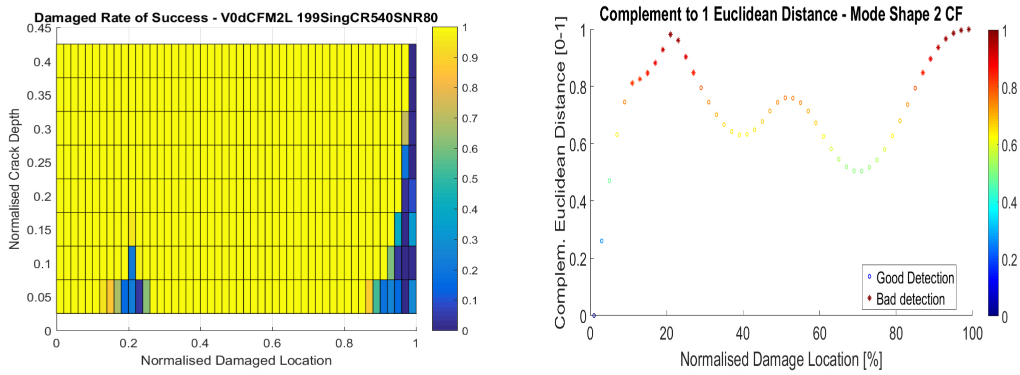

Figure 5.19: CB-MS 2, Rate of success (sx), compl. Euclidean distance (dx)

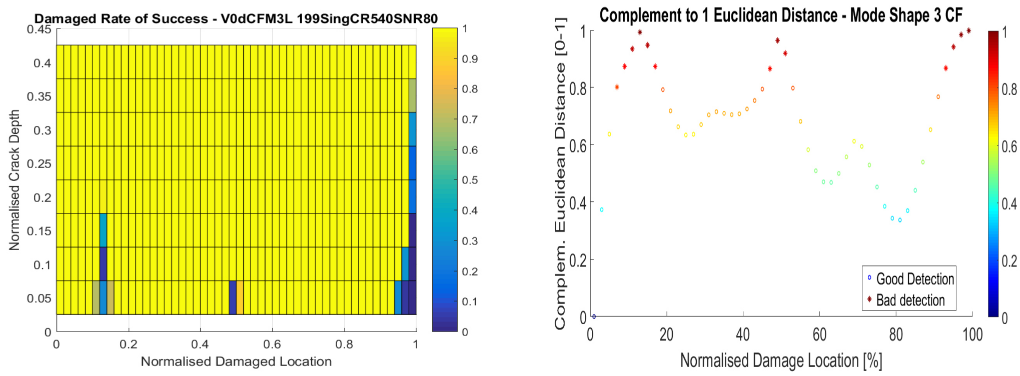

Figure 5.20: CB-MS 3, Rate of success (sx), compl. Euclidean distance (dx)

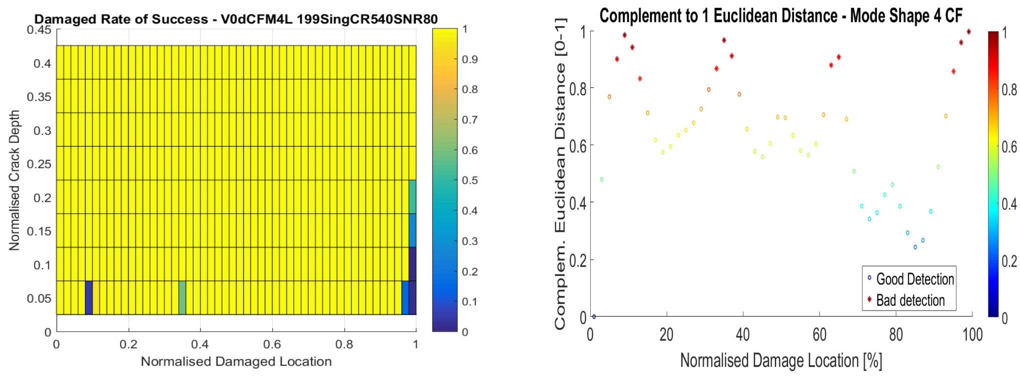

Figure 5.21: CB-MS 4, Rate of success (sx), compl. Euclidean distance (dx)

Hinge/Hinge (HH) - SNR 65 dB

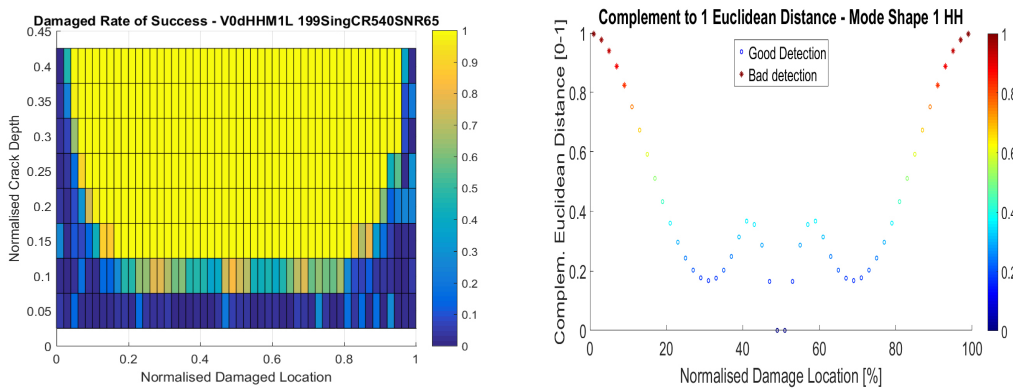

Figure 5.22: HH-MS 1, Rate of success (sx), compl. Euclidean distance (dx)

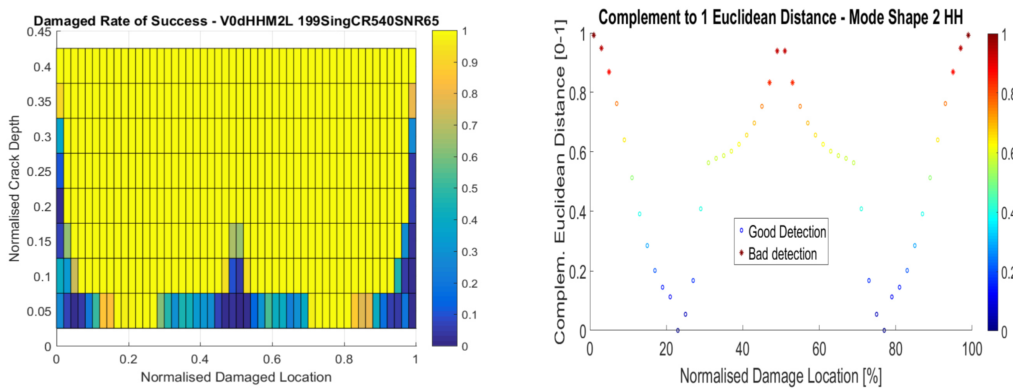

Figure 5.23: HH-MS 2, Rate of success (sx), compl. Euclidean distance (dx)

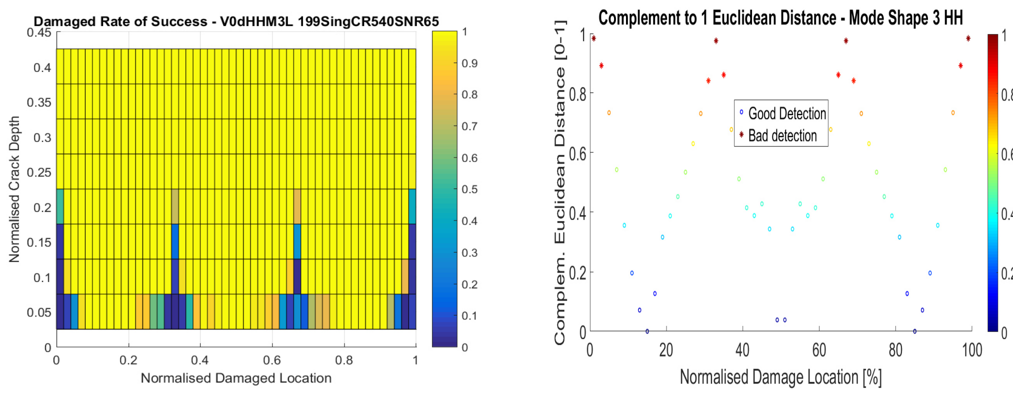

Figure 5.24: HH-MS 3, Rate of success (sx), compl. Euclidean distance (dx)

Hinge/Vertical Slider (HSv) - SNR 65 dB

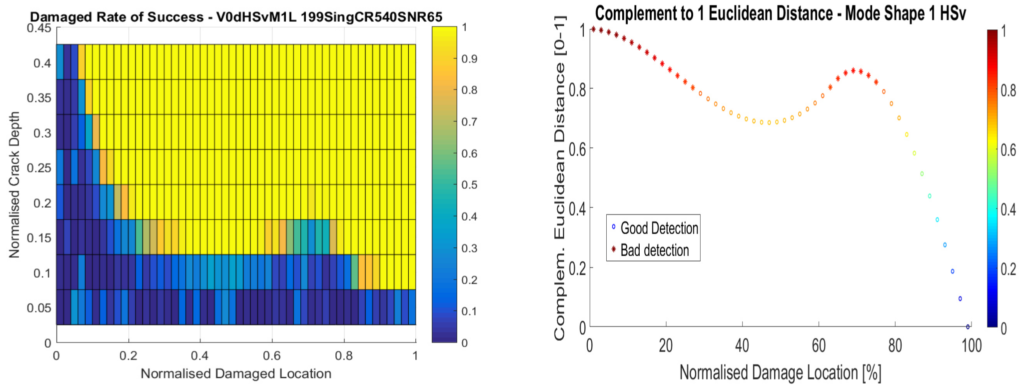

Figure 5.25: HSv-MS 1, Rate of success (sx), compl. Euclidean distance (dx)

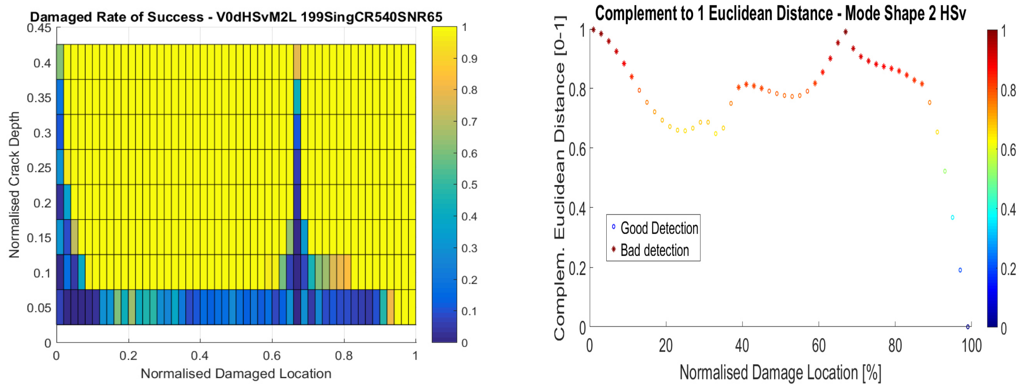

Figure 5.26: HSv-MS 2, Rate of success (sx), compl. Euclidean distance (dx)

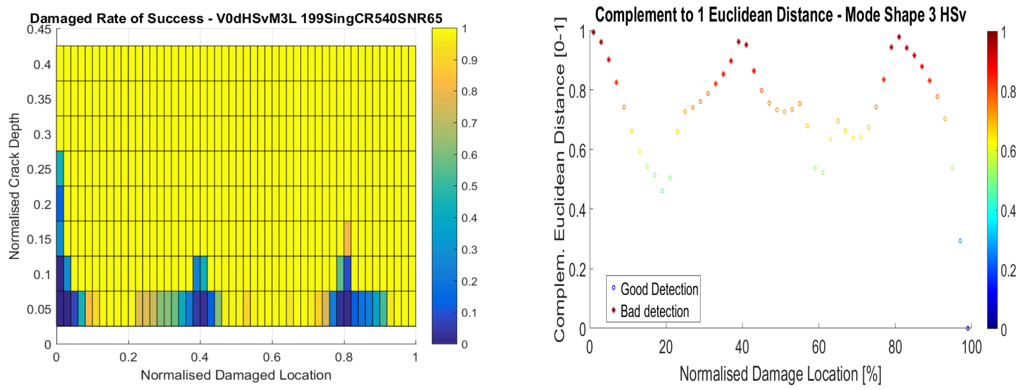

Figure 5.27: HSv-MS 3, Rate of success (sx), compl. Euclidean distance (dx)

Chapter 6

Conclusions and Further Perspectives

The method proposed here shows some advantages, but also some weak points. A first point of interest surely is the capability to work without differentiating transverse displacement data, which always involves a manipulation of values that leads to an amplification of noise. Moreover, from a computational point of view, the algorithm elaborates sufficiently accurate results starting from a reduced number of input data or without a dense discretisation of the structure, remaining able to collect all the available information in the posterior probability in a few seconds per whole cycle with a non-optimised Matlab ® code running on a mid-power personal computer (4 GB RAM, octa-core 2.6 GHz processor). When working with a reduced number of sensors, the "false positive" occurrences decrease significantly because of the diminution of possible false outliers, which is a characteristic of primary importance in the SHM field since it directly influences the cost of the inspection procedures. In spite of this, the presence of less sensitive points such as the modal nodes or crack position corresponding to a minimum Euclidean distance between damaged and undamaged mode shapes locally reduces the effectiveness of the method. Another issue regards the accuracy of the sensors used: the current available measurement technology, state-of-art devices able to consider the vast number of output channels considered in the case here reported, like laser sensors or high resolution cameras, allow to measure transverse displacements with a noise around 3% of the maximum displacement involved, which approximately corresponds to an additive noise level of SNR = 40 dB.

Further improvements of this work can be the extension of the proposed method to multidimensional problems, such as the bi-dimensional case of plates or 2-d frame structures or to multiple crack scenarios. Moreover, the obtained results encourage the development of a damage localisation procedure, but in this case a pointwise approach should be adopted in order to preserve all the nodal information coming from observations. Finally, experimental verifications can validate the damage assessment algorithm and test its susceptibility for real applications.

References

[**1**] M. A. B. Abdo and M. Hori. A numerical study of structural damage detection using changes in the rotation of mode shapes. *Journal of Sound and Vibration*, 251(2):227–239, 2002.

[**2**] R. J. Allemang. The modal assurance criterion - twenty years of use and abuse. *Journal of Sound and Vibration*, 37(8):14–23, 2003.

[**3**] R. J. Allemang and D. L. Brown. A correlation coefficient for modal vector. In *Proceedings of the 1st International Modal Analysis Conference*, volume 365, pages 110–116, 1982.

[**4**] ANAS. Multi-year investment plan 2015-2019. Technical report, Ministero delle Infrastrutture e dei Trasporti, Rome 25/11/2015, 2015.

[**5**] R. J. Astley. *Finite Elements in Solid and Structure*. Chapman and Hall, 1992.

[**6**] C. E. Augarde. Generation of shape functions for straight beam elements. *Computer and Structures*, 68:955–560, 1998.

[**7**] M. Bedworth. Probability moderation for multilevel information processing. Technical report, DRA, 1994.

[**8**] M. Bedworth and J. O'Brien. The omnibus model: a new model of data fusion? *IEEE Aerospace an Electronic Systems Magazine*, 15(4):30–36, 2000.

[**9**] C. Bishop. *Pattern Recognition and Machine Learning*. Springer, 2006.

[**10**] R. Bruson. Ponti e viadotti: procedure per la valutazione della sicurezza delle opere d'arte stradali. Technical report, Collegio degli Ingegneri della Provincia di Vicenza, 2011.

[**11**] P. E. Carden and P. Fanning. Vibration based condition monitoring: a review. *Journal of Structural Health Monitoring*, 3(4):355–377, 2004.

[**12**] A. Carpinteri. *Scienza delle Costruzioni 1.* Pitagora Editrice, 1992.

[**13**] E. Castillo. *Extreme Value Theory in Engineering.* Academic Press Series in Statistical Modelling and Decision Science, 1988.

[**14**] S. Chesné and A. Deraemaeker. Damage localization using trasmissibility functions: a critical review. *Mechanical Systems and Signal Processing*, 38:569–584, 2013.

[**15**] M. Civera, C. Surace, and K. Worden. Detection of cracks in beams using treed gaussian processes. In *Conference Proceedings of the Society for Experimental Mechanics Series*, volume 7 of *Structural Health Monitoring and Damage Detection*, pages 85–97, 2017.

[**16**] D. Clifton, L. Clifton, S. Hugueny, D. Wong, and L. Tarassenko. An extreme function theory for novelty detection. *IEEE Journal of Selected Topics in Signal Processing*, 7(1):28–37, 2013.

[**17**] N. Corrado, N. Durrande, M. Gherlone, J. Hensman, M. Mattone, and C. Surace. Single and multiple crack localisation in beam-like structure usgin a gaussian process regression approach. *Journal of Sound and Vibration*, 24(18):4160–4175, 2017.

[**18**] N. Corrado, C. Surace, L. Montanari, and A. Spagnoli. Comparing three different derivative discontinuities detection methods for the localisation of cracks in beam-like structures. In *Proceedings of the International Workshop on Structural Health Monitoring*, 2015.

[**19**] G. De Roeck. *De eindige elementenmethode - Finite Element Method Course Text.* Acca Katholieke Universiteit Leuven, 2013.

[**20**] S. W. Doebling, C. R. Farrar, and M. B. Prime. A summary review of vibration-based damage identification methods. *The Shock and Vibration Digest*, 30(2):91–105, 1998.

[**21**] S. W. Doebling, C. R. Farrar, M. B. Prime, and D. W. Shevitz. Damage identification and health monitoring of structural and mechanical systems from changes in their vibration characteristics: A literature review. Technical report, Los Alamos National Laboratory, 1996.

[**22**] W. Fan and Q. P. Vibration-based damage identification methods: a review and comparative stud. *Structural Health Monitoring International Journal*, 30(2):91–105, 2011.

[**23**] C. R. Farrar, S. W. Doebling, and D. A. Nix. Vibration-based structural damage identification. *Proceedings of the Royal Society of London A: Mathematical, Physical and Engineering Science*, 359(1778):131–149, 2012.

[**24**] C. R. Farrar and K. Worden. An introduction to structural health monitoring. In *Proceedings of the Royal Society of London A: Mathematical, Physical and Engineering Science*, volume 365, pages 303–315, 2007.

[**25**] S. D. Fassois and S. J. S. Time series methods for fault detection and identification in vibrating structures. *Proceedings of the Royal Society A: Mathematical, Physical and Engineering Science*, 365:411–448, 2007.

[**26**] R. Fisher and L. Tippet. Limiting forms of the frequency distributions of the largest or smallest members samples. *Proceedings of the Cambridge Philosophical Society*, 24:180–190, 1928.

[**27**] R. Fletcher and C. M. Reeves. Function minimization by conjugate gradients. *The computer Journal*, 7(2):149–154, 1964.

[**28**] B. G. Galerkin. Rods and plates. series occurring in various questions concerning the elastic equilibrium of rods and plates. *Engineering Bulletin (Vestnik Inzhenerov)*, 19:897–908, 1915.

[**29**] M. J. Gander and G. Wanner. From euler, ritz and galerkin to modern computing. *SIAM Rev*, 54(4), 2012.

[**30**] D. Goldberg. *Genetic Algorithms in Search, Optimization and Machine Learning*. Addison-Wesley Publishing Company, 1989.

[**31**] M. Gordan, H. A. Razak, Z. Ismail, and K. Ghaedi. Recent developments in damage identification of structures using data mining. *Latin American Journal of Solids and Structures*, 14:2373–2401, 2017.

[**32**] E. Gumbel. *Statistics of Extremes*. Columbia University Press, 1958.

[**33**] S. M. Han, B. Wei, and T. Wei. Dynamics of transversely vibrating beams using four engineering theories. *Journal of Sound and Vibration*, 255(10):935–988, 1999.

[**34**] J. Hesman, C. Surace, and M. Gherlone. Detecting mode-shape discontinuities without differentiation - examining a gaussian process approach. In *Proceedings of 9th International Conference on Damage Assessment of Structures*, pages 1–10, 2011.

[**35**] M. R. Hestenes and E. Stiefel. Methods of conjugate gradients for solving linear systems. *Journal of Research of the National Bureau of Standards*, 49(6):409–436, 1952.

[**36**] M. Hintermüller. Nonlinear optimization - part 1 unconstrained and box-constrained problems basic course, 2011. Berlin School of Mathematics.

[**37**] IlFattoQuotidiano. Photo of collapsed bridge 167, ancona (it), 2017.

[**38**] IlSecoloXIX. Photo of collapsed bridge 626, agrigento (it), 2014.

[**39**] ISTAT. 14^{th} general census of the population and housing. Technical report, Istituto Nazionale Statistica, 2001.

[**40**] J. T. Kim and N. Stubbs. Damage detection in offshore jacket structures from limited modal information. *Journal of Offshore and Polar Engineering*, 5(1):58–66, 1995.

[**41**] D. Kindova-Petrova. A new damage location parameter for beam structures based on mode shape slope. *Journal of Scientific and Engineering Research*, 7(12):1122–1128, 2016.

[**42**] K. Kliewer and B. Glisic. Normalized curvature ratio for damage detection in beam-like structures. *Frontiers in Built Environment*, 3, 50 2017.

[**43**] X. Kong, C. S. Cai, and J. Hu. The state-of-art on framework of vibration-based structural damage identification for decision making. *Applied Sciences SHM of Civil Structures*, 7(5):497, 2017.

[**44**] S. Kotz and S. Nadarajah. *Extreme Value Distributions, Theory and Applications*. Imperial College Press, 2000.

[**45**] LaStampa. Photo of collapsed bridge s. vittoria, cuneo (it), 2017.

[**46**] LaVoceDiGenova. Photo of collapsed bridge polcevera, genoa (it), 2018.

[**47**] D. Martucci, M. Civera, C. Surace, and K. Worden. Novelty detection in a cantilever beam using extreme function theory. Presented at Modern Practice in Stress and Vibration Analysis conference (MPSVA 2018) held by the Institute of Physic at Clare College in Cambridge, UK, 2018.

[**48**] A. Messina, E. J. Williams, and T. Contursi. Structural damage detection by a sensitivity and statistical-based method. *Journal of Sound and Vibration*, 216(5):791–808, 1998.

[**49**] K. Murphy. *Machine Learning A Probabilistic Perspective.* the MIT Press, 2012.

[**50**] J. Nocedal and S. Wright. *Numerical Optimization.* Springer, 1999.

[**51**] I. A. Nophadol. *New plotting position formulas for some well known distributions in engineering hydrology.* PhD dissertation, University of Montreal - Department of Civil Engineering and Applied Mechanics, 1989.

[**52**] OREDA-1992. *Offshore Reliability Data.* DNV Technica, 1992.

[**53**] A. K. Pandey, M. Biswas, and M. M. Samman. Damage detection from changes in curvature mode shapes. *Journal of Sound and Vibration*, 145(2):321–332, 1991.

[**54**] E. Papatheou, N. Dervilis, A. E. Maguire, C. C., I. Antoniadou, and K. Worden. Performance monitoring of a wind turbine using extreme function theory. *Renewable Energy*, 113:1490–1502, 2017.

[**55**] H. Park and H. Sohn. Parameter estimation of the generalized extreme value distribution for structural health monitoring. *Probabilistic Engineering Mechanics*, 21(4):366–376, 2006.

[**56**] F. Pellicano. Meccanica delle vibrazioni, 2009.

[**57**] G. L. Qian, S. N. Gu, and J. S. Jiang. The dynamic behaviour and crack detection of a beam with crack. *Journal of Sound and Vibration*, 138(10):233–243, 1990.

[**58**] P. Qiao and M. Cao. Wafeorm fractal dimension for mode shape-based damage identification of beamtype structures. *International Journal of Solids and Structures*, 45:5946–5961, 2008.

[**59**] A. Qin and P. Suganthan. Self-adaptive differential evolution algorithm for numerical optimization. *Proc. IEEE Congr. Evol. Comput*, 2:1785–1791, 2005.

[**60**] M. Radzienski and M. Krawezuk. Experimental verification and comparison of mode shape-based damage detection methods. In *Proceedings of 7th International Conference on Modern Practice in Stress and Vibration Analysis*, volume 181 of *Journal of Physics: Conference Series*, 2009.

[**61**] R. B. Randall. State of art in monitoring rotating machinery - part 1. *Journal of Sound and Vibration*, 38(3):14–21, 2004.

[**62**] R. B. Randall. State of art in monitoring rotating machinery - part 2. *Journal of Sound and Vibration*, 38(5):10–17, 2004.

[**63**] C. Rasmussen and K. Williams. *Gaussian Process for Machine Learning*. the MIT Press, 2006.

[**64**] C. P. Ratcliffe. Damage detection using modified laplacian operator on mode shape data. *Journal of Sound and Vibration*, 204(3):505–517, 1997.

[**65**] M. Rausand and K. Øien. The basic concepts of failure analysis. *Reliability Engineering and System Safety*, 53(1):78–83, 1996.

[**66**] J. W. S. Rayleigh. *The Theory of Sound 1*. MacMillan and Co., 1896.

[**67**] S. Robert. Novelty detection using extreme value statistics. *IEEE Proceedings in Vision, Image and Signal Processing*, 146:124–129, 1998.

[**68**] S. Rucevskis and M. Wesolowski. Identification of damage ina abeam structure by using mode shape curvature squares. *Shock and Vibration*, 17:601–610, 2010.

[**69**] A. Rytter. *Vibrational Based Inspection of Civil Engineering Structures*. PhD dissertation, University of Aalborg - Department of Building Technology and Structural Engineering, 1993.

[**70**] O. S. Salawu. Detection of structural damage through changes in frequency: a review. *Engineering Structures*, 19(9):718–723, 1997.

[**71**] O. S. Salawu and C. Williams. Damage location using vibration mode shapes. In *Proceedings of the 12th International Modal Analysis Conference*, volume 2251, pages 933–939, 1994.

[**72**] J. Seo, J. W. Hu, and J. Lee. Summary review of structural health monitoring applications for highway bridges. *Journal of Performance of Constructed Facilities*, 30(4), 2016.

[**73**] Z. Y. Shi, S. Law, and L. Zhang. Damage localization by directly using incomplete mode shapes. *Journal of Engineering Mechanics*, 126(6):656–660, 2000.

[**74**] J. J. Sinou. A review of damage detection and health monitoring of mechanical systems from changes in the measurement of linear and nonlinear vibrations. *Mechanical Vibrations: Measurement, Effects and Control*, pages 643–702, 2009.

[**75**] H. Sohn, C. R. Farrar, F. M. Hemez, D. D. Shunk, D. W. Stinemates, B. R. Nadler, and C. J. J. A review of structural health monitoring literature: 1996-2001. Technical report, Los Alamos National Laboratory, 2004.

[**76**] R. Storn and K. Price. Differential evolution: a simple and efficient heuristic scheme for global optimization over continuous spaces. *Journal of Global Optimization*, 11(10):341–359, 1997.

[**77**] S. Timoshenko. *Vibration Problem in Engineering*. Van Nostrand Company, 1937.

[**78**] S. Timoshenko. *Strength of Materials*. Van Nostrand Company, 1940.

[**79**] E. Verstrynge. Inspectie, monitoring en experimentele methodes - vernieuwbouw van structuren course notes, 2009. Katholieke Universiteit Leuven.

[**80**] E. Volterra and E. C. Zachmanoglu. *Dynamic of Vibrations*. Merrill Books Inc., 1965.

[**81**] M. M. A. Wahab and G. DeRoeck. Damage detection in bridges scenario using modal curvatures. *Journal of Sound and Vibration*, 226(2):217–235, 1999.

[**82**] J. Wang and P. Qiao. On irregularity-based damage detection method for cracked beams. *International Journal of Solids and Structures*, 45:688–704, 2008.

[**83**] K. Worden and J. M. Dulieu-Barton. An overview of intelligent fault detection in systems and structures. *Journal of Structural Health Monitoring*, 3(1):85, 2004.

[**84**] K. Worden and C. Farrar. *Structural Health Monitoring: A Machine Learning Perspective*. Wiley and Sons Publication, 2013.

[**85**] K. Worden, C. R. Farrar, J. Haywood, and M. Todd. A review of nonlinear dynamics applications to structural health monitoring. *Structural Control and Health Monitoring*, 15:540–567, 2008.

[**86**] K. Worden, C. R. Farrar, G. Manson, and G. Park. The fundamental axioms of structural health monitoring. *Proceedings of the Royal Society of London A: Mathematical, Physical and Engineering Sciences*, 463(2082):1639–1664, 2007.

[**87**] K. Worden and M. I. Friswell. Modal vibration-based damage identification. In *Encyclopedia of Structural Health Monitoring*, chapter 11. Wiley and Sons, 2009.

[**88**] K. Worden and G. Manson. The application of machine learning to structural health monitoring. *Proceedings of the Royal Society of London A: Mathematical, Physical and Engineering Sciences*, 365:515–537, 2007.

[**89**] K. Worden, G. Manson, and N. R. J. Fieller. Damage detection using outlier analysis. *Journal of sound and Vibrations*, 229(**3**):647–667, 2000.

[**90**] K. Worden, G. Manson, H. Sohn, and C. Farrar. Extreme value statistics from differential evolution for damage detection. *Proceedings of 23rd Int. Modal Analysis Conf.*, 2005.

[**91**] Y. Xia and H. Hao. A genetic algorithm for structural damage detection based on vibration data. In *Proceedings of 19th International Modal Analysis Conferences*, pages 1381–1387, 2001.

[**92**] M. M. F. Yuen. A numerical study of the eigenparameters in a damaged cantilever. *Journal of Sound and Vibration*, 103(3):301–310, 1985.